Measurement of Hansen Solubility Parameters on Surface of Fine Particles Using Capillary-Penetration Method and Their Technical Application

課程博士

学位授与年月：2020 年 9 月

関西大学審査学位論文

Measurement of Hansen Solubility Parameters on Surface of Fine Particles Using Capillary-Penetration Method and Their Technical Application

理工学研究科・総合理工学専攻

環境化学領域

16D6901

堤　慎一

博士論文要旨

理工学研究科総合理工学専攻

環境化学

16D6901

堤　慎一

≪論題≫

Measurement of Hansen Solubility Parameters on Surface of Fine Particles Using Capillary-Penetration Method and Their Technical Application

≪概要≫

　機能性複合材料は、導電性、磁性、熱伝導などの様々な分野で応用されている。無機材料と有機材料からなる機能性複合材料の性能向上には、無機フィラーとポリマー間の親和性改善による無機フィラーの分散性や充填率向上が必要である。一般に、親和性は無機フィラー表面に表面処理を施すことで高められる。但し、その表面処理の種類は多様で、かつ親和性の定量的な評価手法もないため、最適な組合せを見つけることは困難であった。

　一方、物質間の親和性を評価する手法として Hansen Solubility Parameters(HSPs)が注目を浴びている。HSPs は物質における凝集エネルギー密度の平方根で表される物性値であり、HSPs は London 分散力、双極子間力および水素結合力の 3 つの項から成っている。当初、HSPs はポリマーの溶解性等に使用されたが、近年、微粒子の分散等の物質間の相互作用評価にも用いられ始めた。そこで、機能性複合材料であるボンド磁石に HSPs を適用し、親和性の定量的な評価とボンド磁石の性能向上を試みた。

　ボンド磁石の主構成要素である磁石粉末は、比重が 7600 kg/m3 と重く、粒子径も 1～100 μm と比較的大きく、沈降法や粒子径法等の既存の微粒子の HSPs 測定方法では、粒子が測定前に沈降するため測定困難であった。そこで、液体と微粒子の接触角測定方法である浸透速度法を活用し、磁石粉末の HSPs 測定手法を確立した。この手法は粒子を固定し、液体を浸透させるため測定前の沈降等の課題はない。また、新手法は、粒子比重、形状、大きさに制限されず、粒子の HSPs 測定対象を拡大することができたと考える。本手法を用い、表面処理した磁石粉末の HSPs を測定し、磁石粉末と樹脂の HSPs を比較することで、親和性を定量的に評価でき、ボンド磁石性能を大幅に向上できた。

最後に、確立した新手法を用い、非球形で、20～30 μm と比較的大きい花粉粒子の HSPs を測定した。アレルギー予防の観点から、ミストによる花粉の捕集を想定し、花粉粒子の HSPs に近い液体や混合液体を提案した。今後、生体に安全な捕集ミストや、空気清浄機等のフィルタ材料開発に応用できると考える。

≪各章の要旨≫

　第一章では、HSPs の概要や算出方法、測定方法について説明した。また、現在報告されている HSPs 関連の研究について紹介した。今後の HSPs の研究では、ロンドン分散力 δd や水素結合力 δh の分割などにみられる、より詳細なパラメータの理解により、正確性を高める研究がなされると考えられる。また、親和性を評価する方法は様々な提案がなされつつあり、今後分析装置の発展と共に、さらに増えていくものと考えられる。その応用分野では、微粒子の分散に関する研究も盛んで、更にはバイオ、医療、薬品の研究事例が増加しており、今後の広い分野での HSPs の応用について述べた。

　第二章では、筆者が考案した新しい微粒子の HSPs 測定手法について説明した。高比重の粒子は、沈降法や粒子径法等の既存の微粒子の HSPs 測定方法では、粒子が測定前に沈降してしまい測定困難であった。そこで、液体と微粒子の接触角測定方法である浸透速度法を活用し、磁石粉末の HSPs 測定手法を考案した。この手法は粒子を固定し、液体を浸透させるため沈降等の課題はない。本手法を、DLS 法でも測定可能な 1 μm の球形シリカ粒子に用いて、手法の妥当性を検証した。DLS 法と浸透速度法で測定した HSPs の距離 Ra は 1.48 と極めて近い、同等の値が得られ、新手法で HSPs が測定可能であることを明らかにした。また、DLS 法では測定困難な 63 μm 以下の非球形シリカ粒子の測定も行い、1 μm の球形シリカ粒子の HSPs との距離 Ra が 1.5 以下であることを確認し、比較的大きな粒子へも適用可能であることを明らかにした。この新手法は、粒子比重、形状、大きさに制限されず、粒子のHSPs 測定対象を拡大することができたと考える。他方、浸透速度法は、しばしば接触角の絶対値を測定できず、相対比較しかできないと指摘を受ける。しかし、浸透速度法と HSPs を組み合わせると、HSPs という物性値が、接触角の相対値から求まるため、浸透速度法の応用範囲を広めることもできたと考える。

　第三章では、第二章で確立した微粒子の HSPs 測定技術を用いて、非球形で比重が重い磁石粉末を有するボンド磁石の性能改善を試みた。ボンド磁石を含む様々な複合材料は、これまで、過去の経験と知識を頼りに設計が行われてきた。その複合材料設計を定量評価するために HSPs を適用した。磁石粉末と樹脂とを主構成要素とするボンド磁石において、磁石粉末と樹脂との相溶性を改善することができれば、射出流動性と高い磁気特性を両立できる。本章では、まず磁石粉末と樹脂の HSPs を測定し、磁石粉末に表面処理することで磁石粉末表面の HSPs を樹脂の HSPs へ近づけることを試みた。また、選定した表面処理剤と HSPsの関係を明らかにするために、予め表面処理剤の HSPs をグループ寄与法による計算から求めた。また、実際に表面処理した磁石粉末の HSPs も測定した。計算による表面処理剤のHSPs と樹脂の HSPs との距離 Ra と磁石粉末の粘度には、せん断速度で違いはあるが 0.66〜0.9 の相関関係が得られ、グループ寄与法による表面処理剤の計算によって射出流動性の予測が可能であることを明らかにした。さらに、実際に表面処理した磁石粉末の HSPs 測定値と粘度には 0.87〜0.98 の高い相関が得られ、実際に HSPs を測定することで高精度に射出流動性が予測可能であることを明らかにした。最も親和性の高い UPTMS 表面処理剤では、磁粉充填率、磁気特性を変えることなく、せん断速度 760 s-1 での粘度を 1221 Pa·s から 713 Pa·s へと大幅に低減した。この結果は、理論的には、他の複合材料へも応用が可能であり、表面処理剤の HSPs 計算や、フィラー表面の HSPs 測定により複合材料の性能予測が可能であることを示唆している。今後は、ボンド磁石に限らず、構造材料、熱伝導材料、摩擦材料、電気伝導などの様々な複合材料へ展開できると考える。

第四章では、第二章で確立した浸透速度法による HSPs 測定手法を用いて、バイオ粒子への応用を試みた。日本に限らず世界的に、スギ、ブタクサなどの花粉症が問題になっている。これまで、空気清浄機、花粉フィルタ、静電反発など、様々なアレルギー対策がなされている。本章では、花粉を効率的に捕集することを想定して、花粉表面の HSPs を測定した。スギ花粉表面の HSPs は（δd,δp,δh）＝（15.8,5.4,11.7）で、ヒノキ花粉表面の HSPs は（δd,δp,δh）＝（16.0,4.7,11.3）と特定するとともに、花粉表面と親和性の高い混合溶媒を HSPs の３D グラフ上で決定することができた。また、粒子表面の HSPs 測定で常に問題になる良溶媒と貧溶媒を分ける閾値の決定方法も検討し、測定した接触角データを利用して、より正確な HSPs を導き出す新しい手法も提案した。現段階では、化学的な見地からの混合溶媒提案であるため、今後、人体や環境への影響を考慮したクリーンかつ HSPs が花粉と近い液体や、フィルタ材料の検討が必要である。今後の花粉アレルギー対策への HSPs の貢献が期待できる。

　第五章では、各章を総括し、今後の展望および工学的応用について論じた。

以上

Measurement of Hansen Solubility Parameters on Surface of Fine Particles Using Capillary-Penetration Method and Their Technical Application

CONTENTS

Chapter 1 Introduction

1.1 Solubility parameter

1.1.1 Solubility indicators

Various indexes are available to indicate the solubility of a substance, including the Kauri-butanol value, solubility grade, cloud point of aniline, heptane number, and wax number. The Kauri-butanol (KB) value indicates the maximum amount of solvent that can be added to a stock solution of Kauri resin in butanol without causing haze. The method uses the property of the Kauri resin that it is easily dissolved in butanol, but does not dissolve in hydrocarbon solvents. A solvent with a high KB value, such as toluene, can dissolve more resin than a solvent with a low KB value, such as hexane. The solubility grade index indicates the strength of a solvent required to dissolve a particular polymer; a numerical value is assigned to each polymer. The cloud point of aniline is used as a solubility index by using the property that aniline is easily soluble in aromatic hydrocarbons, but only slightly soluble in aliphatic hydrocarbons. The heptane number is an index indicating how much heptane can be added to a solvent/resin solution. The wax number is an indicator of how much solvent can be added to a benzene/beeswax solution. Each of these methods, however, deals only with a specific phenomenon and a theory for comprehensively evaluating the phenomenon is not discussed.

This study focused on the Hansen solubility parameters (HSPs) as one of the cohesive energy density, which is used as an index to comprehensively evaluate the surface properties of substances, affinity between substances, and their interactions. The HSPs is described in Section 1.1.3; however, the Hildebrand solubility parameter, on which the HSPs is based, is first described in detail.

1.1.2　Hildebrand Solubility parameters

The Hildebrand solubility parameter as cohesive energy density is defined by the regular solution theory that was introduced by Hildebrand and is a measure of the extent of solubility of a binary solution.[1-1] The energy required for mixing two types of liquids is the difference between the cohesive energy when component 1 and component 2 are each present as a pure substance and that when the components are mixed. This energy difference is given by Equation 1-1:

$$\Delta E_M = \frac{n_1 V_1 \cdot n_2 V_2}{n_1 V_1 + n_2 V_2} \left\{ \left(\frac{\Delta E_1^V}{V_1} \right)^{1/2} - \left(\frac{\Delta E_2^V}{V_2} \right)^{1/2} \right\}^2 \tag{1-1}$$

where ΔE_M [J·mol] is the energy required for mixing, n is the number of moles of the respective component, V_i [cm^3/mol] is the molar volume of component i, and ΔE^V is the evaporation energy of the component. Subscripts 1 and 2 indicate components 1 and 2, respectively. Hildebrand defined $\Delta E^V/V$ in Equation 1-1, the energy required for mixing, as the solubility parameter δ [(MPa)$^{1/2}$], given by Equation 1-2:

$$\delta = \left(\frac{\Delta E^V}{V} \right)^{1/2} \tag{1-2}$$

where ΔE [J/mol] is the cohesive energy. The solubility parameter is the cohesive energy density and represents the energy required for mixing per unit volume; therefore, it can be used as an index to indicate the intermolecular force between the components. Substituting the solubility parameter δ in Equation 1-2 into Equation 1-1 yields Equation 1-3:

$$\Delta E_M = \frac{n_1 V_1 \cdot n_2 V_2}{n_1 V_1 + n_2 V_2} (\delta_1 - \delta_2)^2 \tag{1-3}$$

2

Therefore, when the difference between the solubility parameters of components 1 and 2 is small, the components are easily dissolved because the energy required for their mixing is small.

1.1.3   Hansen solubility parameters

The Hildebrand parameter as cohesive energy density, discussed in Section 1.1.2, became widely known and exhibited excellent results. However, the Hildebrand parameter was limited because it was determined solely based on the evaporation energy of the components; in other words, it was based on the assumption that components with similar evaporation energies had high mutual solubility, rather than components with similar chemical structures. The Hildebrand parameters are good for regular solutions, but not for polar solvents that involve electrostatic interactions, associations, and dipole interactions. Various methods for adding or modifying terms to the Hildebrand solubility parameter were studied.[1-2] Of these, Hansen categorized the solubility parameters into three types of interactions: the London dispersion force δ_d, the dipole force δ_p, and the hydrogen-bonding force δ_h.[1-3] The cohesive energy ΔE is given by the sum of the energies resulting from these three forces, as defined by Equations 1-4 and 1-5:

$$\Delta E = \Delta E_d + \Delta E_p + \Delta E_h$$

;   (1-4)

$$\delta_d = \frac{\Delta E_d}{V}, \quad \delta_p = \frac{\Delta E_p}{V}, \quad \delta_h = \frac{\Delta E_h}{V}$$

,   (1-5)

where the subscripts d, p, and h represent the dispersion, dipole, and hydrogen-bonding force terms, respectively. The HSPs and Hildebrand solubility parameter have the relationship shown in Equation 1-6:

$$\delta^2 = \delta_d^2 + \delta_p^2 + \delta_h^2$$

.   (1-6)

3

To date, HSPs have been reported for more than 1200 organic compounds, including liquids, gases, and solids, and for more than 500 polymers.[1-4] The HSPs database is extended through, for example, updating the current version of the calculation software Hansen Solubility Parameter in Practice (HSPiP). The values in this database are determined from those obtained from physical properties, such as latent heat of vaporization, the force between dipoles, and the molecular structure: there is no absolute value; however, adjustment is made so that there is no inconsistency between the actual phenomena for thousands of solvents. The solubility, as given by the HSPs, can be quantitatively evaluated by R_a [(MPa)$^{1/2}$], shown in Equation 1-7:

$$R_a = \left\{ 4(\delta_{d1} - \delta_{d2})^2 + \left(\delta_{p1} - \delta_{p2}\right)^2 + (\delta_{h1} - \delta_{h1})^2 \right\}^{1/2}$$
.   (1-7)

The coefficient 4 applied to the δ_d term was introduced to correct the influence of the dispersion force on the dipole and hydrogen-bonding forces. Introducing this coefficient has the following merit: when the solubility is expressed in a three-dimensional space having δ_d, δ_p, and δ_h as the three Cartesian axes, the area in which the solvent that dissolves a certain substance changes shape from an ellipse to a sphere, which facilitates data handling. Later, Yamamoto's work showed that the coefficient 4 originated from a value in which δ_d included van der Waals and dispersive forces.[1-5] The further subdivision of δ_d may be used to get a more detailed understanding; however, evaluation in a three-dimensional space in which δ_d is not divided is visually easy to understand, and will be continued in the future. The HSPs have been shown to provide strong predictive performance in fields such as industrial products, pharmaceuticals, and foods, and it is expected that examples of other applications will be further expanded in the future.[1-3]

1.2   Calculation of solubility parameter

1.2.1   Calculation using physical property values

The solubility parameter is used as a measure of intermolecular forces and therefore correlates with various physical properties. Hildebrand's solubility parameter was derived from regular solution theory, in which the force acting between a solvent and solute is treated only as an intermolecular force; therefore, the solubility parameter is expressed as in Equation 1-8 from the relationship between the cohesive energy of the liquid and the enthalpy of evaporation:

$$\delta = \sqrt{\frac{\Delta H - RT}{V}}$$

,   (1-8)

where ΔH [J] is the evaporation enthalpy, R [J/K·mol] is the gas constant, T [K] is temperature, and V [cm^3/mol] is the molar volume for the solute. Given the enthalpy of evaporation and molar volume data for a substance, the Hildebrand solubility parameter for that substance can be calculated.

In addition, there is a relationship between surface tension and the change in evaporation enthalpy, as represented by Equation 1-9:

$$\gamma = \frac{K(\Delta H^V - RT)}{V^{2/3}}$$

,   (1-9)

where γ [mN/m] is the surface tension, K is a constant, and ΔH^V [J] is the enthalpy of evaporation. Equation 1-10 is derived from Equations 1-8 and 1-9:

$$\delta = K'\left(\frac{\gamma}{V^{1/3}}\right)^{1/2}$$

,   (1-10)

where K' [–] is a constant. Becher determined constants for liquids other than those containing OH and COOH functional groups, and proposed Equation 1-11:[1-6]

$$\delta = 7.653\left(\frac{\gamma}{V^{1/3}}\right)^{1/2}$$

(1-11)

Given the surface tension and molar volume data for a substance, the Hildebrand solubility parameter for that substance can be calculated using Equation 1-11. Equation 1-12 was proposed for substances containing OH and COOH groups:[1-7]

$$\delta = 12.13\left(\frac{\gamma}{V^{0.45}}\right)^{1/2}$$

(1-12)

The constant in this formula and the multiplier of the molar volume were determined using data for fifty compounds that contained OH and COOH groups.

Calculation using physical property values for the dispersion force term δ_d of the HSPs was proposed by Blank and Prausnitz.[1-2] Blank et al. found that, for hydrocarbons, cycloalkanes, and aromatic hydrocarbons, there was a relationship between molar volume, evaporation, and cohesive energy densities. Furthermore, δ_d was determined by calculating the evaporation energy and cohesive energy density from the molar volume using the critical temperature T_r. Hansen described the relationship between refractive index and δ_d as shown in Equation 1-13:[1-3]

$$\delta_d = \frac{n_D - 0.784}{0.0395}$$

(1-13)

where n_D is the refractive index. The coefficients in Equation 1-13 were determined using data for 540 compounds.[1-3] Solubility parameters for polarization were reported by Blanks and Prausnitz.[1-2] They reported a single parameter, a combination of the dipole force δ_p and hydrogen-bonding force δ_h terms, expressed as the HSPs, as the polar term. For the

6

calculation of δ_p using physical properties, Hansen and Skaarup reported using Böttcher's equation:[1-8]

$$\delta_p^2 = \frac{12108}{V^2} \frac{\varepsilon - 1}{2\varepsilon - n_D^2} (n_D^2 + 2)\mu^2$$

, (1-14)

where δ_p [cal/cm^3] is the dipole force term of the HSPs, ε [F/m] is the dielectric constant, and μ [D] is the dipole moment. Equation 1-14 requires data for many physical properties, so Equation 1-15, as simplified by Hansen and Beerbower, is generally used:[1-9]

$$\delta_p = \frac{37.4\mu}{V^{1/2}}$$

. (1-15)

The hydrogen-bond term δ_h of the HSPs has not been reported for calculation from physical properties. This value may be obtained by calculating the total evaporation energy of a substance and subtracting the dispersion and dipole energies.[1-3]

1.2.2   Group contribution method

In addition to experimentally measuring physical properties to determine the HSPs, the theoretically calculated group-contribution method was proposed. The group-contribution method is based on a group solution model that estimates physical properties based on the chemical structure of the components that make up the solution using the thermodynamic method proposed by Wilson and Deal.[1-10] The method assumes that physical property values depend on the number and type of functional groups, such as methyl, hydroxyl, amino, and benzene-ring groups, so the structure of the target substance is divided into functional groups and parameters are assigned to each group. This method calculates a physical property value by using typical values for a specific group. Various methods for predicting physical properties, such as density, viscosity, surface tension, critical value,

and vapor–liquid equilibria, of organic compounds have been proposed[1-11,1-12,1-13,1-14,1-15] and various proposals made for HSPs estimation using this method. The van Krevelen and Hoftyzer method, used in the estimation described in Chapter 3, is explained below.

van Krevelen and Hoftyzer proposed a group-contribution method for estimating the HSPs, assuming that the aggregation energies ΔE_{dv}, ΔE_{pv} and ΔE_{hv} depend on the type and number of substituents.[1-16] The Krevelen and Hoftyzer method has been proposed to calculate HSPs for organic compounds, including polymers. Equation 1-16 is used to estimate δ_d:

$$\delta_d = \frac{\sum F_{di}}{V}$$

$$,\qquad(1\text{-}16)$$

where F_{di} [(MJ/m^3)$^{1/2}$/mol] is a molar attraction constant caused by the dispersion force. The energy of the variant component is calculated by simple addition of the group parameters. Equation 1-17 is used to estimate δ_p:

$$\delta_p = \frac{\sqrt{\sum F_{pi}^2}}{V}$$

$$,\qquad(1\text{-}17)$$

where F_{pi} [(MJ/m^3)$^{1/2}$/mol] is a molar attraction constant caused by the dipole force. Owing to the interaction between polar groups, addition of the dipole force is not a simple addition: when the same polar group is present at a symmetric position (for example, as in hydroquinone), δ_p is corrected as shown in Table 1-1. Equation 1-18 is used to estimate δ_h:

$$\delta_h = \sqrt{\frac{\sum E_{hi}}{V}}$$

$$,\qquad(1\text{-}18)$$

where E_{hi} [J/mol] is the hydrogen-bonding energy. Hansen reported that the hydrogen-bond energy per structural group is almost constant, so the sum of the hydrogen-bond energies is expressed in the form of Equation 1-18.

Table 1-1 Group parameters of van Krevelen and Hoftyzer for estimation of HSPs

Structural group	F_{di} [(MJ/m³)$^{1/2}$/mol]	F_{pi} [(MJ/m³)$^{1/2}$/mol]	E_{hi} [J/mol]
-CH$_3$	420	0	0
-CH$_2$-	270	0	0
>CH-	80	0	0
>C<	-70	0	0
=CH$_2$	400	0	0
=CH-	200	0	0
=C<	70	0	0
—⟨cyclohexane ring⟩	1620	0	0
—⟨benzene ring⟩	1430	110	0
—⟨benzene ring⟩= (o, m, p)	1270	110	0
-F	(220)	-	-
-Cl	450	550	400
-Br	(550)	-	-
-CN	430	1100	2500
-OH	210	500	20,000
-O-	100	400	3000
-COH-	470	800	4500
-CO-	290	770	2000
-COOH	530	420	10,000
-COO-	390	490	7000
HCOO-	530	-	-
-NH$_2$	280	-	8400
-NH-	160	210	3100
>N-	20	800	5000
-NO$_2$	500	1070	1500
-S-	440	-	-
=PO$_4$	740	1890	13,000
Ring	190	-	-
One plane of symmetry	-	0.50×	-
Two planes of symmetry	-	0.25×	-
More planes of symmetry	-	0×	0×

10

1.3 Measurement of solubility parameter meter

1.3.1 Hansen solubility sphere method

Methods of estimating the HSPs using physical property values and the group-contribution method are described in Section 1.2. There is also a method of experimentally measuring the solubility parameter for a particle surface or of a substance for which the chemical structure is not known: this is the Hansen solubility sphere method. By measuring the solubility and dispersibility of the substance to be measured in a solvent, a Hansen solubility sphere can be created and the HSPs calculated. Evaluation of the solubility can be visualized by expressing it in a three-dimensional graph with coordinates of δ_d, δ_p, and δ_h. When the solubility parameters of good and poor solvents for a target substance are plotted in such a three-dimensional diagram, the good solvents gather in similar places. This collection of solvents forms a spherical region that is called Hansen's solubility sphere. The solubility sphere is such that a good solvent for the target substance falls inside the sphere and poor solvents fall outside the sphere. The center of the sphere is defined as the solubility parameter of the target substance;[1-17, 1-18, 1-19] the radius of the sphere is called the interaction radius R_O [(MPa)$^{1/2}$].

The concept of the Hansen solubility sphere is based on the theory that the smaller the difference between their solubility parameters, the more soluble are two substances. Figure 1-1 shows an example of a Hansen sphere created using this method. The RED (relative energy difference) [−] is expressed by the ratio of R_O and R_a [(MPa)$^{1/2}$], as calculated by Equation 1-15:

$$\mathrm{RED} = \frac{R_a}{R_0}. \tag{1-19}$$

If RED ≤ 1, a solvent is considered good; if RED > 1, the solvent is poor. The sphere can therefore be used as an index of solubility.

The Hansen solubility sphere is an experimental method of calculating HSPs because it is necessary to determine whether a particular compound is a good or poor solvent for the target substance. This solubility evaluation is based on measurement of solubility,[1-17] average particle diameter of particles,[1-18] and aggregation point.[1-20]
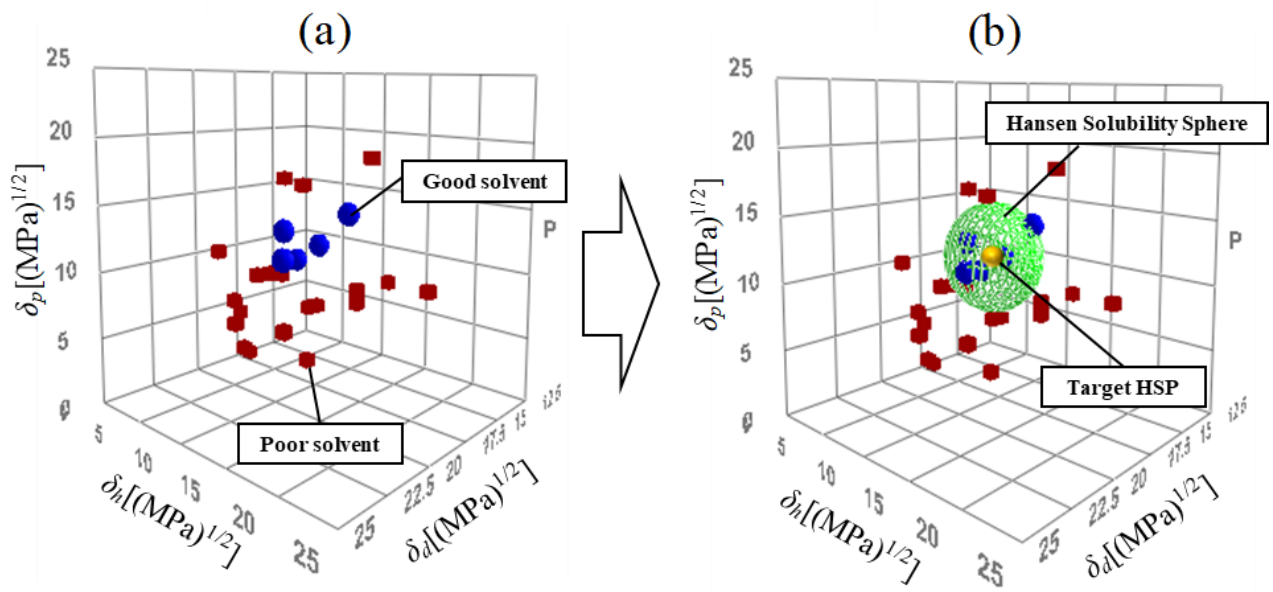
Figure 1-1 Example of use of Hansen solubility sphere method to identify good and poor solvents for a target substance

1.3.2   Solid measurement methods

Here, the solubility of a solid using the Hansen solubility sphere method is described in detail. For example, when it is desired to specify HSPs of a solid such as a resin, the affinity between the target substance and a pure solvent, for which the HSPs is known, is experimentally evaluated. In the case of a resin, the affinity is confirmed by whether or not the resin dissolves or swells in the solvent. First, various organic solvents with known HSPs are added to a predetermined amount of the sample. The ratio between the sample and solvent amounts is determined by conducting a preliminary experiment to ensure that a difference in the dissolution behavior between the organic solvents appears. The sample and solvent are then allowed to stand for a predetermined time, usually 24 h; however, when the dissolution behavior is fast and there is no difference in affinity between the solvents, the standing time is shortened (and the opposite is also true). After standing, the affinity is determined. Figure 1-2 shows an example of affinity evaluation. A solvent in which the sample dissolves is determined to be good; one in which the sample is insoluble is determined to be poor. HSPs are then calculated using the Hansen solubility sphere method based on the affinity evaluation.
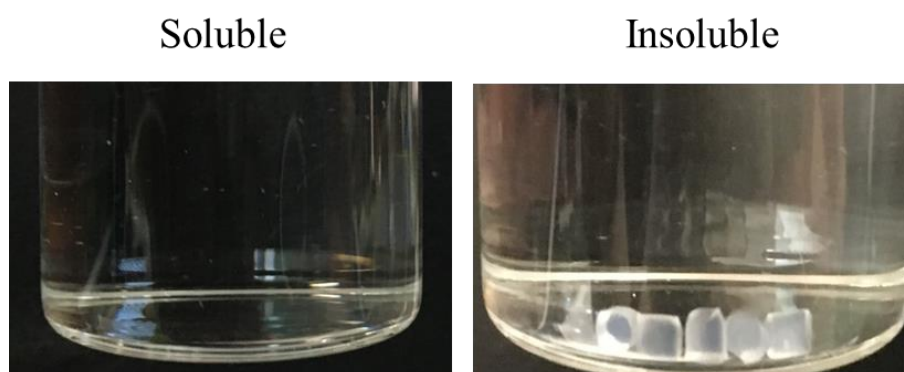
Figure 1-2 Example of affinity evaluation for solubility tes

1.3.3　Measurement of fine particle surface

In the measurement of the HSPs of a surface of fine particles, a sedimentation or dynamic light-scattering (DLS) method is used. Here, the DLS method is described. In the DLS method, Brownian motion of fine particles in a liquid phase is measured as a function of frequency change and the particle size distribution is determined from diffusion coefficients to evaluate affinity. The particle diameter is calculated from the Stokes–Einstein equation (Equation 1-19):

$$d = \frac{kT}{3\pi\eta D},$$
(1-19)

where d is the Stokes diameter [m], k is the Boltzmann constant [J/K], η is the viscosity of the solvent [Pa·s], and D is the diffusion coefficient [m^2/s]. A good solvent has highly dispersed particles, so its useful diameter is close to that of the primary particles; the useful diameter of a poor solvent is larger than that of the primary particles. Figure 1-3 shows a photograph of the dispersion state. If the affinity between the solvent and particles is low, the particles aggregate and precipitate; when the affinity is high, the particles are dispersed and spread throughout the solvent.

DLS is suitable for measuring the diameter of spherical particles of approximately 10 nm to 1 μm dispersed in a solvent. It is widely used for measuring nanospherical particles in a liquid phase because the measurement time is short, the only physical properties required are the solvent viscosity and refractive index, and there are no influencing factors due to the sample.[1-21]

Figure 1-3 Example of dispersion-stability evaluation experiment

1.4 Application of Hansen solubility parameters

The HSPs as one of the cohesive energy density have been applied in various fields by many researchers in recent years. Here, I introduce some recent research content. The number of proposals for new measurement methods, such as those proposed in Chapter 2, and reports of research on improving the accuracy of HSPs measurement are increasing.

Lim et al. measured HSPs of multi-walled carbon nanotubes by reverse gas chromatography and compared the values with those reported by sedimentation and molecular dynamics simulations.[1-22] Vebber et al. applied a genetic algorithm to determine the Hansen sphere and tested it using polyethersulfone, bitumen, and lignin. According to the genetic algorithm, fitting of the Hansen sphere improved.[1-23] Weng et al. applied a hybridization algorithm to the determination of the Hansen sphere: verification with polyethersulfone, bitumen, and lignin showed that use of this method improved its accuracy.[1-24] Louwerse and colleagues modified the HSPs from a thermodynamic point of

view to improve accuracy. Improvements were made to fitting and predictability in four areas: solvent molecule size, solid crystal-structure destruction, specificity of hydrogen-bond interactions, and solubility prediction at the estimated temperature.[1-25] Andecochea Saiz et al. applied HSP technology to the field of organic solvent nanofiltration and predicted the behavior of solvents and solutes. The affinity was evaluated by the flow rate of the solvent passing through a ceramic membrane and the HSPs of the membrane was calculated.[1-26]

Reports on the dispersion of fine particles, the subject of this research, are also increasing. For example, Ma et al. applied HSP technology to predict the dispersion and interfacial properties of octadecylamine-functionalized single-walled carbon nanotubes in a polyvinylidene difluoride polymer matrix.[1-27] Gårdebjer et al. used the HSP technique to disperse cellulose nanocrystals in a hydrophobic polymer to achieve good dispersion.[1-28] Huth et al. applied HSP technology to investigate the effect of different surface energies on lipophilic fluoromica exfoliation. The Flory–Huggins parameter was calculated from the HSP of lipophilic fluoromica and chloroform: when the parameter was high, the fluoromica dispersion was aggregated; when it was close to zero, it was considered to be dispersed.[1-29] Besides chloroform, which is known as a solvent for lipophilic fluoromica, proposed candidate solvents such as trichloroethylene and benzyl ethyl ether[1-30] were identified. Süß et al. measured the Hansen dispersibility parameter (HDP) of micro- and nanoparticle surface properties using analytical centrifugation, where the term HDP is defined as expressing the dispersion of particles with respect to HSP, expressing the dissolution of resin or the like.[1-31]

The use of HSPs in the medical and pharmaceutical fields is also increasing. Carberry et al. applied HSP technology to optimize surface treatment to improve the insertion of urinary catheters into the body.[1-32] Paseta et al. used HSP to optimize the encapsulation of caffeine in a metallo-organic structure to control the release of medicinal caffeine into the

16

body.[1-33] Hossin et al. applied HSPs to assess the penetration of drugs into nails for the treatment of onychomycosis (a fungal infection of the nail).[1-34] Devalapalli et al. used HSP technology to select mobile and stationary phases in high-performance liquid chromatography analysis of blood plasma components.[1-35] Obradović et al. determined the HSPs of the antipsychotic drug ziprasidone using partial least-squares regression, artificial neural networks, regression trees, and boost trees.[1-36]

Research on alternative solvents to those traditionally used is also continuing. For example, Nakamura et al. selected a non-toxic solvent from determination of the HSPs of cell components, based on the assumption that solvents that do not dissolve in cell components are non-toxic [1-37]. Liu et al. applied HSP technology to search for alternative solvents to replace chlorobenzene-type solvents for solution processing of polymer solar cells; terpinolene, a natural and safe substance that is used in food and cosmetic additives, was selected.[1-38]

Studies of HSP are also increasing in other fields, such as food and engineering. For example, Bonnet et al. determined the gelling spheres of a low-molecular-mass gelling agent by a solubility test and argued that if HSP of an untested liquid enters the gelling sphere, the liquid may gel with small-molecule gelling agents.[1-39] These authors also examined the quantitative effect of structural changes in the gelling agent on gel-forming ability. As the length of the alkyl group in the gelling agent increased, its polarity decreased and the solubility sphere gradually moved to lower δ_p and δ_h values.[1-40] Diehn et al. argued that applying HSP technology to the gelation of organic liquids would allow inference of the state of gelation. Dissolving spheres, slow-gelling spheres, fast-gelling spheres, and insoluble spheres can be drawn on concentric circles of Hansen spheres, which is useful for predicting the gelation state.[1-41] Fardi et al. applied HSP to the selection of solvents used to preserve handicrafts.[1-42] Aghanouri and colleagues applied HSP to soy protein, a potential alternative to petroleum-based rigid polymers, and confirmed that the HSP can

17

predict the solubility behavior of organic solvent systems for soy protein if the candidate solvent meets the basic principles of structural similarity with biopolymers.[1-43] Liu et al. predicted the gelation performance of low-molecular-mass organogelators by using HSPs. Various ratios of ternary solvent mixtures consisting of octane, 1-octanol, and 1-octylamine were mixed with low-molecular-mass organogelators, and their gel-forming ability was considered.[1-44] Tang et al. studied the HSPs of polyglycolic acid, a biodegradable thermoplastic used in medical applications, such as drug-release control systems, orthopedic fasteners, and scaffolds. The values of δ_d, δ_p, and δ_h were 17.094, 8.206, and 7.912, respectively [1-45]. De La Peña-Gil et al. examined a simple method for calculating HSPs in edible fats and oils. Although the calculation was difficult using the general group-contribution method, δ_d, δ_p, and δ_h were estimated by simplifying the calculation by assuming that vegetable oil was composed of simple neutral fats in the same proportion as fatty acids.[1-46] Seo et al. applied HSPs to a method that uses the dissolution of a supercritical fluid in solution to make the solvent poorer and thereby precipitate solutes.[1-47] Tamizifar et al. analyzed the affinity of initiators, monomers, and solvents for polyethylene terephthalate using HSP to control surface radical-graft polymerization on its surfaces. [1-48] Agata et al. determined the HSP of an ionic liquid consisting of a combination of cations and anions by applying the double-sphere method.[1-49] Fujiwara et al. applied HSP technology to evaluate the adsorptivity of organic solvents to surface-modified hydrophobic silica adsorbents. The HSP distance between the adsorbent and organic solvent and the amount of adsorption have a high correlation, so the adsorbability can be evaluated using HSPs.[1-50]

As described above, HSPs are a powerful tool for evaluating the affinity between substances and have a wide range of applications. It is expected that research will be expanded not only in applications of organic solvents and polymers, but also in fine particle dispersion and medical fields.

1.5   References

[1-1] Hildebrand, J. H.; Scott, R. L. The Solubility of Nonelectrolytes, 3rd ed.,Dover PublicationsInc.: 1950.

[1-2]Blanks, R. F.;Prausnitz, J. M. Ind. and Eng. Chem. Fundamen.1964, 3, 1-8.

[1-3] Hansen, C. M. The Three Dimensional Solubility Parameter and Solvent Diffusion Coefficient and Their Importance in Surface Coating Formulation. (1967).

[1-4] Hansen, C. M. Hansen Solubility Parameters: A User's Handbook,CRC Press: Boca Raton, FL, 1999; ISBN: 0-8493-1525-5.

[1-5] H. Team, H. Yamamoto, S. Abbott, C.M. Hansen, Consideration of Hansen Solubility Parameters . Part 1 Dividing the dispersion term (δ_D) and new HSP distance, 13 (2017) 1–13.

[1-6] P. Becher, The calculation of cohesive energy density from the surface tension of liquids, J. Colloid Interface Sci. 38 (1972) 291–293.

[1-7] T.J. Sheldon, C.S. Adjiman, J.L. Cordiner, Pure component properties from group contribution: Hydrogen-bond basicity, hydrogen-bond acidity, Hildebrand solubility parameter, macroscopic surface tension, dipole moment, refractive index and dielectric constant, Fluid Phase Equilib. 231 (2005) 27–37.

[1-8] Hansen, C. M.; Skaarup, K. J. paint technol.1967, 39, 511-514.

[1-9] Hansen, C.; Beerbower, A. Solubility parameters. In Kirk-OthmerEncyclopedia of Chemical Technology, 1971.

[1-10] Wilson, G. M.; Deal, C. H. Ind. Eng. Chem. Fundamen.1962, 1, 20–23.

[1-11] Elbro, H. S.; Fredenslund A.; Rasmussen, P. Ind. Eng. Chem. Res.1991, 30, 2576-2582.

[1-12] C. Yang, H. Lai, Z. Liu, P. Ma, Density and viscosity of binary mixtures of diethyl carbonate with alcohols at (293.15 to 363.15) K and predictive results by UNIFAC-VISCO group contribution method, J. Chem. Eng. Data. 51 (2006) 1345–1351.

[1-13] H. Laux, I. Rahimian, T. Butz, E. Darwish, T.A. Al-Sahhaf, M.A. Fahim, R.C. Little, Prediction of the surface tension of petroleum cuts using a modified UNIFAC group contribution method, J. Colloid Interface Sci. 67 (1995) 229–239.

[1-14] X. Yan, Q. Dong, X. Hong, Reliability analysis of group-contribution methods in predicting critical temperatures of organic compounds, J. Chem. Eng. Data. 48 (2003)

[1-15] K. Tochigi, K. Yoshida, K. Kurihara, K. Ochi, J. Murata, M. Yasumoto, T. Sako, Prediction of vapor-liquid equilibrium for systems containing hydrofluoroethers using ASOG group contribution method, Fluid Phase Equilib. 183–184 (2001) 173–182.

[1-16] van Krevelen, D. W.; Hoftyzer, P. J. Properties of Polymers2nd Edition, 1976.

[1-17] C.M. Hansen, A.L. Smith, Using Hansen solubility parameters to correlate solubility of C 60 fullerene in organic solvents and in polymers, Carbon N. Y. 42 (2004) 1591–1597.

[1-18] J.U. Wieneke, B. Kommob, O. Gaer, I. Prykhodko, M. Ulbricht, Systematic investigation of dispersions of unmodified inorganic nanoparticles in organic solvents with focus on the hansen solubility parameters, Ind. Eng. Chem. Res. 51 (2012) 327–334.

[1-19] S. Acevedo, A. Castro, E. Vásquez, F. Marcano, M.A. Ranaudo, Investigation of physical chemistry properties of asphaltenes using solubility parameters of asphaltenes and their fractions A1 and A2, Energy and Fuels. 24 (2010) 5921–5933.

[1-20] H. Laux, I. Rahimian, T. Butz, Theoretical and practical approach to the selection of asphaltene dispersing agents, Fuel Process. Technol. 67 (2000) 79–89.

[1-21] A. K. Jack, R. Isabelle, H. Frédéric, Biochemistry, 44 (2005) 13122-13131

[1-22] H.J. Lim, K. Lee, Y.S. Cho, Y.S. Kim, T. Kim, C.R. Park, Experimental consideration of the Hansen solubility parameters of as-produced multi-walled carbon nanotubes by inverse gas chromatography, Phys. Chem. Chem. Phys. 16 (2014) 17466–17472.

[1-23] G.C. Vebber, P. Pranke, C.N. Pereira, Calculating hansen solubility parameters of polymers with genetic algorithms, J. Appl. Polym. Sci. 131 (2014).

[1-24] M. Weng, Determination of the Hansen solubility parameters with a novel optimization method, J. Appl. Polym. Sci. 133 (2016).

[1-25] M.J. Louwerse, A. Maldonado, S. Rousseau, C. Moreau-Masselon, B. Roux, G. Rothenberg, Revisiting Hansen Solubility Parameters by Including Thermodynamics, ChemPhysChem. 18 (2017) 2999–3006.

[1-26] C. Andecochea Saiz, S. Darvishmanesh, A. Buekenhoudt, B. Van der Bruggen, Shortcut applications of the Hansen Solubility Parameter for Organic Solvent Nanofiltration, J. Memb. Sci. 546 (2018) 120–127.

[1-27] J. Ma, R.M. Larsen, Use of Hansen solubility parameters to predict dispersion and strain transfer of functionalized single-walled carbon nanotubes in poly(vinylidene fluoride) composites, J. Thermoplast. Compos. Mater. 27 (2014) 801–815.

[1-28] S. Gårdebjer, M. Andersson, J. Engström, P. Restorp, M. Persson, A. Larsson, Using Hansen solubility parameters to predict the dispersion of nano-particles in polymeric films, Polym. Chem. 7 (2016) 1756–1764.

[1-29] M. Huth, C.W. Chen, V. Wagner, Measurement of Hansen solubility parameters for organophilic fluoromica and evaluation of potential solvents for exfoliation, Appl. Clay Sci. 155 (2018) 120–125.

[1-30] M. Huth, C.W. Chen, J. Köhling, V. Wagner, Influence of Hansen solubility parameters on exfoliation of organophilic fluoromica, Appl. Clay Sci. 161 (2018) 412–418.

[1-31] S. Süß, T. Sobisch, W. Peukert, D. Lerche, D. Segets, Determination of Hansen parameters for particles: A standardized routine based on analytical centrifugation, Adv. Powder Technol. 29 (2018) 1550–1561.

[1-32] B.J. Carberry, J. Farrell, J.E. Kennedy, Evaluation and characterisation of urinary catheter coating utilising Hansen solubility parameters and FEA analysis, Surf. Coatings Technol. 276 (2015) 456–463.

[1-33] L. Paseta, G. Potier, S. Abbott, J. Coronas, Using Hansen solubility parameters to study the encapsulation of caffeine in MOFs, Org. Biomol. Chem. 13 (2015) 1724–1731.

[1-34] B. Hossin, K. Rizi, S. Murdan, Application of Hansen Solubility Parameters to predict drug-nail interactions, which can assist the design of nail medicines, Eur. J. Pharm. Biopharm. 102 (2016) 32–40.

[1-35] M.M.R. Devalapalli, H.S. Cheruvu, T. Yertha, V.B. Veeravalli, S. Sampathi, S. Shivakumar, Hansen solubility parameters for assay method optimization of simvastatin, ramipril, atenolol, hydrochlorothiazide and aspirin in human plasma using liquid chromatography with tandem mass spectrometry, J. Sep. Sci. 40 (2017) 3662–3674.

[1-36] D. Obradović, F. Andrić, M. Zlatović, D. Agbaba, Modeling of Hansen's solubility parameters of aripiprazole, ziprasidone, and their impurities: A nonparametric comparison of models for prediction of drug absorption sites, J. Chemom. 32 (2018) 1–12.

[1-37] D. Nakamura, M. Hirano, R. Ohta, Nontoxic organic solvents identified using an: a priori approach with Hansen solubility parameters, Chem. Commun. 53 (2017) 4096–4099.

[1-38] C. Liu, Y. Zhu, J. Chen, H. Wang, Y. Cao, J. Chen, Terpinolene processed PTB7:PC71BM blend film for polymer solar cells: a non-aromatic and non-chlorinated solvent predicted by Hansen solubility parameters, Synth. Met. 242 (2018) 17–22.

[1-39] J. Bonnet, G. Suissa, M. Raynal, L. Bouteiller, Organogel formation rationalized by Hansen solubility parameters: Dos and don'ts, Soft Matter. 10 (2014) 3154–3160.

[1-40] J. Bonnet, G. Suissa, M. Raynal, L. Bouteiller, Organogel formation rationalized by Hansen solubility parameters: Influence of gelator structure, Soft Matter. 11 (2015) 2308–2312.

[1-41] K.K. Diehn, H. Oh, R. Hashemipour, R.G. Weiss, S.R. Raghavan, Insights into organogelation and its kinetics from Hansen solubility parameters. Toward a priori predictions of molecular gelation, Soft Matter. 10 (2014) 2632–2640.

[1-42] T. Fardi, E. Stefanis, C. Panayiotou, S. Abbott, S. van Loon, Artwork conservation materials and Hansen solubility parameters: A novel methodology towards critical solvent selection, J. Cult. Herit. 15 (2014) 583–594.

[1-43] A. Aghanouri, G. Sun, Hansen solubility parameters as a useful tool in searching for solvents for soy proteins, RSC Adv. 5 (2015) 1890–1892.

[1-44] C. Liu, M. Corradini, M.A. Rogers, Self-assembly of 12-hydroxystearic acid molecular gels in mixed solvent systems rationalized using Hansen solubility parameters, Colloid Polym. Sci. 293 (2015) 975–983.

[1-45] S. Tang, R. Zhang, F. Liu, X. Liu, Hansen solubility parameters of polyglycolic acid and interaction parameters between polyglycolic acid and solvents, Eur. Polym. J. 72 (2015) 83–88.

[1-46] A. De La Peña-Gil, J.F. Toro-Vazquez, M.A. Rogers, Simplifying Hansen Solubility Parameters for Complex Edible Fats and Oils, Food Biophys. 11 (2016) 283–291.

[1-47] M.D. Jones, G. Buckton, Comparison of the cohesion-adhesion balance approach to colloidal probe atomic force microscopy and the measurement of Hansen partial solubility parameters by inverse gas chromatography for the prediction of dry powder inhalation performance, Int. J. Pharm. 509 (2016) 419–430.

[1-48] B. Seo, T. Kim, H.J. Park, J.Y. Kim, K.D. Lee, J.M. Lee, Y.W. Lee, Extension of the Hansen solubility parameter concept to the micronization of cyclotrimethylenetrinitramine crystals by supercritical anti-solvent process, J. Supercrit. Fluids. 111 (2016) 112–120.

[1-49] M. Tamizifar, G. Sun, Control of surface radical graft polymerization on polyester fibers by using Hansen solubility parameters as a measurement of the affinity of chemicals to materials, RSC Adv. 7 (2017) 13299–13303.

[1-50] Y. Agata, H. Yamamoto, Determination of Hansen solubility parameters of ionic liquids using double-sphere type of Hansen solubility sphere method, Chem. Phys. 513 (2018) 165–173.

[1-51] N. Fujiwara, H. Yamamoto, Evaluation of adsorption of organic solvents to modified hydrophobic silica adsorbents based on Hansen solubility parameter, Sep. Purif. Technol. 210 (2019) 907–912.

Chapter 2 Determination of HSPs by capillary penetration method

2.1   Introduction

Functional particles are widely used in composite materials applied in industrial fields. To enable effective use of such functional particles, their compatibility with other materials needs to be improved. Therefore, a good understanding of the physical properties of the particle surface is important. Hansen solubility parameters have attracted attention in the fields of carbon materials and petroleum and gas as a universal method to evaluate the affinity between materials [2-1,2-2,2-3,2-4,2-5]. The solubility parameter δ_t (MPa)$^{1/2}$ is used to describe the affinity between substances and it has three components: a dispersion force term δ_d, a dipole interaction term δ_p, and a hydrogen-bonding force term δ_h [2-6,2-7]. Recently, HSP has also been used as a method for evaluating the affinity of the material surface, and HSP on the surface of titanium dioxide and zirconia particles has been reported [2-8, 2-9].

Sedimentation velocity measurements and dynamic light scattering (DLS) are currently used to determine the HSPs of particles [2-10]. When the affinity between the particles and solvent is high, the particles are well dispersed and the sedimentation rate is low. Conversely, when the affinity between the particles and solvent is low, the particles aggregate and the sedimentation rate becomes high, enabling the affinity between the particles and solvent to be evaluated from this difference. DLS measures the diameter of particles dispersed in various solvents. When the affinity between particles and the solvent is high, the particles are well dispersed and the particle diameter is close to that of the primary particles. Conversely, when the affinity between the particles and solvent is low, particles aggregate, which leads to larger particle diameters. The solvent–particle affinity is evaluated from these differences. However, in the sedimentation method, non-spherical particles feature a wide range of sedimentation rates and in the case of highly dense particles, it becomes difficult to determine their differences if the sedimentation rate is too high. Furthermore, highly dense particles can precipitate immediately in DLS

measurements, and measurable particles are limited to sizes of less than approximately 1 μm because of the measurement principle of DLS. However, relatively large particles of micrometer size and highly dense particles are frequently used in industry. Therefore, it is challenging to determine the HSPs of technologically relevant particles using existing methods.

In the present study, to measure HSPs regardless of particle density, configuration, and size, particles are not dispersed in a solvent, as is typical for the sedimentation velocity and DLS methods; instead, the particles are fixed on a surface. The sessile drop and Wilhelmy plate methods can be used to measure the contact angles of particles; however, here I use the capillary penetration method because of its simplicity and reproducibility [2-11, 2-12, 2-13, 2-14, 2-15, 2-16, 2-17]. I measure the HSPs of spherical silica particles with a diameter of 1 μm by the capillary penetration method. The capillary penetration method is also used to determine the HSPs of non-spherical silica particles with a diameter of <63 μm, which are representative of particles that are difficult to assess by the sedimentation rate method or DLS.

2.2   Experimental

2.2.1   Materials

To confirm the effectiveness of HSP measurement by the capillary penetration method, I measured the HSPs of spherical silica particles (Haipureshika FR and N2N; Ube-exsymo Ltd. Tokyo, Japan) with a mean spherical particle size of 1 μm, which could also be measured by DLS to validate my approach. The mean particle size of the 1-μmspherical silica particles determined by the Coulter method was 1.01 μm. Non-spherical silica particles with particle diameters of<63 μm (SiO_2/quartz powder sieved through a 63-μm mesh; Kojundo Chemical Laboratory Co., Ltd, Saitama, Japan) were also assessed as representative particles that are difficult to measure particles by DLS. The mean particle

size of the<63-µm non-spherical silica particles was 33.6 µm, as measured with a laser diffraction-type particle counter. Scanning electron microscope (SEM; JSM-6600A, JEOL Ltd, Tokyo, Japan) images of the silica particles are shown in Figure 2-1 and Fourier transform infrared (FT-IR) spectra (FT/IR-6200, JASCO, Tokyo, Japan) are presented in Figure 2-2. Both types of particles showed typical FT-IR peaks of silica [2-18].
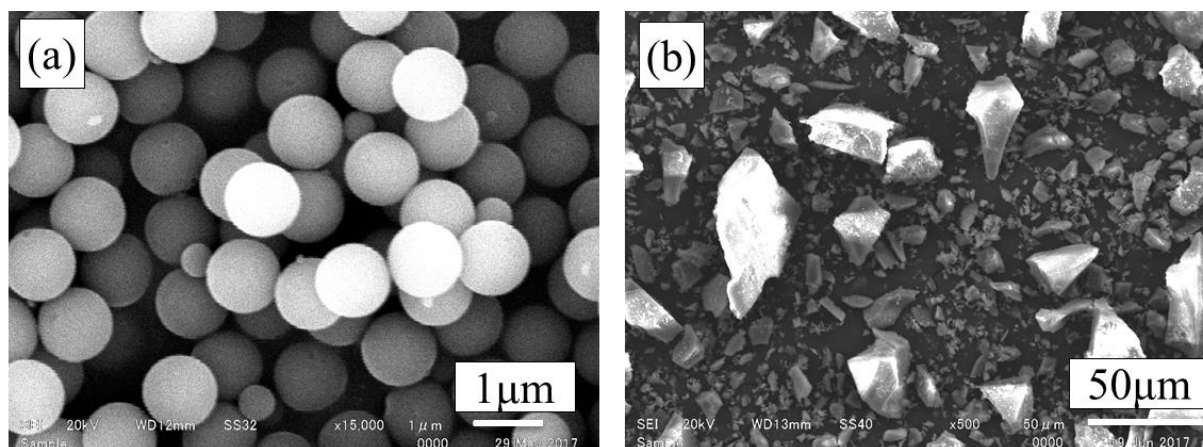
Figure 2-1. SEM images of (a) 1-µm spherical and (b) <63-µm non-spherical silica particles.
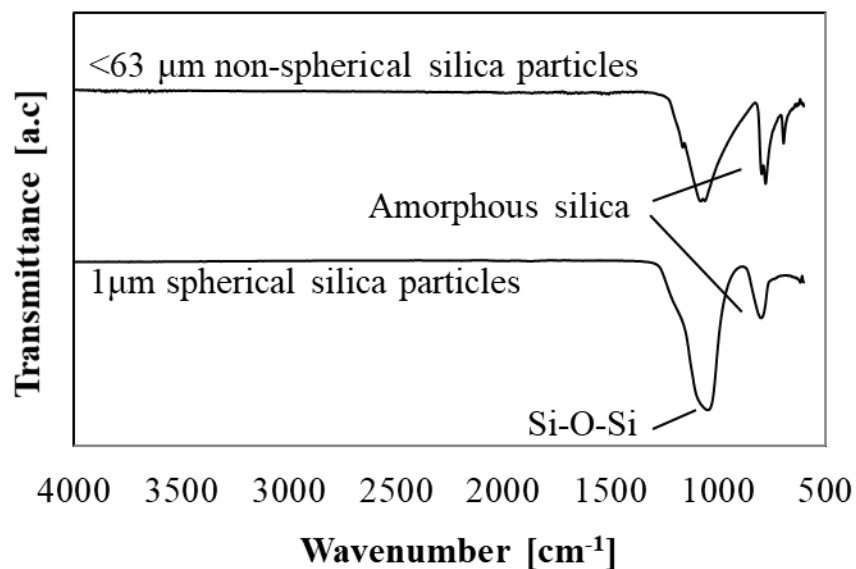
Figure 2-2. FT-IR spectra of 1-µm spherical and <63-µm non-spherical silica particles.

2.2.2   Measurement of HSPs using the capillary penetration method

The contact angles of the particles in various solvents were measured with the device shown in Figure 2-3. The Hansen sphere method was used to determine the difference between the contact angles of the particles in various solvents, from which the HSPs were calculated. In this procedure, the solvents used in the evaluation are first plotted in a three-dimensional HSP space. Next, I determined a sphere of the smallest radius for good solvents.

Solutes with HSPs lying outside this sphere were considered to be poor solvents. The center coordinates of the sphere were determined to be the HSPs of the target material. To judge whether a solvent is good or poor, an arbitrary threshold value was set for the contact angle between various solvents and the material being measured. For results lower than the threshold value, the solvent was considered good and for results above the threshold value, I judged that the solvent was poor. HSPiP software (HSPiP 5th Edition 5.0.06) was used for the Hansen sphere calculation. Also, in many measurements of HSPs, irregularities occur in which a poor solvent enters the sphere or a good solvent exits the sphere. In the HSPiP program, the validity of a sphere is evaluated, including irregularities.
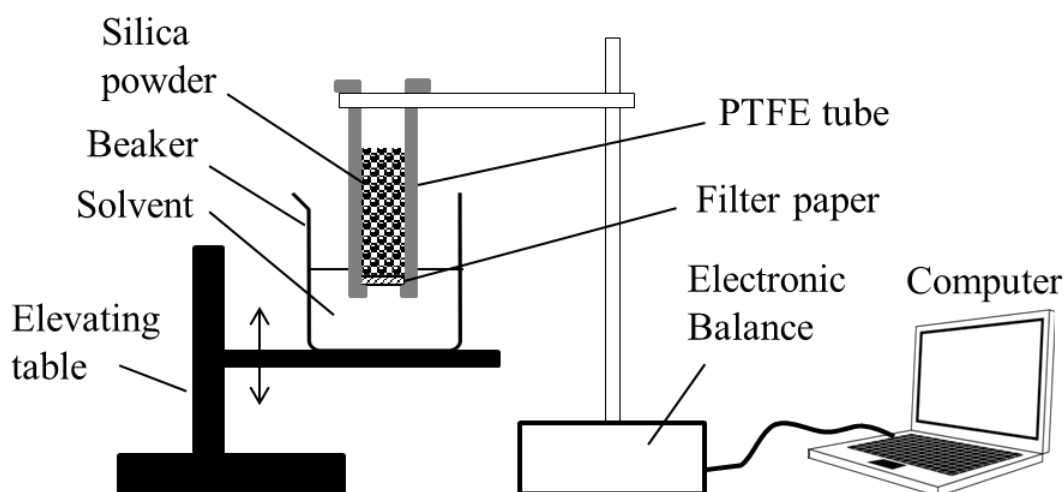
Figure 2-3. Schematic diagram of the experimental apparatus used for the capillary penetration measurements.

28

The validity of the sphere was evaluated by the parameter "fitting" available in the HSPiP program. The fitting value ranges from 0 to 1, where 0 is inaccurate and 1 is accurate. Empirically, when the fitting value is 0.8 or more, it is considered valid as an HSP [2-19]. The contact angles of the particles were calculated using Equation 2-1 below obtained by converting the permeation height of the solvent in the Washburn equation [Equation 2-2] into the permeation weight. When measuring the penetration rate, either the penetration height of the liquid or the penetration weight can be used; however, because the penetration height includes a considerable human error, I measured the penetration weight:

$$m^2 = \left(A^2 \varepsilon^2 \rho^2\right) \frac{r\gamma \cos\theta}{2\eta} t \qquad (2\text{-}1)$$

where m is the permeation weight of the liquid, A is the cross-sectional area of the container, ε is the interparticle void ratio, ρ is the liquid density, γ is the surface tension of the liquid, η is the viscosity of the liquid, θ is the contact angle, t is the penetration time, and r is the effective radius of an individual capillary tube in the capillary bundles.

$$h^2 = \frac{r\gamma \cos\theta}{2\eta} t \qquad (2\text{-}2)$$

where h is the height of infiltration of the liquid.

HSPs were determined using the capillary penetration method as follows. The bottom of the container was soaked in the test solvent after the particles were compressed in a container with filter paper on the bottom (Figure 2-3). The test solvent infiltrated through the filter paper into the fine pores between particles. The weight change of the penetrating solvent was recorded by an electronic balance, which was capable of measuring the change

29

of weight over time. The contact angle between each solvent and the particles was calculated from the Equation 2-1. Polytetrafluoroethylene (PTFE) with a high solvent resistance was used as the container for the 1-µm spherical silica particles because many solvents with different solubilities were used. The container had an inner diameter of 10 mm, height of 70 mm, and a hole with a diameter of 8mm on its lower surface to allow solvent penetration. This PTFE container was not used for measurements of the<63-µm non-spherical particles because their sharp edges damaged the container. Instead, a container made of hardened steel with the same dimensions was used. Filter paper was placed oven the hole to prevent particles from falling through the hole while allowing penetration of the solvent. The particles were packed by a compression method under a constant load after the particles were added to the container to ensure a constant gap between the particles and improve the repetition accuracy of loading.

Figure 2-4 shows the relationships between the packing volume and packing pressure for the spherical and non-spherical silica particles. The packing volume was saturated at 185 MPa for both types of particles. In addition, to confirm that the compression pressure did not crush the particles, I observed the particle shape after compression at 185 MPa. An SEM image of the 1-µm spherical particles after compression is presented in Figure 2-5. This image indicates that the particle shape was not changed under a compression pressure of 185 MPa. Therefore, a compression pressure of 185 MPa was used in subsequent experiments. In the calculation of θ using Equation 2-1, ε after compression was calculated using the density of the silica particles (2200 kg/m^3) and the compression volume. Also, because it is difficult to determine r, I calculated r assuming that the lowest θ of the solvent with the highest solvent–particle affinity was 0° and the value of r was considered to be constant. Furthermore, t was calculated as m^2/t according to the relationship between m and t.
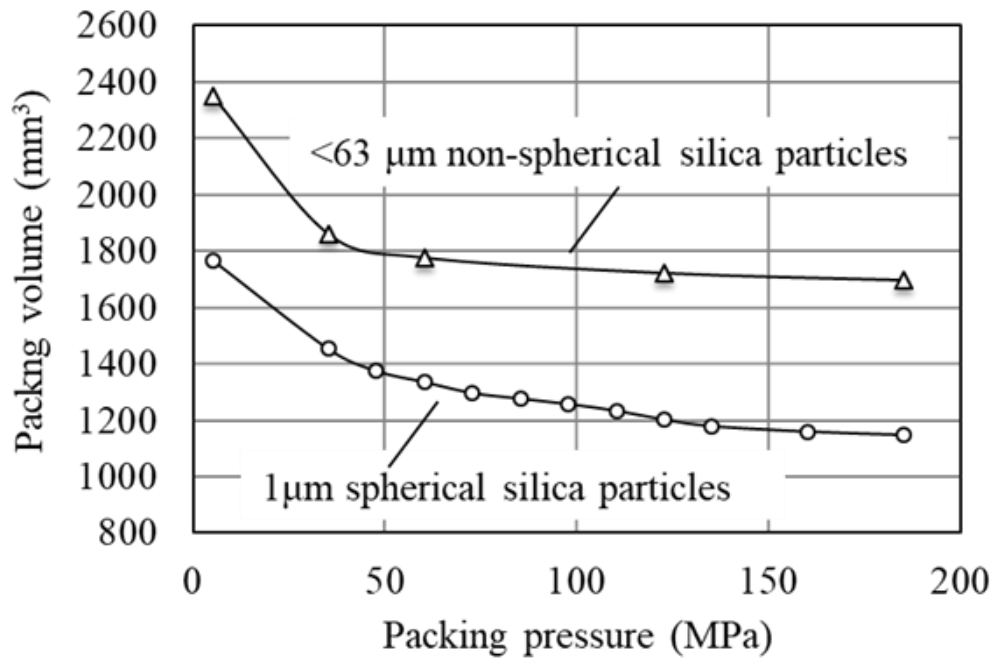
30

Figure 2-4. Relationship between the packing pressure and packing volume for 1-µm spherical and <63-µm non-spherical silica particles
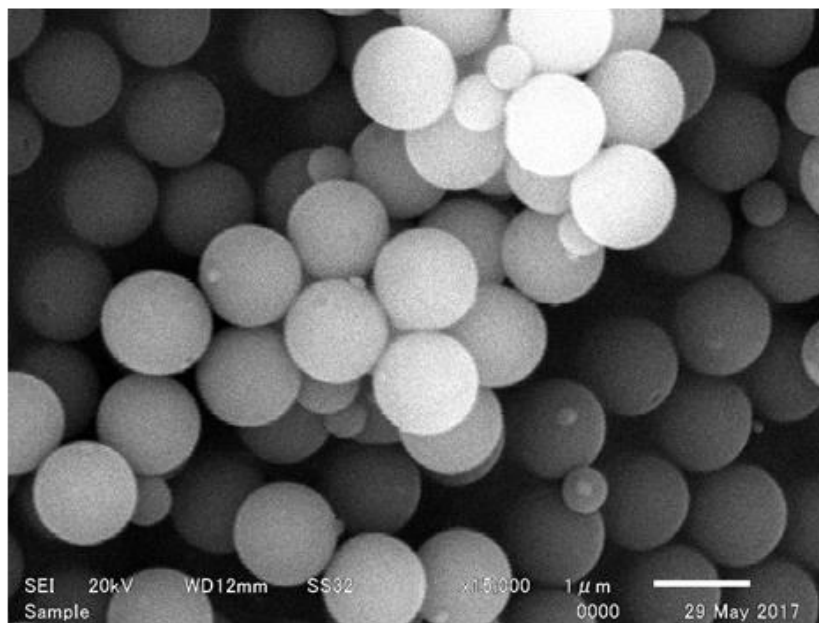
Figure 2-5. SEM image of 1-µm spherical silica particles after

2.2.3 HSP measurements by DLS

The grain diameters of the particles dispersed in various solvents were determined by DLS using the Hansen sphere method based on the different behaviors of the particles in various solvents, from which HSPs were calculated. When particles are dispersed in a solvent, DLS can be used to determine the compatibility between the particles and solvent provided that the particles have small diameters. The particles adhere when their compatibility with the solvent is poor, which causes the observed particle diameter to increase. Therefore, twice the average particle diameter of the measured particles was set as a threshold to distinguish good and poor solvents. The DLS method enables measurement of the diameter of fine particles by capturing the light scattered upon irradiating the suspension with a laser beam. For the actual measurement, a dispersion of 1-μm spherical silica particles (50 kg/m^3) was prepared, ultrasonicated for 10 min, and then the particle size was determined by a particle size analyzer (FPAR-1000, Otsuka Electronics Co., Ltd, Osaka, Japan).

2.3 Results and discussion

2.3.1 Repetition accuracy of the capillary penetration method

I determined the repetition accuracy of the capillary penetration method. Firstly, the repetition accuracy of the compressed state was confirmed. The compression height and weight of the 1-μm spherical silica particles compressed at 185 MPa in the PTFE container were measured and then the filling properties were confirmed by calculating the porosity from the filling volume, weight, and particle specific gravity. The results of 20 repeated measurements gave an average porosity of 58.7% with a standard deviation of 0.79%, maximum porosity of 59.97%, and minimum porosity of 57.97%, which indicated that a stable compressed state formed. Next, the repetition accuracy of solvent permeation was confirmed by packing 1-μm silica particles (1 g) into a PTFE container, compressing the particles at 185 MPa, and then introducing one of the three solvents; namely, acetone,

ethanol, or 1- methylnaphthalene. These measurements were conducted three times for each solvent. Figure 2-6 shows the infiltration weight change of each solvent. Each solvent had a different slope and the repetition accuracy was adequate. The contact angles calculated using Equation 2-1 from the weight increase of each solvent are shown in Table 2-1. The repetition accuracy of the contact angles was sufficient.
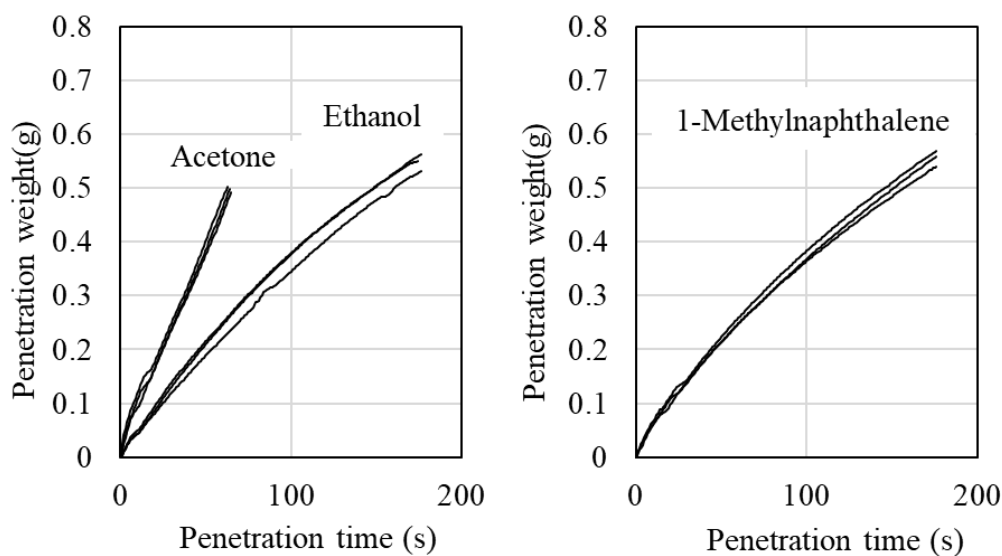
Figure 2-6. Penetration weight change of 1-µm spherical silica particles in acetone, ethanol, and 1-methylnaphthalene.

Table 2-1. Contact angles of 1-µm spherical silica particles measured in ethanol, acetone, and 1-methylnaphthalene.

	Contact Angle (°)		
	Ethanol	Acetone	1-Methyl-naphthalene
1	63	71	71
2	65	70	69
3	66	71	70
Average	65	71	70
Standard deviation	1.53	0.58	1
95%-confidence interval	1.73	0.65	1.13

2.3.2   HSPs of 1-μm silica particle surfaces determined by the capillary penetration method

   Because the repetition accuracy of the capillary penetration method was adequate, I determined the HSPs of the 1-μm spherical silica particles using this method. The 19 solvents used for the capillary penetration measurements are listed in Table 2-2.

  The θ values of the particles in different solvents were calculated using Equation 1-1. The HSPs of the particles and density, surface tension, and viscosity of the solvents are presented in Table 2-2. The solvent parameters in Table 2-2 were obtained from the literature [20]. The weight of the measured sample was 1 g. ε after compression was calculated using the density of the silica particles (2200 kg/m^3) and compression volume. Because it is difficult to determine r, I calculated r assuming that the lowest θ of the solvent with the best affinity was 0°, and r was considered to remain constant. Among the 19 solvents used for the determination, o-dichlorobenzene displayed the highest affinity for the silica particles. Therefore, r was calculated by considering that θ of o-dichlorobenzene was 0°, which gave r=0.21 μm. Table 2-2 lists the θ values calculated from this method and corresponding scores (good solvent: 1, poor solvent: 0). The threshold value used to distinguish good and poor solvents was 52°, which was obtained for tetrahydrofuran; this value was selected by considering various thresholds. Figure 2-7 shows representative HSPs, fittings and Hansen spheres obtained when changing the θ threshold of 1-μm spherical silica particles measured by the capillary penetration method. Blue circles denote good solvents, red square denote poor solvents, and the green balls are Hansen spheres with centers defining by the HSPs. When the θ threshold is large, the Hansen sphere is also large. In an ideal Hansen sphere with high precision, the outer shell of the sphere is defined by many poor solvents, and the fitting is high. As shown in Figuire 2-7(a), because the number of good solvents was too small, the fitting was as high as 1, but the outer shell of the sphere was not defined by the poor solvents, so this scenario is inaccurate. Conversely, as shown in Figure 2-7(c) and (d), when the number of good solvents was too large, the outline of the

34

sphere was not defined and the sphere diverged to the high δ_d side. In the case of Figure 2-7(b), where the threshold value was set to 52°, the outer shell of the Hansen sphere was defined by a large number of poor solvents, and the fitting value was high and accurately measured. Therefore, the scenario in Figure 2-7(b) with a threshold of 52° was adopted. The calculated HSPs of the 1-µm spherical silica particles were δ_d=18.61, δ_p=7.77, and δ_h=5.67.

Here I consider the combination of capillary penetration and HSP methods. It is difficult to determine absolute values of θ by the capillary penetration method. However, in the HSP method, HSPs can be determined using relative θ values. Therefore, combining the capillary penetration and HSP methods is considered to be a useful approach to evaluate wettability.

Table 2-2. Properties of 1-μm spherical silica particles measured by the capillary penetration method and various solvent characteristics.

Solvent	Hansen solubility parameter			Density	Viscosity	Surface tension	Contact angle	Score
	δ_d	δ_p	δ_h					
	$(MPa)^{1/2}$	$(MPa)^{1/2}$	$(MPa)^{1/2}$	kg/m^3	$mPa \cdot s$	mN/m	$^{\circ}$	
o-Dichlorobenzene	19.2	6.3	3.3	1306	1.324	26.8	0	1
Pyridine	19	8.8	5.9	983	0.952	36.9	14	1
Bromobenzene	19.2	5.5	4.1	1495	1.13	36.2	37	1
Benzyl Benzoate	20	5.1	5.2	1114	8.45	49	40	1
Nitrobenzene	20	10.6	3.1	1204	2.01	43.4	41	1
Tetrahydrofuran	16.8	5.7	8	889	0.55	26.4	52	1
Toluene	18	1.4	2	867	0.587	28.5	56	0
Salicylaldehyde	19	10.5	12	1146	2.5	49	59	0
1,4-Dioxane	17.5	1.8	9	1034	1.31	36.9	60	0
Aniline	20.1	5.8	11.2	1022	4.429	42.8	62	0
1-Methoxy-2-propanol	15.6	6.3	11.6	923	1.75	27.1	62	0
1-Methyl-2-Pyrrolidone	18	12.3	7.2	1028	1.65	41	62	0
Ethanol	15.8	8.8	19.4	789	1.06	22.1	65	0
Ethyl Acetate	15.8	5.3	7.2	901	0.449	23.8	66	0
2-Butanone	16	9	5.1	800	0.365	24	69	0
Acetone	15.5	10.4	7	785	0.316	23.7	71	0
N,N-Dimethyl Formamide	17.4	13.7	11.3	944	0.802	35.2	74	0
γ-Butyrolactone	18	16.6	7.4	1125	1.7	44.6	76	0
Dimethyl Sulfoxide	18.4	16.4	10.2	1096	1.996	42.9	80	0

(a) Contact angle of Bromobenzen(37°)			
δd	δp	δh	Fitting
19.11	7.21	4.91	1.00

(b) Contact angle of THF(52°)			
δd	δp	δh	Fitting
18.61	7.77	5.67	1.00

(c) Contact angle of Salicylaldehyde(59°)			
δd	δp	δh	Fitting
19.05	6.6	5.16	0.859

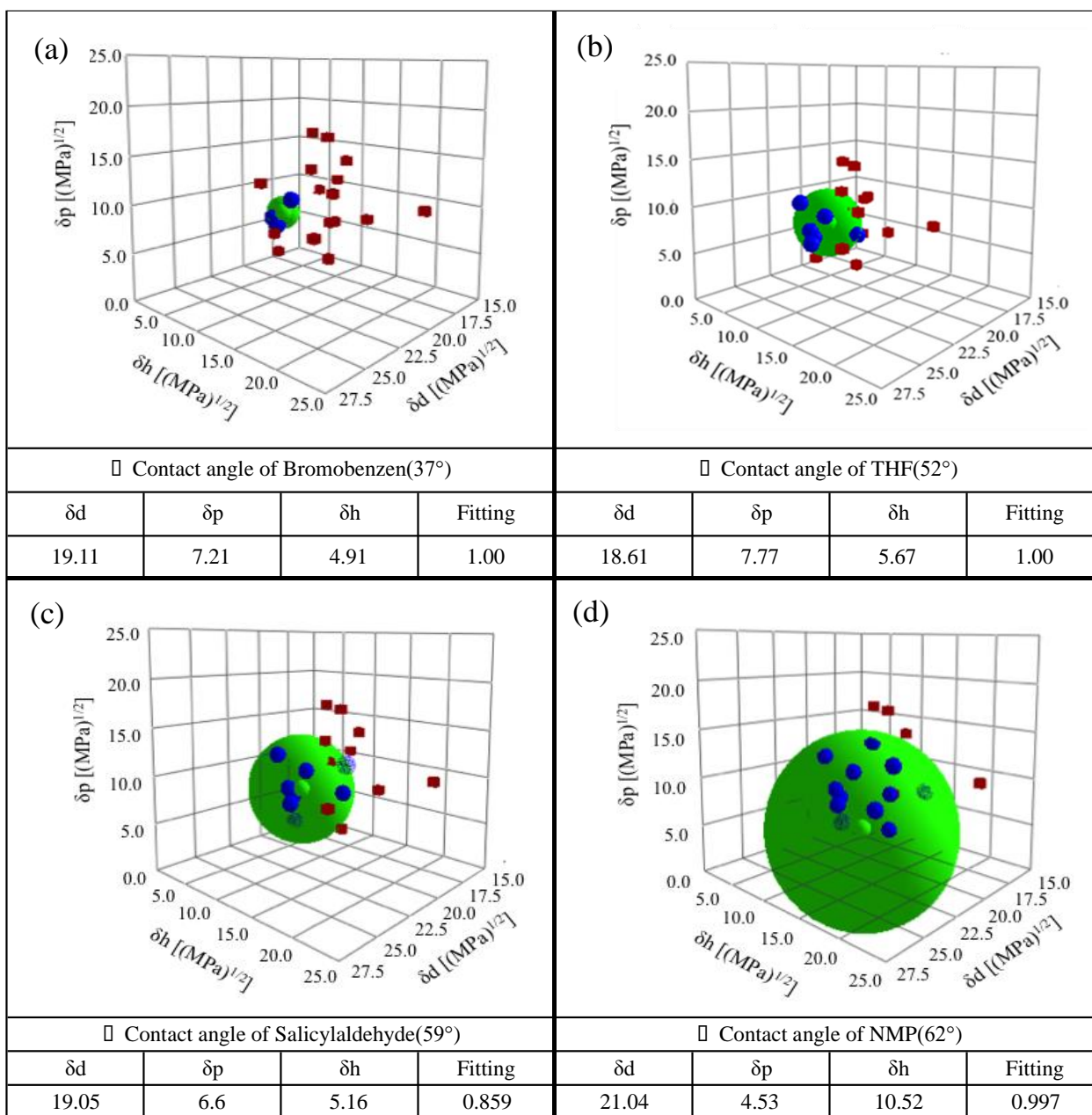| (d) Contact angle of NMP(62°)			
δd	δp	δh	Fitting
21.04	4.53	10.52	0.997

Figure 2-7. Representative Hansen spheres with different contact angle thresholds for the 1-μm spherical silica particles measured by the capillary penetration method. Blue spheres denote good solvents and red cubes denote poor solvents.

2.3.3 HSPs of 1-μm spherical silica particle surface determined by DLS

To validate the HSPs determined by the capillary penetration method, the HSPs of the 1-μm spherical silica particles were also determined by DLS. The HSPs, particle diameters, and scores (0 or 1) for the 35 solvents considered are listed in Table 2-3. The threshold used to determine the scores for the solvents was 2 μm, which is twice the diameter of the silica particles. The hyphens in the table indicate poor solvents for which it was impossible to collect measurements because of precipitation induced by particle aggregation. Figure 2-8 shows the Hansen sphere obtained from the DLS results. Similar to the capillary penetration method, blue spheres indicate good solvents, red cubes indicate poor solvents, and the green sphere is the Hansen sphere, the center of which defines the HSPs. As indicated in Figure 2-8, some poor solvents (e.g., Methylene Dichloride) were located inside the sphere and some good solvents (e.g., Tetrahydrofuran) were located outside the sphere. However, I confirmed the fitting, as described in Section 2.2.2. The fitting value in this case exceeded 0.8, so it is considered sufficiently valid. The HSPs of 1-μm spherical silica particles determined from the DLS results were $\delta_d = 19.45$, $\delta_p = 7.52$, and $\delta_h = 6.65$.

Table 2-3. HSP results obtained for solvents by DLS measurements.

Solvent	Hansen solubility parameter			Reflective index	Particle size	Score
	δ_d (MPa)$^{1/2}$	δ_p (MPa)$^{1/2}$	δ_h (MPa)$^{1/2}$	—	nm	
Benzaldehyde	19.4	7.4	5.3	1.544	1352	1
Pyridine	19	8.8	5.9	1.507	1352	1
o-Dichlorobenzene	19.2	6.3	3.3	1.549	1405	1
Dibenzyl Ether	19.6	3.4	5.2	1.539	1566	1
p-Chlorotoluene	19.1	6.2	2.6	1.519	1600	1
Nitrobenzene	20	10.6	3.1	1.55	1666	1
Phenyl Acetonitrile	19.5	12.3	3.8	1.523	1723	1
Bromobenzene	19.2	5.5	4.1	1.557	1742	1
Trichloroethylene	18	3.1	5.3	1.478	1749	1
Aniline	20.1	5.8	11.2	1.584	1787	1
1-Bromonaphthalene	20.6	3.1	4.1	1.656	1877	1
Benzyl Benzoate	20	5.1	5.2	1.496	1877	1
1,1,2,2-Tetrabromoethane	21	7	8.2	1.632	1887	1
Tetrahydrofuran	16.8	5.7	8	1.405	1934	1
2-Butanone	16	9	5.1	1.377	1990	1
Salicylaldehyde	19	10.5	12	1.57	2433	0
γ-Butyrolactone	18	16.6	7.4	1.435	2712	0
Toluene	18	1.4	2	1.494	-	0
N-Methyl-2-Pyrrolidone	18	12.3	7.2	1.468	-	0
1,4-Dioxane	17.5	1.8	9	1.42	-	0
1-Methoxy-2-propanol	15.6	6.3	11.6	1.404	-	0
Ethanol	15.8	8.8	19.4	1.359	-	0
Ethyl Acetate	15.8	5.3	7.2	1.37	-	0
Acetone	15.5	10.4	7	1.356	-	0
Dimethyl Formamide	17.4	13.7	11.3	1.428	-	0
Dimethyl Sulfoxide	18.4	16.4	10.2	1.478	-	0

Table 2-3. (Continued)

| Solvent	Hansen solubility parameter			Reflective index	Particle size	Score
	δ_d $(MPa)^{1/2}$	δ_p $(MPa)^{1/2}$	δ_h $(MPa)^{1/2}$	—	nm	
Methylene Dichloride	17	7.3	7.1	1.425	-	0
Methyl Isobutyl Ketone	15.3	6.1	4.1	1.394	-	0
N,N-Dimethyl Acetamide	16.8	11.5	9.4	1.436	-	0
Cyclohexane	16.8	0	0.2	1.444	-	0
Chlorobenzene	19	4.3	2	1.522	-	0
Acetonitrile	15.3	18	6.1	1.342	-	0
1-Methylnaphthalene	19.7	0.8	4.7	1.615	-	0
Methanol	14.7	12.3	22.3	1.327	-	0
Hexane	14.9	0	0	1.375	-	0
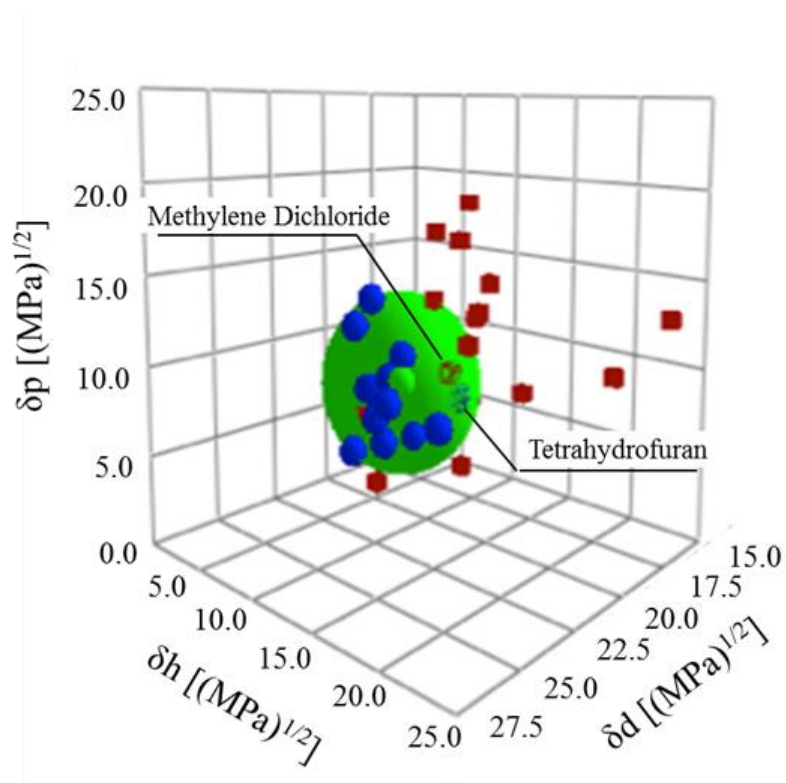
Figure 2-8. Hansen sphere (green) of 1-µm silica particles measured by DLS. Blue spheres denote good solvents and red cubes denote poor solvents.

2.3.4   Comparison of HSPs determined by the capillary penetration and DLS methods

The HSP values of 1-µm silica particles determined by the capillary penetration and DLS methods are given in Table 2-4. To analyze the measurement methods in more detail, the θ values determined by the capillary penetration method were compared with the particle diameters determined by DLS; Figure 2-9 shows the relation between these parameters. Although this is an empirical correlation, its correlation coefficient of R=0.82 indicates a strong correlation between θ and particle diameter. Thus, the effectiveness of the capillary penetration method for HSP determination was confirmed, although it was not the same for each solvent.

Table 2-4. HSPs of 1-µm silica particles determined by capillary penetration and DLS measurements.

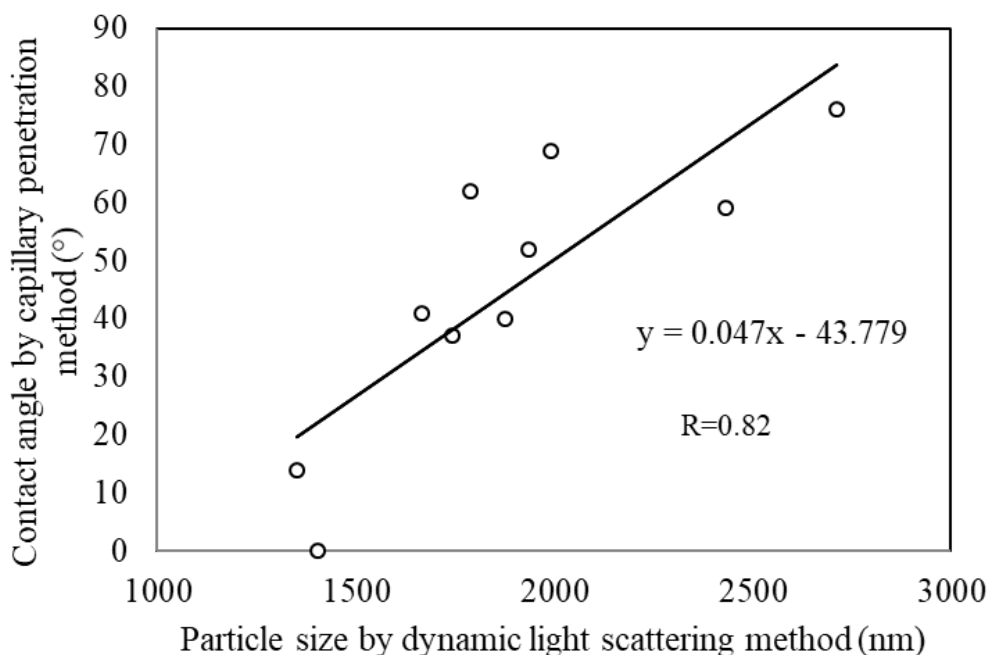| Measurement method	Hansen solubility parameter			
	δ_d $(MPa)^{1/2}$	δ_p $(MPa)^{1/2}$	δ_h $(MPa)^{1/2}$	δ_t $(MPa)^{1/2}$
Capillary Penetration method	18.61	7.77	5.67	20.94
Dynamic light scattering method	19.45	7.52	6.65	21.89

Figure 2-9. Relationship between contact angle by capillary penetration method and particle size by dynamic light scattering method.

2.3.5　HSPs of < 63-μm non-spherical silica particle surfaces determined by the capillary penetration method

Having confirmed the effectiveness of HSP determination by the capillary penetration method, I next applied my technique to large non-spherical silica particles. An SEM image of the silica powder with particle sizes of < 63 μm is shown in Figure 2-1(b). The small gaps between the silica particles meant that only a small amount of solvent could be absorbed. Thus, these non-spherical silica particles had short permeation- weight change times, which were difficult to measure; to counteract this, I increased the filling weight of the particles in the container to 2 g for these measurements. The HSPs, θ, and scores for 19 solvents are listed in Table 2-5. The density, surface tension, and viscosity of each solvent were the same as the values listed in Table 2-2 for the 1- μm spherical silica particle measurements by the capillary penetration method. The θ value was determined twice for

42

each solvent; average values are listed along with their score (1: good solvent; 0: poor solvent). The threshold was determined by the same method as that described in Section 2.3.2, from which the θ value of pyridine of 49° or less was taken to represent a good solvent. The obtained Hansen sphere is depicted in Figure 2-10.

The solvent 1-methyl-2-pyrrolidone was a poor solvent but was located inside the sphere, as indicated by a red cube. Meanwhile, 1- methoxy-2-propanol was a good solvent but was located outside the sphere. This case was also evaluated using the fitting parameter, which was more than 0.8 and thus considered adequately valid. The HSPs of the < 63-µm non-spherical silica particles were δ_d = 18.81, δ_p = 6.77, and δ_h = 6.69. The < 63-µm non-spherical silica particles and 1-µm-spherical silica particles are expected to have similar surface properties and HSPs even though their sizes and shapes are different. To quantitatively evaluate the similarity of the surface properties of these two types of particles, the distance Ra, which is used generally in HSP evaluations, was determined using Equation 2-3,

$$R_a = \left\{ 4\left(\delta_{d1} - \delta_{d2}\right)^2 + \left(\delta_{p1} - \delta_{p2}\right)^2 + \left(\delta_{h1} - \delta_{h2}\right)^2 \right\}^{1/2}$$

(2-3)

The distance between the 1-µm silica particles determined by DLS was Ra=1.48. The distance between the 1-µm silica particles and < 63-µm non-spherical silica particles determined by the capillary penetration method was also Ra=1.48 in both cases. Thus, I confirmed that Ra was 1.5 or less and the HSPs of the two types of silica particles were similar. Figure 2-11 shows a plot of the three above-mentioned approaches used to measure the HSPs of silica particles in HSP space. The parameters obtained by the different methods agreed well, which confirmed the effectiveness of HSP determination by the capillary penetration method.

43

Table 2-5. Properties of <63-µm non-spherical silica particles determined by the capillary penetration method.

| Solvent	Hansen solubility parameter			Contact angle			
	δ_d	δ_p	δ_h	1	2	Ave.	Score
	$(MPa)^{1/2}$	$(MPa)^{1/2}$	$(MPa)^{1/2}$	°	°	°	
o-Dichlorobenzene	19.2	6.3	3.3	0	3.6	1.8	1
Benzyl Benzoate	20	5.1	5.2	27.6	29.5	28.6	1
Aniline	20.1	5.8	11.2	32.2	39.4	35.8	1
Nitrobenzene	20	10.6	3.1	38	41.8	39.9	1
1-Methoxy-2-propanol	15.6	6.3	11.6	43.6	44.6	44.1	1
Bromobenzene	19.2	5.5	4.1	43.8	45.7	44.8	1
Tetrahydrofuran	16.8	5.7	8	47.4	46.2	46.8	1
Pyridine	19	8.8	5.9	50.3	48.2	49.3	1
1-Methyl-2-Pyrrolidone	18	12.3	7.2	48.8	53.9	51.4	0
Dimethyl Sulfoxide	18.4	16.4	10.2	49.6	51.8	50.7	0
γ-Butyrolactone	18	16.6	7.4	50.7	52.8	51.8	0
Toluene	18	1.4	2	51.4	53.8	52.6	0
Ethyl Acetate	15.8	5.3	7.2	50.8	58.7	54.8	0
Salicylaldehyde	19	10.5	12	53.8	59.1	56.5	0
1,4-Dioxane	17.5	1.8	9	52	59.6	55.8	0
N,N-Dimethyl Formamide	17.4	13.7	11.3	55.7	57.6	56.7	0
2-Butanone	16	9	5.1	56.2	59.1	57.7	0
Acetone	15.5	10.4	7	61.1	63	62.1	0
Ethanol	15.8	8.8	19.4	62.7	64	63.4	0
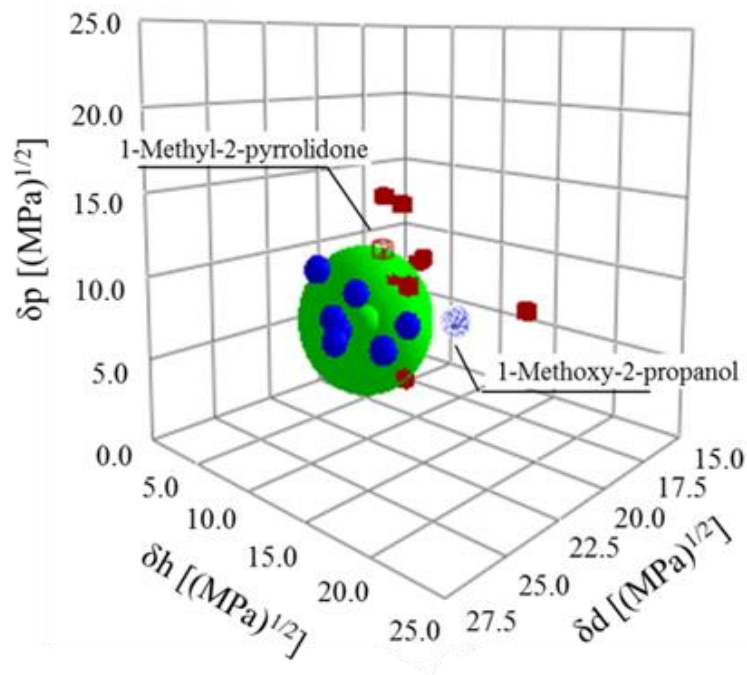
Figure 2-10. Hansen sphere of <63-µm non-spherical silica particles measured by the capillary penetration method. Blue spheres denote good solvents and red cubes denote poor solvents.
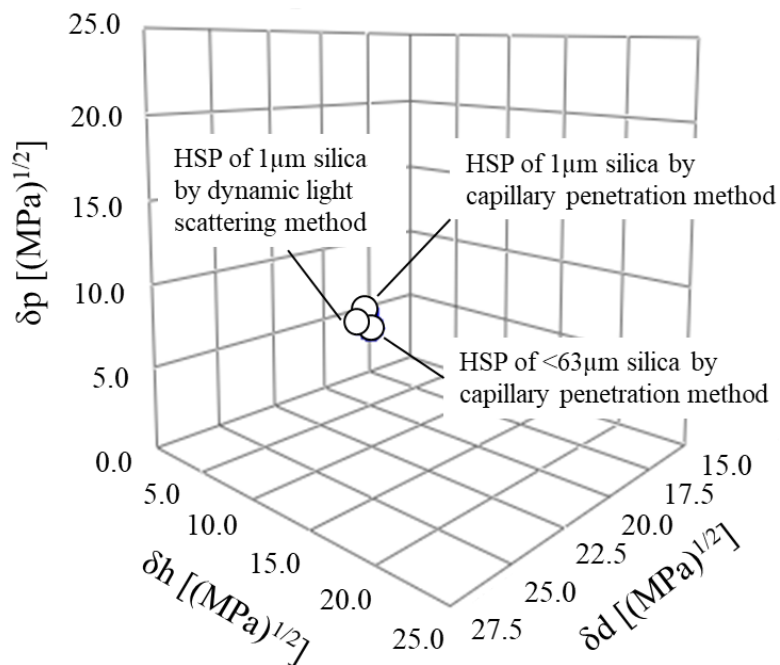

Figure 2-11. HSPs of silica particles measured by the capillary penetration and DLS methods.

2.4 Conclusions

To determine the HSPs of highly dense, large, or non-spherical particles, which are difficult to measure by conventional HSP determination methods, I used a capillary penetration method to measure θ of the particles. I accurately determined the HSPs of silica particles using the capillary penetration method. For 1-μm spherical silica particles, the DLS results were δ_d=19.45, δ_p=7.52, and δ_h=6.65. These results agreed well with those obtained by the capillary penetration method (δ_d = 18.61, δ_p = 7.77, and δ_h = 5.67). The HSPs of<63-μm non-spherical silica particles, which represent a system that is difficult to measure by DLS, were measured by the capillary penetration method, providing values of δ_d = 18.81, δ_p = 6.77, and δ_h = 6.69. Ra for the<63-μm non-spherical and 1-μm spherical silica particles determined by DLS and the capillary penetration methods were less than 1.5, which confirmed their good agreement. The above results indicate that the capillary penetration method is effective for HSP determination even for highly dense non-spherical particles. Clarifying the affinities of various particles for solvents should be useful in the study of polymer composite materials including, conductive, magnetic, heat-conducting, sliding, sealing, damping, and structural materials.

2.5 References

[2-1] C. M.Hansen, A. L.Smith, Using Hansen solubility parameters to correlate solubility of C60 fullerene in organic solvents and in polymers. Carbon. 42 (2004) 1591–1597.

[2-2] H. T.Ham, Y. S.Choi, I. J.Chung, An explanation of dispersion states of single-walled carbon nanotubes in solvents and aqueous surfactant solutions using solubility parameters. J. Colloid Interface Sci. 286 (2005) 216-223.

[2-3] S.Acevedo, A.Castro, E.Vasquez, F.Marcao, M. A.Ranaudo, Investigation of Physical Chemistry Properties of Asphaltenes Using Solubility Parameters of Asphaltenes and Their Fractions A1 and A2. Energy Fuels. 24 (2010) 5921-5933.

[2-4] T.;Sato, S.Araki, M.Morimoto, R.Tanaka, H.Yamamoto, Comparison of Hansen Solubility Parameter of Asphaltenes Extracted from Bitumen Produced in Different Geographical Regions. Energy Fuels. 28 (2014) 891-897.

[2-5] T.Sato, Y.Hamada, M.Sumikawa, S.Araki, H.Yamamoto, Solubility of Oxygen in Organic Solvents and Calculation of the Hansen Solubility Parameters of Oxygen. Ind. Eng. Chem. Res. 53 (2014) 19331-19337.

[2-6] J. H.Hildebrand, R. L.Scott, The Solubility of Nonelectrolytes, 3rd ed.; Dover Publications Inc.: New Yoke, 1950.

[2-7] C. M.Hansen, Hansen Solubility Parameters: A User's Handbook; CRC Press: Boca Raton, FL, 1999.

[2-8] J. U.Wieneke, B.Kommoß, O.Gaer, I.Prykhodko, M.Ulbricht, Systematic Investigation of Dispersions of Unmodified Inorganic Nanoparticles in Organic Solvents with Focus on the Hansen Solubility Parameters. Ind. Eng. Chem. Res. 51 (2012) 327-334.

[2-9] S.Wang, J.Liu, C.Pai, C.Chen, P.Chung, A. S.Chiang, S. J.Chang, Hansen solubility parameter analysis on the dispersion of zirconia nanocrystals. J Colloid Interface Sci. 407 (2013) 140-147.

[2-10] S.Süß, T.Sobisch, W.Peukert, D.Lerche, D.Segets, Original Research Paper Determination of Hansen parameters for particles: A standardized routine based on analytical centrifugation. Advanced Powder Technol. 29 (2018) 1550-1561.

[2-11] M.Lazghab, K.Saleh, I.Pezron, P.Guigon, L.Komunjer, Wettability assessment of finely divided solids. Powder Technol. 157 (2005) 79–91.

[2-12] A.Roman-Gutierrez, J.Sabathier, S.Guilbert, L.Galet, B.Cuq, Characterization of the surface hydration properties of wheat flours and flour components by the measurement of contact angle. Powder Technol. 129 (2003) 37–45.

[2-13] J. W.Dove, G.Buckton, C.Doherty, A comparison of two contact angle measurement methods and inverse gas chromatography to assess the surface energies of theophylline and caffeine. Int. J. Pharm. 138 (1996) 199–206.

[2-14] G.Buckton, Assessment of the wettability of pharmaceutical powder. J. Adhes. Sci. Technol. 7 (1993) 205–219.

[2-15] M. V.Hammes, A. H.Englert, C. P. Z.Noreña, N. S. M.Cardozo, Study of the influence of soy lecithin addition on the wettability of buffalo milk powder obtained by spray drying. Powder Technol. 277 (2015) 237–243.

[2-16] S.OKA, H.Emady, O.Kaspar, V.Tokarova, F.Muzzio, F.Stepanec, et al. The effects of improper mixing and preferential wetting of active and excipient ingredients on content uniformity in high shear wet granulation. Powder Technol. 278 (2015) 266–277.

[2-17] J. E.Jaine, M. R.Mucalo, Measurements of the wettability of catalyst support materials using the Washburn capillary rise technique. Powder Technol. 276 (2015) 123–128.

[2-18] S. Sompech, T. Dasri, S. Thaomola. Preparation and characterization of amorphous silica and calcium oxide from agricultural wastes. Oriental J. Chem. 32 (2016) 1923–1928.

[2-19] M. Levin, P. Redelius, Determination of three-dimensional solubility parameters and solubility spheres for naphthenic mineral oils, Energy and Fuels. 22 (2008) 3395–3401.

[2-20] Organic Synthetic Chemistry Association, Solvents Pocket Book; Ohmsha, Ltd.: Tokyo, 1967.

Chapter 3 Functional composite design with HSPs

3.1   Introduction

Functional composite materials have been applied in various fields, such as conductivity, magnetism, heat conduction, and as structural materials. The reason for enhancing the performance of functional composite materials is, in general, to improve the compatibility of the inorganic filler and the polymer material to achieve higher dispersion and improve various properties [3-1, 3-2, 3–3].

Generally, to enhance the compatibility between the inorganic filler and the polymer, the surface of the inorganic filler is subjected to a surface treatment, such as by a silane coupling agent. For example, Dang et al. improved the strength of composite materials by treating TiO_2 nanoparticles with a silane coupling agent to increase the dispersion in the composite material of TiO_2 nanoparticles and silicone rubber [3-4]. Additionally, Mallakour et al. improved the thermal stability by treating the surface of TiO_2 nanoparticles with a silane coupling agent that was added to PVA [3-5]. In a composite material of aluminum and epoxy, Zhou et al. treated aluminum particles with a silane coupling agent to improve the dispersibility of copper and enhance the thermal conductivity [3-6]. For a composite of SiO_2 particles and cyanate ester resin, Chuang et al. treated the surface of the SiO_2 particles with a silane coupling agent to strengthen interfacial bonding and improve the heat resistance and friction properties of the material [3-7]. Moreover, in a composite material of boron nitride and an epoxy resin, Jang et al. treated the boron nitride with a silane coupling agent to achieve high dispersion and improve the thermal conductivity of the material [3-8]. Furthermore, even in the case of a bonded magnet, the magnetic powder particles are treated with a silane coupling agent to achieve high dispersion and achieve high packing of the magnetic powder particles [3-9,3-10]. As mentioned above, the selection of the silane coupling agent is important for the characteristic improvement of a composite material. However, so far, there has not been much quantitative evaluation between coupling agents.

However, a quantitative evaluation of the compatibility between two substances can be achieved by the Hansen solubility parameters as cohesive energy density. The solubility parameter δ_t (MPa$^{1/2}$) has been defined by J. H. Hildebrand as an indicator of the affinity [3-11]. C. M. Hansen divided δ_t into three parts, a dispersion term δ_d, an interdipolar force term δ_p, and a hydrogen bonding term δ_h, and expressed the affinity between substances in more detail [3-12]. This solubility parameter is called the Hansen solubility parameter. This HSP is also attracting attention in the fields of carbon materials, oil and gas [3-13, 3-14, 3-15, 3-16, 3–17]. In recent years, it has begun to be used for the affinity evaluation of particle surfaces, and HSPs, such as titanium oxide and zirconia, have been reported [3-18, 3-19].

HSPs have also begun to be used in the field of composite materials Su et al. evaluated the mechanical strength of composite materials with HSPs [3-20]. There are also papers that compare HSPs before and after surface treatment with copper particles, with a composite material in mind [3-21]. However, there have only been a few reports that have confirmed a property change of the applied material by measuring the particle surface before and after surface treatment.

In this paper, the Hansen solubility parameter is applied to bonded magnets used in motors and sensors. The relationship between the change of HSP of the particle surface arising from surface treatment and the flowability during injection molding of the bonded magnet is clarified, and the compatibility between the magnet powder surface and the resin is evaluated. Bonded magnets, which contain plastic in addition to magnet powder, can be molded into various shapes by injection molding, thereby increasing the degree of freedom in motor design and contributing to the downsizing and high power output of the motor. However, since the bonded magnet contains a plastic component, there is also the problem where the magnetic properties of the magnet are degraded as compared with a magnet having 100% of the magnet component. To further improve the magnetic properties of this bonded magnet, it is necessary to obtain injection-moldable fluidity even with a high filling

51

of the magnet powder. Therefore, to enhance the compatibility with the plastic, the magnet powder is surface-treated to improve the flowability of the bonded magnet. The HSP was applied as follows. The HSP of polyamide 6 resin, which is a matrix resin of the bonded magnet, was measured. Next, the HSPs of the surface treatment agents were calculated by the group contribution method to predict the effect of the surface treatment agent. Moreover, the HSP of the magnet powder surface treated by the coupling agent was measured. However, since the magnetic powder had a high specific gravity and a non-spherical shape, which was difficult to measure by the existing particle diameter method or sedimentation method, it was measured by the capillary penetration method proposed by the authors [3-22]. Finally, the flowability and magnetic properties of the produced bonded magnet were measured. By comparing and examining these results, the applicability of HSP technology to composite materials was examined.

3.2   Material and methods

3.2.1   Measurement sample

As the magnet powder, two types of NdFeB-based magnet powders having different particle sizes were used. One was a NdFeB-based magnet powder (manufactured by Neo Performance Materials, model: MQFP-14- 12-AA4) having an average particle size of 5 μm. The other type was a NdFeB-based magnet powder (manufactured by Neo Performance Materials, model: MQP-14-12-AA4) of 106 μm or less. Both magnet powder densities were 7620 kg/m^3. Figure 3-1 shows the scanning electron microscopy (SEM) photographs. Both powders were produced by crushing with a thin ribbon, and when the particle diameter was large, the shape of the thin ribbon remained, and as the particles became finer, the ribbon exhibited lumps. As a resin, powdery polyamide 6 resin (Unitika, Model: A1012N) was used. The coupling agents used for treating the magnet powder surface were 3-(acrylolyoxy) propyltrimethoxysilane (ALTMS, Tokyo Chemical Industry Co., Ltd. Model: A1597), 3-

Aminopropyltrimethoxysilane (APTMS, Tokyo Chemical Industry Co., Ltd. Model: A2628),
N-phenyl-3-aminopropyltrimethoxysilane (NPTMS, Tokyo Chemical Industry Co., Ltd.
Model: P1458), (3-ureidopropyl) trimethoxysilane (UPTMS, Tokyo Chemical Industry Co.,
Ltd. Model: T1915). The chemical structure of the silane coupling agent is shown in Figure
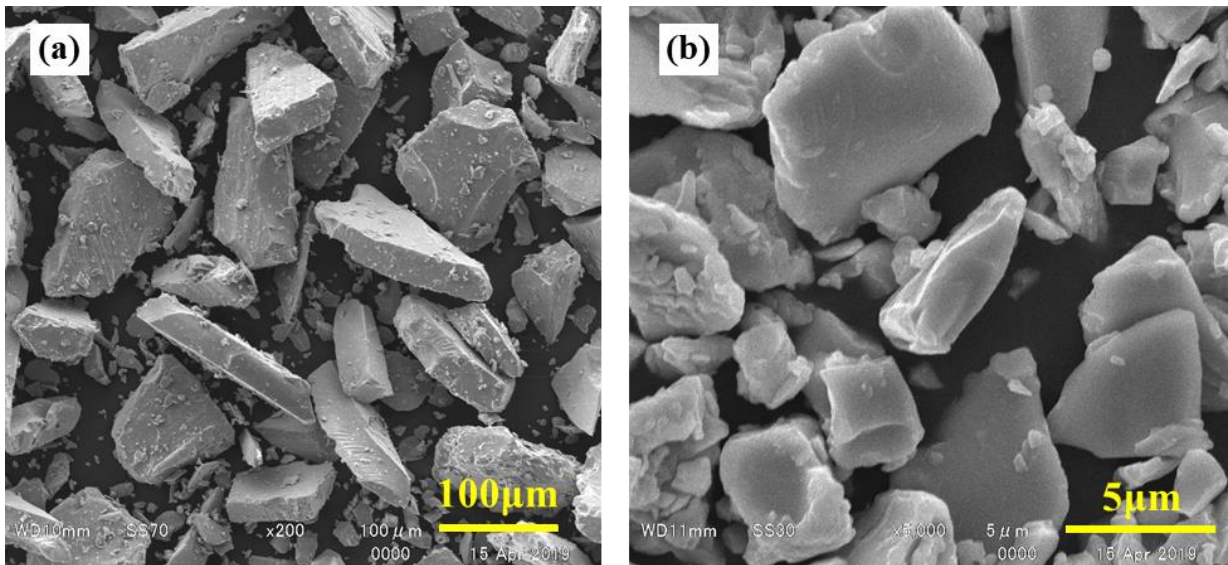3-2.

Figure 3-1. Electron micrographs of magnet powder of (a) 106 µm or less and (b) magnet powder of 5 µm on average.
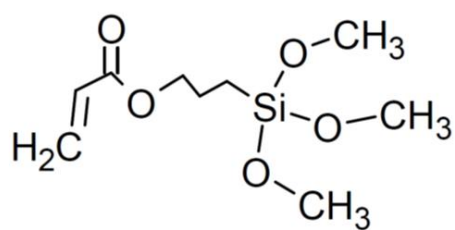
ALTMS
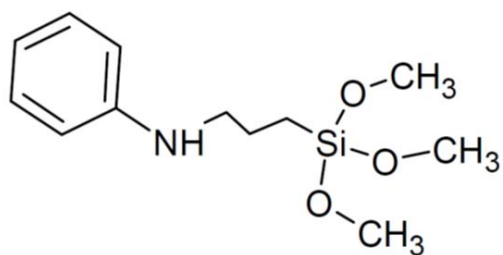
NPTMS
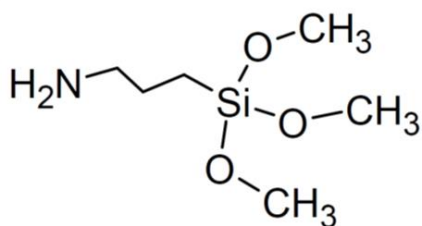
APTMS
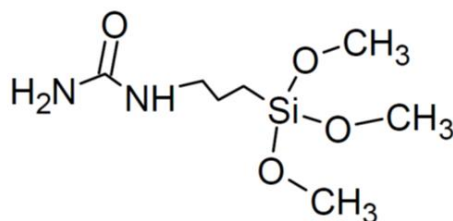
UPTMS

Figure 3-2. Chemical structure of silane coupling agent used in the experiment.

3.2.2   Bonded magnet fabrication and analysis method

Next, the method used to produce a bonded magnet will be described. Figure 3-3 shows the flow chart for the method to produce a bonded magnet. First, the magnet powder was surface treated with a coupling agent. Thereafter, the coupling agent-treated magnet powder and the polyamide 6 were kneaded and pelletized. Injection molding was performed to obtain a desired magnet shape, and finally, the mold was magnetized to become a magnet. The silane coupling agent treatment was implemented as follows. In advance, the silane coupling agent (2 g) was added to a mixed solution of pure water (50 mL) and ethanol (50 mL) to prepare the coupling agent solution. The magnet powder (100 g) was added to the

solution, and was sonicated for 10 min. Thereafter, it was allowed to stand with a thermostat at 110 ℃. for 20 min. Finally, it was washed with ethanol and dried at 80 ℃. for 30 min.

The state of the surface-treated magnet powder was confirmed by Xray photoelectron spectroscopy (XPS JEOL Ltd. Model: JPS-9010).

```
                              ┌─────────────────┐
                              │  Magnet powder  │
                              └─────────────────┘
                                       │
                                       ▼
┌─────────────────┐          ┌─────────────────┐
│ Coupling agent  │─────────▶│ Surface treatment│
└─────────────────┘          └─────────────────┘
                                       │
                                       ▼
┌─────────────────┐          ┌─────────────────┐
│   Polyamide 6   │─────────▶│     Kneading    │
└─────────────────┘          └─────────────────┘
                                       │
                                       ▼
                              ┌─────────────────┐
                              │   Pelletizing   │
                              └─────────────────┘
                                       │
                                       ▼
                              ┌─────────────────┐
                              │ Injection molding│
                              └─────────────────┘
                                       │
                                       ▼
                              ┌─────────────────┐
                              │   Magnetizing   │
                              └─────────────────┘
```
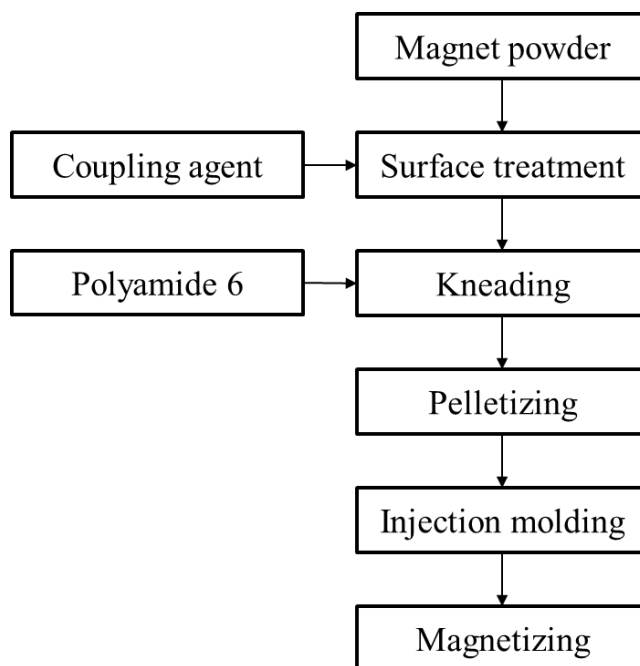
Figure 3-3. Manufacture method of bonded magnet by injection mold.

The HSPs of the polyamide 6 resin were calculated by the Hansen sphere method described in Section 1.1.3. After adding the resin (50 mg) in various solvents (20 mL) and leaving it to stand for 24 h, it was judged to be a good solvent if the resin dissolved, and a poor solvent if it did not. Commercial HSPiP software (HSPiP 5th Edition 5.0.06) was used for the actual calculation of the HSPs. The built-in fitting value of the software was used to check the accuracy of the Hansen ball. The fitting value is an index for evaluating the accuracy of a sphere, and takes a value of 0–1. Empirically, HSPs are considered valid if the fitting is greater than 0.8 [3-23].

The HSPs of the coupling agents were calculated from the chemical structure by the group contribution method. Here, the coupling agent was calculated from the structure of the part excluding the methyl group because the methyl group is released when bonded to the magnetic powder. The measurement of the HSPs of the surface-treated magnet powder was not possible because the specific gravity of the magnet powder particle was as large as 7620 kg/m^3 and the magnet powder immediately settled out by the sedimentation method [3-24] or the particle size method [3-18, 3-19]. Therefore, the capillary penetration method was used [3-22]. An outline is shown below. The magnetic powder (8 g) was filled in an iron container and compressed at 0.62 MPa. The inner diameter of the container was 10 mm and the height was 70 mm, and the lower surface had a hole that allowed the solvent to penetrate to a depth of 8 mm in diameter. Each of the 18 organic solvents was infiltrated into the compressed magnet powder, and the penetration weight was measured every second. After the contact angle was calculated using Washburn's equation [3-22] and the threshold values for the poor solvent and the good solvent were determined, the HSPs were determined using the Hansen sphere method.

The fluidity after forming a bonded magnet pellet was measured using a capillary rheometer (TOYO SEIKI SEISAKU-SHO, LTD. Model: CAPILOGRAPH 1C). The capillary diameter was 2 mm, and the measurement temperature was 300 ℃, which was the injection molding temperature of the bonded magnet. The magnetic properties were measured with a vibrating sample magnetometer (RIKEN Electronics Co., Ltd. Model: BHV-55) after injection molding the pellet into a cylindrical shape (diameter of 5 mm, height of 5 mm) and magnetizing with a magnetic field of 4000 kA/m.

3.3 Results and discussion

3.3.1 HSPs of polyamide 6 resin

If the HSP of the polyamide 6 resin and the HSP of the magnet powder surface are close to each other, the resin will cover the magnet powder surface, so that the friction between the magnet powder can be reduced, and the flowability is expected to improve. Therefore, first, the HSP of the polyamide 6 resin was measured. Table 3-1 shows the HSP values and scores of the 33 solvents used for the measurement. The score was 1 when dissolved and 0 when not dissolved. There were five solvents in which the polyamide 6 resin was dissolved. Then, the good solvents and the poor solvents were divided according to the presence or absence of dissolution, and the HSP was calculated using the Hansen sphere method introduced in Section 1.1.3. The calculated HSPs were $(\delta_d, \delta_p, \delta_h)$ ¼ (17.4, 9.6, 12.0), and the fitting value was 0.921. The Hansen sphere of the polyamide 6 resin is shown in Figure 3-4. In this resin measurement, it was difficult to find a solvent that could dissolve the resin, so a relatively large number of solvents were used. However, as hexafluoroisopropanol is used for molecular weight analysis of polyamide resins, a solvent close to hexafluoroisopropanol was found relatively easily from Hansen's solvent list. The solvents close to hexafluoroisopropanol were 2-fluorophenol, 2,2,2-trifluoroethanol, p-chlorophenol, acetic acid and trifluoroacetic Acid. The HSP distances Ra with hexafluoroisopropanol were 5.00, 5.50, 6.47, 6.55 and 6.94. When I tested the solvents with similar HSP values, multiple solvents were found in which the polyamide was soluble. If more than one solvent is able to dissolve the polyamide, an increasingly accurate Hansen sphere can be obtained.
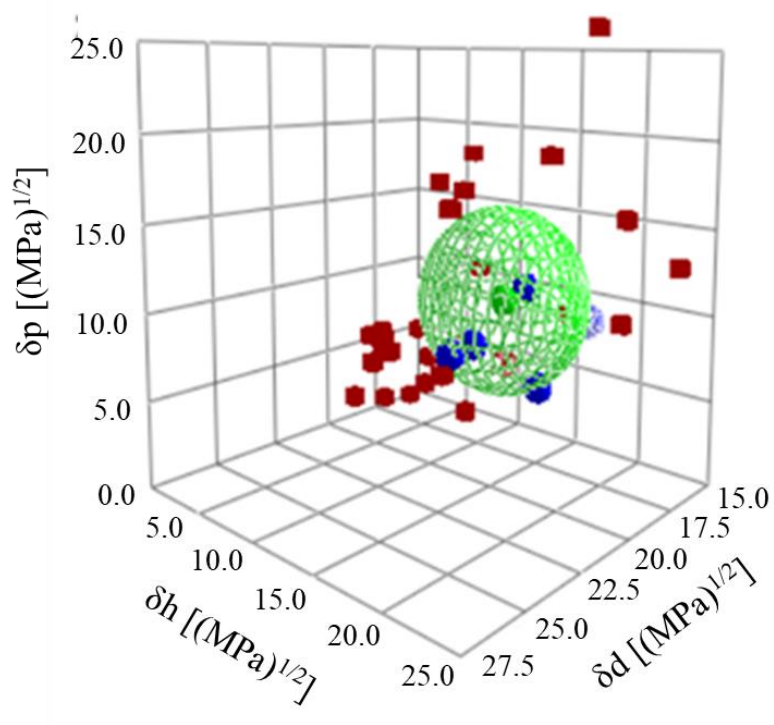
Figure 3-4. Hansen sphere for polyamide 6. Blue spheres are for "good" solvents, and red cubes are for "bad" solvents.

Table 3-1. Hansen solubility parameter of the solvent used for the dissolution test of polyamide 6 and the test result. Score = 1 means dissolution, Score = 0 means insoluble.

Solvents	δ_d $[(MPa)^{1/2}]$	δ_p $[(MPa)^{1/2}]$	δ_h $[(MPa)^{1/2}]$	Score
p-Chlorophenol	19.65	6.8	11.16	1
Trifluoroacetic Acid	15.6	9.7	11.4	1
Hexafluoro Isopropanol	17.2	4.5	14.7	1
2,2,2-Trifluoro Ethanol	15.4	8.3	16.4	1
2-Fluorophenol	18.27	6.83	10.83	1
Acetic Acid	14.5	8	13.5	0
Acetone	15.5	10.4	7	0
Acetonitrile	15.3	18	6.1	0
Aniline	20.1	5.8	11.2	0
Benzyl Alcohol	18.4	6.3	13.7	0
Bromobenzene	19.2	5.5	4.1	0
1-Bromonaphthalene	20.6	3.1	4.1	0
γ-Butyrolactone (GBL)	18	16.6	7.4	0
1-Chlorobutane	16.2	5.5	2	0
Chloroform	17.8	3.1	5.7	0
p-Chlorotoluene	19.1	6.2	2.6	0
o-Dichlorobenzene	19.2	6.3	3.3	0
Dimethyl Sulfoxide (DMSO)	18.4	16.4	10.2	0
1,4-Dioxane	17.5	1.8	9	0
Ethanol	15.8	8.8	19.4	0
Ethanolamine	17	15.5	21	0
Fluorobenzene	18.1	6.1	2	0
Formamide	17.2	26.2	19	0
Methanol	14.7	12.3	22.3	0

Table 3-1. (Continued)

Solvents	δ_d [(MPa)$^{1/2}$]	δ_p [(MPa)$^{1/2}$]	δ_h [(MPa)$^{1/2}$]	Score
N-Methyl Formamide	17.4	18.8	15.9	0
1-Methyl Imidazole	19.7	15.6	11.2	0
Octane	15.5	0	0	0
Quinoline	20.5	5.6	5.7	0
1,1,2,2-Tetrabromoethane	21	7	8.2	0
Tetrahydrofuran (THF)	16.8	5.7	8	0
Toluene	18	1.4	2	0
1,1,2-Trichloroethane	18.2	5.3	6.8	0
4-(Trifluoromethyl) Acetophenone	18.8	6.1	3.5	0

3.3.2 HSPs of coupling agents

Next, the HSP of the coupling agent was calculated by the group contribution method. If there is a correlation between the difference of the HSP of the coupling agent from that of the resin calculated from the group contribution method and the fluidity of the bonded magnet, the fluidity can be estimated from the coupling agent chemical structure, so this will become a very effective tool.

When the coupling agent is bound to the magnetic powder, the methyl group is detached, so HSPs were calculated only for the part excluding the methyl group. The calculated HSPs are shown in Table 3-2. Also described is the difference R_a between the HSPs of the polyamide 6 resin measured in Section 3.3.1 and the calculated HSPs of the coupling agent. When the calculated difference R_a was confirmed, UPTMS and ALTMS were estimated to be effective coupling agents because R_a with the polyamide 6 resin was small.

Table 3-2. Distance Ra between HSP of polyamide 6 by measurement and HSP of silane coupling agent calculated by group contribution method.

Coupling agent	δ_d $[(MPa)^{1/2}]$	δ_p $[(MPa)^{1/2}]$	δ_h $[(MPa)^{1/2}]$	δ_t $[(MPa)^{1/2}]$	Ra
ALTMS	16.5	7.6	8.9	18.9	4.1
APTMS	15.2	6.3	10.5	20.9	5.6
NPTMS	19.5	7	10.3	20.0	5.3
UPTMS	15.5	9.3	13.1	25.4	3.9

3.3.3 Surface state and HSPs of magnet powder

Next, the magnet powder was surface-treated with various coupling agents by the method described in Section 2.2. To confirm the surface condition, elemental analysis of the surface of the magnet powder was performed by XPS. Figure 3-5 shows the Si and N XPS peaks of the surfacetreated magnet powder. While there was no Si peak on the magnet powder without surface treatment, a Si peak was observed from the surface-treated magnet powder. Moreover, the nitrogen peak was confirmed from the magnet powder surface-treated by APTMS, NPTMS and UPTMS, which contained nitrogen in the molecular structure of the coupling agent. Furthermore, UPTMS containing two nitrogen atoms in the coupling agent had a slightly higher peak than APTMS and NPTMS, which contained one nitrogen atom in the coupling agent. From the above, it was confirmed that the coupling agent was present on the magnet powder, though qualitatively.
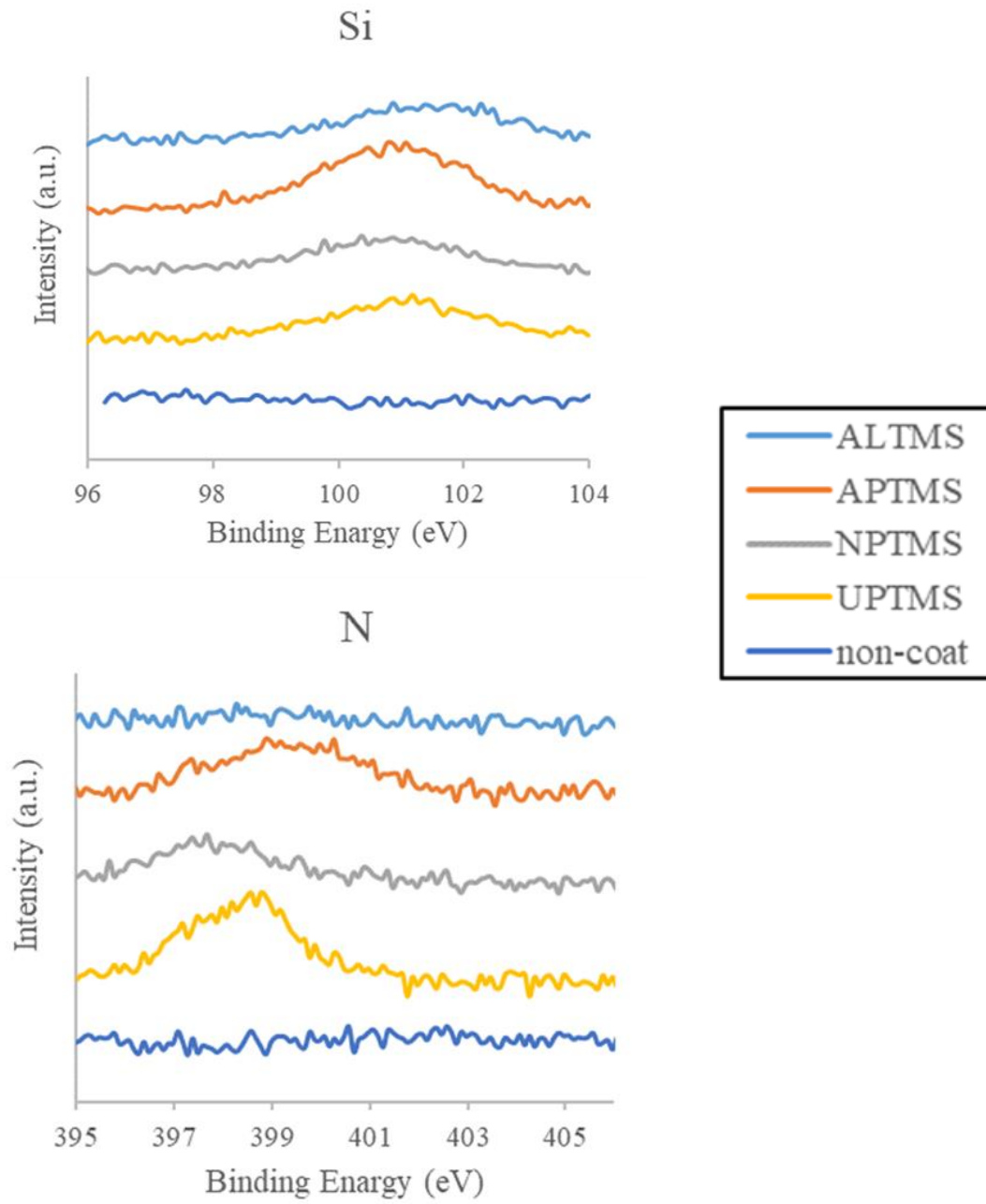
Figure 3-5. XPS spectra of magnet powder surface-treated with silane coupling agent.

Next, the HSPs of the surface-treated magnet powders were measured. First, Table 3-3 shows the measurement results of the 18 types of solvents used for the measurement and the respective magnet powders. The values of the density, viscosity and surface tension in Table 3-3 were taken from the literature [3-25], and used for calculation of the contact angle by using the Washburn equation. The threshold for separating the poor solvent from the good solvent at the contact angle was the median of the contact angle, and the score for the good solvent was 1 and that for the poor solvent was 0 [3-24]. HSPs were calculated from the Hansen sphere method described in Section 1.1.3 using the scores in Table 3-3. The results are shown in Table 3-4. Table 3-4 also shows the surface-treated HSPs, fitting values, and the differences Ra between the HSPs of the polyamide 6 resin and the HSPs of the measured magnet powder surface. The trend of Ra calculated from the actual measurements was the same as that for Ra calculated by the group contribution method. However, Ra calculated from the measured value was larger than Ra obtained from the group contribution method, and was somewhat distant from the resin HSPs. The HSPs measured on the surface of the magnet powder are shown in Figure 2-6. The calculated HSPs and HSPs of polyamide 6 resin are also shown in the figure. The group contribution method HSPs were closer to the polyamide 6 resin, and the measured value was located between the two values.

The calculated value by the group contribution method was calculated for the coupling agent alone. For this reason, the magnetic powder coated with the coupling agent and the coupling agent alone were in different states. Therefore, the true value of HSPs was not the same value in the first place. However, since the surface HSPs of the magnetic powder after the coupling treatment were considered to be close to the HSPs of the coupling agent, it was considered to be effective to estimate the effect with the calculated value of the coupling agent. In addition, the HSPs on the surface of the magnetic powder were considered to change if the coating state of the coupling agent was different. Therefore, as

the coupling agent coverage on the magnet powder increased, the measured value approached the calculated HSPs of the coupling agent.

Although there was a variation, the measured value approached the coupling agent side. Among the coupling agents investigated, the magnet powder treated with UPTMS showed the smallest value of Ra ¼ 4.9.

Table 3-3. Various properties of the solvent used for HSP measurement of the magnet powder surface, and the measurement results.

Solvents	δ_d [(MPa)$^{1/2}$]	δ_p [(MPa)$^{1/2}$]	δ_h [(MPa)$^{1/2}$]	Density kg/m^3	Viscosity mPa·s	Surface tension mN/m	Non-coat Contact angle °	Non-coat Score -	ALTMS Contact angle °	ALTMS Score -	APTMS Contact angle °	APTMS Score -	NPTMS Contact angle °	NPTMS Score -	UPTMS Contact angle °	UPTMS Score -
o-Dichlorobenzene	19.2	6.3	3.3	1306	1.324	26.8	32	1	37	1	42	1	39	1	31	1
Nitrobenzene	20	10.6	3.1	1204	2.010	43.4	50	1	54	0	69	0	54	1	52	1
Benzyl Benzoate	20	5.1	5.2	1114	8.450	49.0	54	1	61	0	77	0	56	1	46	1
Bromobenzene	19.2	5.5	4.1	1495	1.130	36.2	55	1	87	0	51	0	55	1	87	0
Ethyl Acetate	15.8	5.3	7.2	901	0.449	23.8	57	0	60	0	43	1	60	0	60	0
Toluene	18	1.4	2	867	0.587	28.5	62	0	54	0	47	1	56	1	56	0
Aniline	20.1	5.8	11.2	1022	4.429	42.8	63	0	52	1	62	0	48	1	48	1
γ-Butyrolactone (GBL)	18	16.6	7.4	1125	1.700	44.6	63	0	57	0	81	0	59	0	59	0
2-Butanone	16	9	5.1	800	0.365	24.0	64	0	60	0	49	1	64	0	62	0
Tetrahydrofuran (THF)	16.8	5.7	8	889	0.550	26.4	64	0	52	1	33	1	56	1	55	1
N-Methyl-2-Pyrrolidone (NMP)	18	12.3	7.2	1028	1.650	41.0	64	0	54	0	67	0	59	0	55	1
Pyridine	19	8.8	5.9	983	0.952	36.9	64	0	59	0	56	0	61	0	59	0
Acetone	15.5	10.4	7	785	0.316	23.7	64	0	59	0	54	0	64	0	63	0
1,4-Dioxane	17.5	1.8	9	1034	1.310	36.9	65	0	57	0	50	0	57	0	58	0
Quinoline	20.5	5.6	5.7	1090	3.635	42.6	66	0	30	1	57	0	33	1	60	0
Dimethyl Sulfoxide (DMSO)	18.4	16.4	10.2	1096	1.996	42.9	68	0	55	0	85	0	61	0	63	0
Dimethyl Formamide (DMF)	17.4	13.7	11.3	944	0.802	35.2	71	0	55	0	64	0	59	0	59	0
Chloroform	17.8	3.1	5.7	1490	0.563	27.1	55	1	62	0	49	1	58	0	57	0

Table 3-4. Distance R_a between surface-treated magnet powder HSPs and polyamide 6 resin HSPs.

Product number	δ_d [(MPa)$^{1/2}$]	δ_p [(MPa)$^{1/2}$]	δ_h [(MPa)$^{1/2}$]	δ_t [(MPa)$^{1/2}$]	Fitting	Ra
ALTMS	19.7	6.6	8.3	18.9	0.89	6.7
APTMS	16.4	5.9	3.2	20.9	1.00	9.8
NPTMS	19.3	5.4	5.6	20.0	0.89	8.6
UPTMS	18.6	9.4	7.9	25.4	0.89	4.9
Non-coat	19.6	7.4	2.2	21.1	0.94	11.1
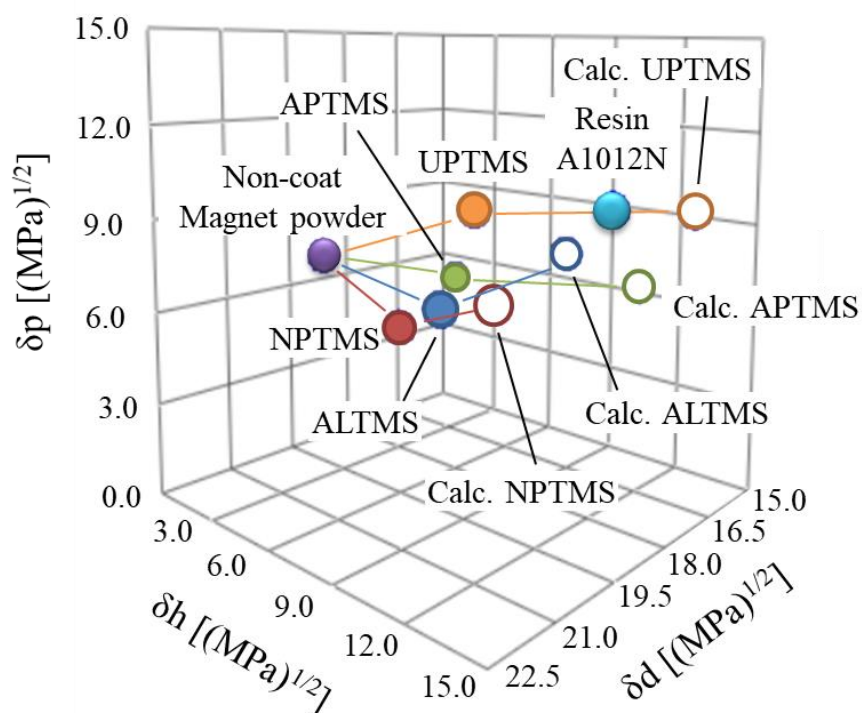
Figure 3-6. Positional relationship in HSP space between HSP of coupling agent calculated by group contribution method and HSP measurement value of coupling treated magnetic powder.

3.3.4 Bonded magnet flowability and HSP comparison

Bonded magnet pellets were prepared from each of the surfacetreated magnet powders according to the bonded magnet manufacturing method of Section 3.2.2, and the fluidity was measured using a capillary rheometer. The measured shear rate and viscosity values are shown in Table 3-5. The relationship between the shear rate and shear viscosity is shown in Figure 3-7. Compared with the pellet without surface treatment, the pellet using the surface-treated magnet powder had a lower viscosity and improved fluidity. Among them, UPTMS showed the best viscosity, and the tendency was consistent with the calculated HSPs and the measured HSPs.

Table 3-5. Measurement values of shear rate and shear viscosity of bonded magnet materials treated with various coupling agents.

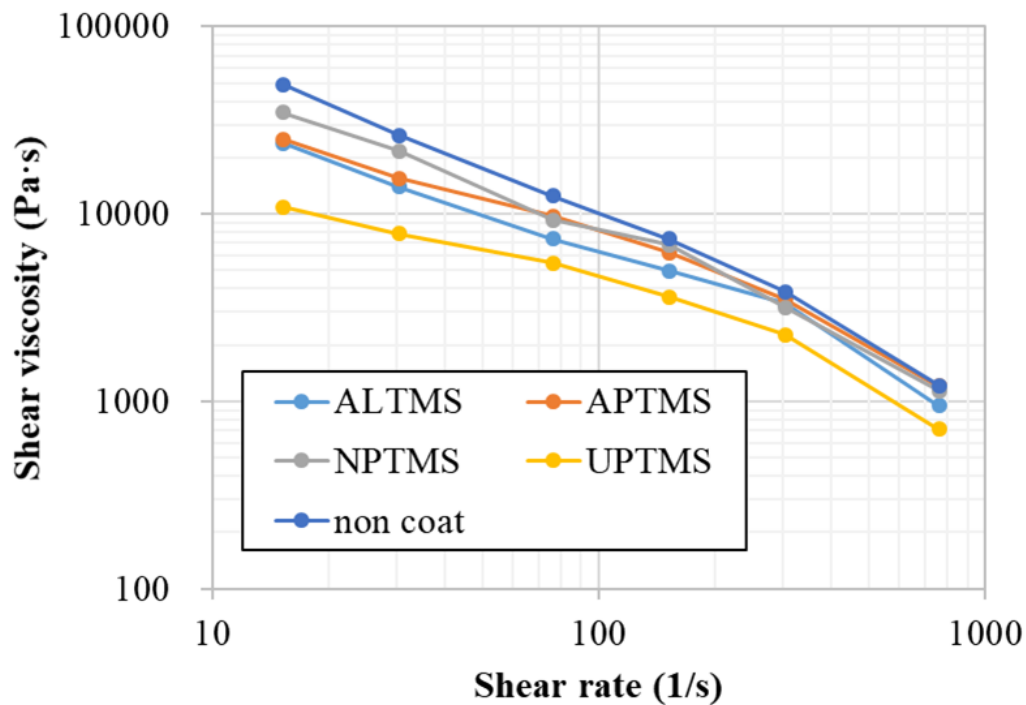| Shear rate [1/s]	Shear viscosity				
	ALTMS [Pa·s]	APTMS [Pa·s]	NPTMS [Pa·s]	UPTMS [Pa·s]	non coat [Pa·s]
15.2	23854	25008	34809	10913	49292
30.4	13971	15460	21756	7836	26392
76	7371	9731	9261	5459	12461
152	4993	6228	6876	3612	7393
304	3336	3537	3188	2277	3843
760	946	1205	1142	713	1221

Figure 3-7. Relationship between shear rate and shear viscosity of bonded magnet materials treated with various coupling agents.

For a detailed analysis, the relationship between the difference of the HSP for the magnet powder surface and the HSP of polyamide 6 resin and the shear viscosity is shown in Figures 3-8 and 3-9. Figure 3-8 shows HSPs of coupling agents according to the group contribution method, and Figure 3-9 shows the measured HSPs. Part (a) in each figure shows the shear viscosity at a shear rate of 15.2/s, and part (b) shows the shear viscosity at a shear rate of 760/s. A graph of the two shear rates is shown as a visual representation. The correlation coefficient between the HSP distance Ra at each shear rate and the shear viscosity of the bonded magnet material was calculated. Table 3-6 shows the calculated correlation coefficients. The correlation coefficient from the HSPs of coupling agents calculated by the group contribution method was as high as 0.66 to 0.90. Furthermore, the correlation coefficient from the HSPs of the surface-treated magnet powder by actual measurement was

0.87–0.98, which was a higher value. From this result, if the HSPs of the coupling agent is calculated by the group contribution method and the HSPs difference from the matrix resin is determined, the influence on the fluidity of the bonded magnet can be roughly understood. In addition, if the surface-treated magnet powder is actually measured, the influence on the flowability can be evaluated more accurately. However, on occasion, the measured HSPs differed from the calculated HSPs, and the deviation was sometimes large. A future topic will be to clarify the difference between HSPs for the coupling agent alone and the state where it is surface-treated with the filler, and the relationship between surface coverage and HSPs.

Finally, the density and magnetic properties of each bonded magnet were evaluated. The results are shown in Table 2-7. From these results, it can be seen that the surface-treated bonded magnets had no significant difference in density and magnetic properties, and that only the fluidity was improved by the surface treatment.
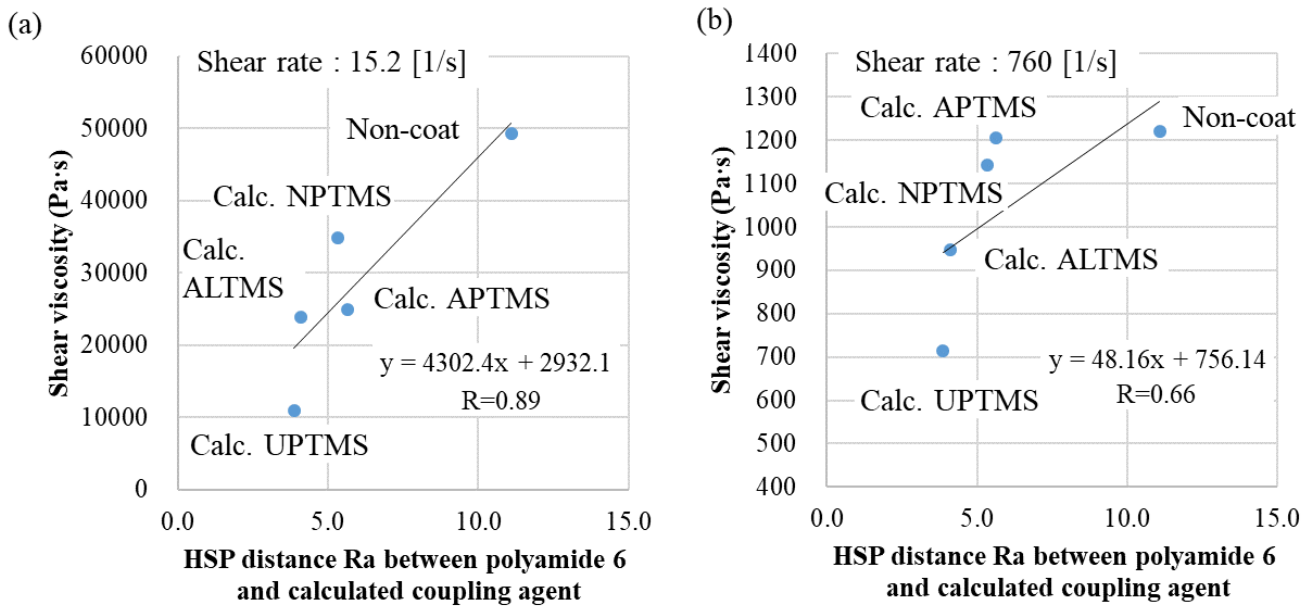
Figure 3-8. Relationship between HSP distance R_a and shear viscosity of the bonded magnet material. This HSP distance R_a is the distance between polyamide 6 and the coupling agent calculated by the group contribution method. (a) At a shear rate of 15.2 [1 / s], and (b) at a shear rate of 760 [1 / s].
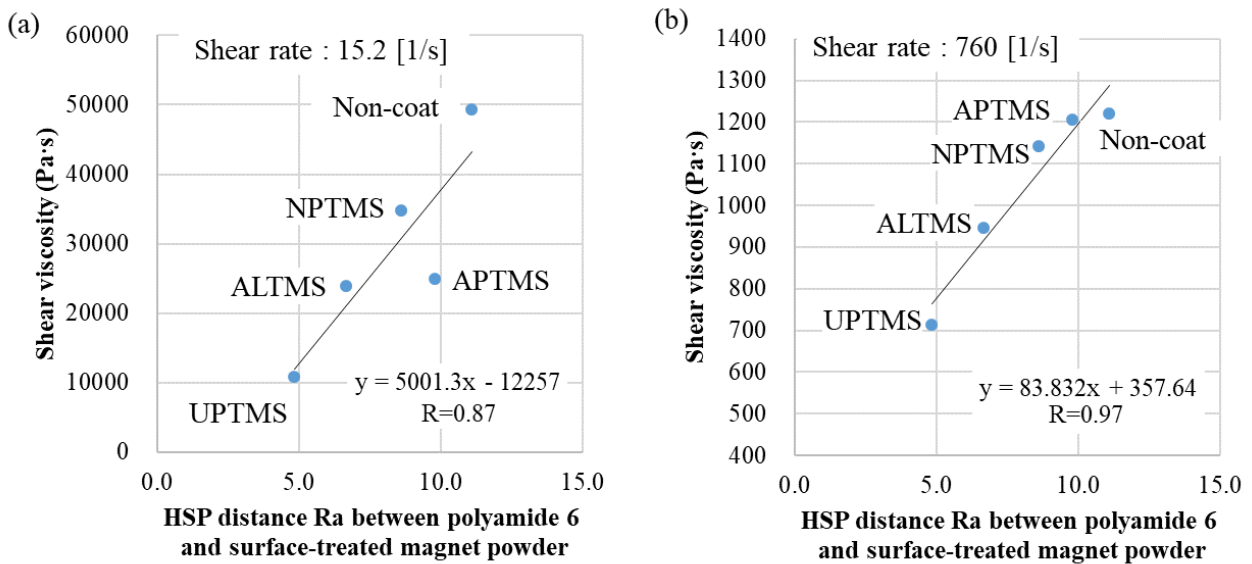

Figure 3-9. Relationship between HSP distance R_a and shear viscosity of the bonded magnet material. This HSP distance R_a is the distance between polyamide 6 and the surface-treated magnet powder measured by the capillary penetration method. (a) At a shear rate of 15.2 [1 / s], and (b) is at a shear rate of 760 [1 / s]

71

Table 3-6. Correlation coefficient between HSP distance R_a at each shear rate and shear viscosity of the bonded magnet material.

Shear rate	Correlation coefficient of HSP distance Ra and shear viscosity	
[1/s]	Calculated	Measured
15.2	0.89	0.87
30.4	0.83	0.87
76	0.90	0.98
152	0.75	0.94
304	0.70	0.90
760	0.66	0.97

Table 3-7. Density and Magnetic Properties of Bonded Magnets Treated with Various Coupling Agents.

	Density	B_r	H_{cJ}	$(BH)_{max}$
	[kg/m^3]	[mT]	[kA/m]	[kJ/m^3]
ALTMS	5703	608	405	61
APTMS	5825	620	406	63
NPTMS	5771	617	409	63
UPTMS	5824	623	414	64
non-coat	5716	611	404	62

3.3.5 Conclusion

HSPs were applied for the evaluation of surface treatment agents for composite materials. If there is a correlation between the HSPs easily calculated from the chemical structure of the surface treatment agent and the performance of the composite material, or if there is a correlation between the HSPs of the filler surface and the performance of the composite material, design will become theoretical and easy.

In this paper, I applied HSPs to the coupling agent treatment of a bonded magnet to the magnet powder surface and verified its effect. As a result, there is a correlation between the HSPs and fluidity calculated from the chemical structure of the coupling agent, and the fluidity of the bonded magnet can be predicted from the chemical structure of the coupling agent. Furthermore, it was found that when the HSPs of the coupling-treated magnetic powder are measured, the influence on the fluidity can be evaluated more accurately. However, in certain cases, the measured HSP differs from the calculated HSPs and the deviation was sometimes large. A future strategy will be to clarify the difference between HSPs for the coupling agent alone and the state where it is surfacetreated with the filler, and the relationship between surface coverage and HSPs.

Compared with the published research, this paper reports a series of evaluations of HSP measurements of surface-treated material and property measurements of composite material obtained from HSPs calculation by the group contribution method of a surface treatment agent. Furthermore, I expect that the number of HSP applications will increase for composite materials other than as bonded magnets.

3.3.6 References

[3-1] X.W. Li, R.G. Song, Y. Jiang, C. Wang, D. Jiang, Surface modification of TiO$_2$ nanoparticles and its effect on the properties of fluoropolymer/TiO$_2$ nanocomposite coatings, Appl. Surf. Sci. 276 (2013) 761–768.

[3-2] S. Kango, S. Kalia, A. Celli, J. Njuguna, Y. Habibi, R. Kumar, Surface modification of inorganic nanoparticles for development of organic-inorganic nanocomposites - A review, Prog. Polym. Sci. 38 (2013) 1232–1261.

[3-3] S.H. Wang, Y. Sen Sun, A.S.T. Chiang, H.F. Hung, M.C. Chen, K. Wood, Carboxylic acid-directed clustering and dispersion of ZrO2 nanoparticles in organic solvents: A study by small-angle x-ray/neutron scattering and NMR, J. Phys. Chem. C. 115 (2011) 11941–11950.

[3-4] Z.M. Dang, Y.J. Xia, J.W. Zha, J.K. Yuan, J. Bai, Preparation and dielectric properties of surface modified TiO 2/silicone rubber nanocomposites, Mater. Lett. 65 (2011) 3430–3432.

[3-5] S. Mallakpour, A. Barati, Efficient preparation of hybrid nanocomposite coatings based on poly(vinyl alcohol) and silane coupling agent modified TiO2 nanoparticles, Prog. Org. Coatings. 71 (2011) 391–398.

[3-6] W. Zhou, Effect of coupling agents on the thermal conductivity of aluminum particle/epoxy resin composites, J. Mater. Sci. 46 (2011) 3883–3889.

[3-7] W. Chuang, J. Geng-sheng, P. Lei, Z. Bao-lin, L. Ke-zhi, W. Jun-long, Influences of surface modification of nano-silica by silane coupling agents on the thermal and frictional properties of cyanate ester resin, Results Phys. 9 (2018) 886–896.

[3-8] I. Jang, K.H. Shin, I. Yang, H. Kim, J. Kim, W.H. Kim, S.W. Jeon, J.P. Kim, Enhancement of thermal conductivity of BN/epoxy composite through surface modification with silane coupling agents, Colloids Surfaces A Physicochem. Eng. Asp. 518 (2017) 64–72.

[3-9] Q. Chen, J. Asuncion, J. Landi, B.M. Ma, The effect of the coupling agent on the packing density and corrosion behavior of NdFeB and SmCo bonded magnets, J. Appl. Phys. 85 (2002) 5684–5686.

[3-10] J.U. Otaigbe, J. Xiao, H. Kim, S. Constantinides, Influence of filler surface treatments on processability and properties of polymer-bonded Nd-Fe-B magnets, J. Mater. Sci. Lett. 18 (1999) 329–332.

[3-11] J. H.Hildebrand, R. L.Scott, The Solubility of Nonelectrolytes, 3rd ed.; Dover Publications Inc.: New Yoke, (1950).

[3-12] C. M.Hansen, Hansen Solubility Parameters: A User's Handbook; CRC Press: Boca Raton, FL, (1999).

[3-13] C.M. Hansen, A.L. Smith, Using Hansen solubility parameters to correlate solubility of C 60 fullerene in organic solvents and in polymers, Carbon N. Y. 42 (2004) 1591–1597.

[3-14] H.T. Ham, Y.S. Choi, I.J. Chung, An explanation of dispersion states of single-walled carbon nanotubes in solvents and aqueous surfactant solutions using solubility parameters, J. Colloid Interface Sci. 286 (2005) 216–223.

[3-15] S. Acevedo, A. Castro, E. Vásquez, F. Marcano, M.A. Ranaudo, Investigation of physical chemistry properties of asphaltenes using solubility parameters of asphaltenes and their fractions A1 and A2, Energy and Fuels. 24 (2010) 5921–5933.

[3-16] T. Sato, S. Araki, M. Morimoto, R. Tanaka, H. Yamamoto, Comparison of hansen solubility parameter of asphaltenes extracted from bitumen produced in different geographical regions, Energy and Fuels. 28 (2014) 891–897.

[3-17] T. Sato, Y. Hamada, M. Sumikawa, S. Araki, H. Yamamoto, Solubility of oxygen in organic solvents and calculation of the Hansen solubility parameters of oxygen, Ind. Eng. Chem. Res. 53 (2014) 19331–19337.

75

[3-18] J.U. Wieneke, B. Kommob, O. Gaer, I. Prykhodko, M. Ulbricht, Systematic investigation of dispersions of unmodified inorganic nanoparticles in organic solvents with focus on the hansen solubility parameters, Ind. Eng. Chem. Res. 51 (2012) 327–334.

[3-19] S.H. Wang, J.H. Liu, C.T. Pai, C.W. Chen, P.T. Chung, A.S.T. Chiang, S.J. Chang, Hansen solubility parameter analysis on the dispersion of zirconia nanocrystals, J. Colloid Interface Sci. 407 (2013) 140–147.

[3-20] X. Su, B. Shi, Effect of silane coupling agents with different non-hydrolytic groups on tensile modulus of composite PDMS crosslinked membranes, React. Funct. Polym. 98 (2016) 1–8.

[3-21] N. Fujiwara, S. Imai, H. Yamamoto, Evaluation of the influence of fine particle surface modification with the Hansen solubility parameters, Mater. Chem. Phys. 229 (2019) 139–148.

[3-22] S. Tsutsumi, K. Kondo, Y. Kato, N. Fujiwara, H. Yamamoto, Determination of Hansen solubility parameters of particles using a capillary penetration method, Chem. Phys. 521 (2019) 115–122.

[3-23] M. Levin, P. Redelius, Determination of three-dimensional solubility parameters and solubility spheres for naphthenic mineral oils, Energy and Fuels. 22 (2008) 3395–3401.

[3-24] S. Süß, T. Sobisch, W. Peukert, D. Lerche, D. Segets, Determination of Hansen parameters for particles: A standardized routine based on analytical centrifugation, Adv. Powder Technol. 29 (2018) 1550–1561.

[3-25] Organic Synthetic Chemistry Association, Solvents Pocket Book, Ohmsha Ltd., Tokyo, (1967).

Chapter 4 Hansen solubility parameters of pollen particle surface

4.1 Introduction

Pollen from species such as cedar and ragweed can negatively affect human health, and this is a problem around the world. It has been suggested that 20%−30% of people in developed countries suffer from pollen allergies [4-1]. Ragweed and rice pollen are common causes of allergies in Europe and the USA, and cedar and cypress pollen are common causes of allergies in Japan [4-2,4-3,4-4,4-5,4-6,4-7].

Pollen counts have been monitored to allow people to take measures to protect themselves from pollen [4-8]. Studies of the effects of removing pollen from air using air purifiers [4-9], pollen filters [4-10], and nasal filters [4-11] have also been performed. The possibility of preventing exposure to pollen by repelling the pollen using electrostatic barriers has also been studied [4-12]. Studies of methods of alleviating allergic symptoms using antihistamines [4-13], immunotherapy [4-14], and other methods have also been performed.

I have focused on efficiently collecting pollen to avoid the pollen becoming dispersed. Achieving this requires the physical properties of the pollen surfaces to be understood, to allow efficient air cleaners and pollen-collection mists to be designed. I therefore investigated the surface properties of pollen particles by determining the Hansen solubility parameters (HSPs) of the surfaces.

The solubility parameter δ_t as cohesive energy density is a physical property defined by Hildebrand et al. as an index representing the affinity of the chemical of interest for another [4-15]. Hansen defined HSPs (which are physical properties) as the δ_t divided into three components describing the affinities of the chemical of interest for various other substances [4-16]. HSPs have attracted attention in the carbon material field and petroleum and gas research field as universal parameters for evaluating affinities between materials [4-17,4-18,4-19,4-20,4-21]. HSPs have also recently been used to evaluate the affinities of surfaces for other

77

substances, and the HSPs of titanium oxide and zirconia surfaces have been determined [4-22, 4-23].

The HSPs of nanoparticles are currently measured by making sedimentation velocity measurements and dynamic light scattering measurements. However, sedimentation velocity measurements and dynamic light scattering measurements are not suitable for evaluating pollen particles with diameters of 10–60 μm and complicated shapes. I therefore developed a method for measuring HSPs based on the capillary penetration method. This method can be used to make measurements regardless of the shapes and sizes of the particles of interest [4-24]. In the study described here, I measured the HSPs of cedar and cypress pollen, which cause health problems in Japan, to determine the affinities of these types of pollen for various liquids and mixtures.

4.2　Material and methods

4.2.1　Material

Measurements were made using cedar pollen and cypress pollen (obtained from Yamizo Pollen Research Group, Ibaraki, Japan) collected in Taizo Town, Kuji-gun, Ibaraki Prefecture, Japan. The pollen sample was already dried and frozen to prevent mold. Therefore, it was left at room temperature for 60 min just before the experiment and thawed. Freezing at the Yamizo Pollen Research Group was performed as follows. The pollen samples were dried, passed through a 53 μm sieve to remove foreign particles with diameters >53 μm, dehumidified at a humidity of 10% or less, and then frozen and stored. Scanning electron micrographs of the cedar pollen and cypress pollen are shown in Figure 4-1. The micrographs were acquired using a S-4800 scanning electron microscope (Hitachi High-Technologies Corp., Tokyo, Japan). The particle size distributions are shown in Figure 4-2. The particle size distributions were determined using a SALD-2100 laser diffraction particle size analyzer (Shimadzu Corp., Kyoto, Japan). The particle size

distribution for each pollen sample was determined in triplicate. The mean cedar pollen particle diameter was 28.4 μm, and the standard deviation was 0.36 μm. The mean cypress pollen particle diameter was 23.7 μm, and the standard deviation was 0.31 μm. The densities of the pollen samples were determined using an AccuPyc II 1340 V 2.0 dry-type automatic density meter (Shimadzu Corp.). The density of each pollen sample was determined 10 times. The cedar pollen density was 1393.4 kg/m^3, and the standard deviation was 1.4 kg/m^3. The cypress pollen density was 1413.6 kg/m^3, and the standard deviation was 1.1 kg/m^3. Fouriertransform infra-red spectra of the cedar and cypress pollen samples are shown in Figure 4-3. Cedar and cypress pollen had very similar spectra.
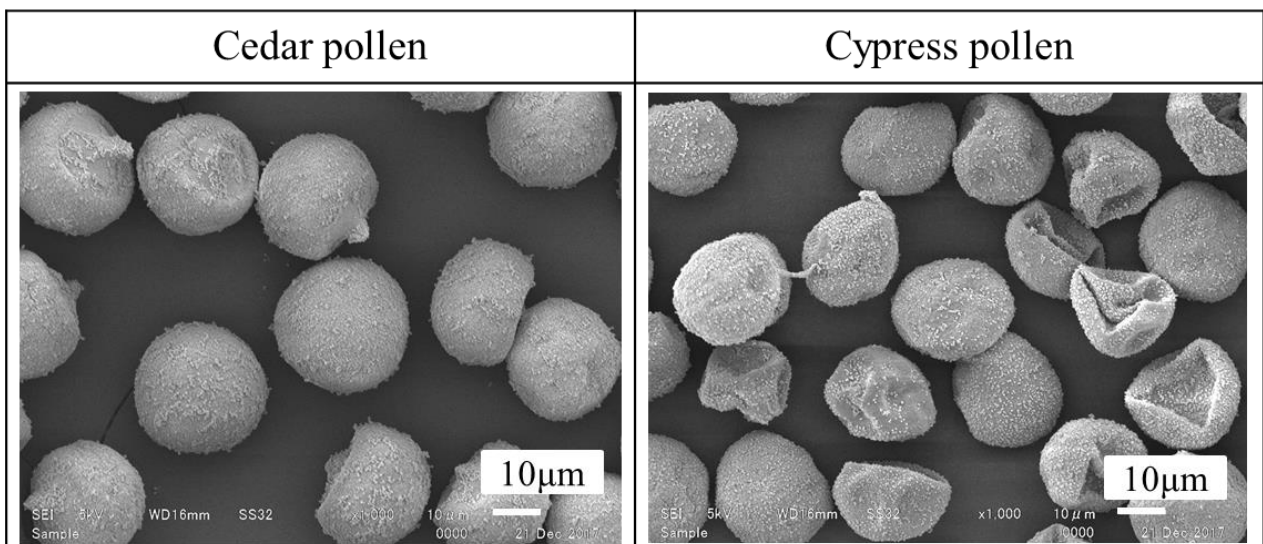

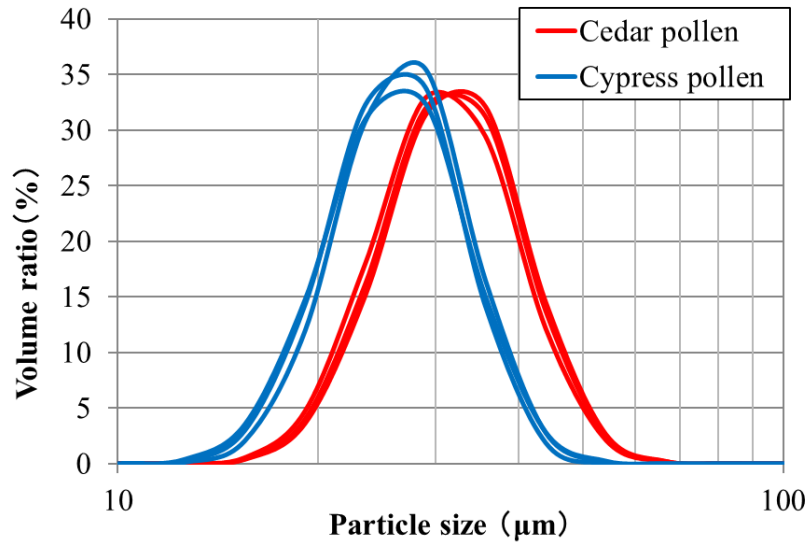Figure 4-1. Electron micrographs of cedar pollen and cypress pollen.

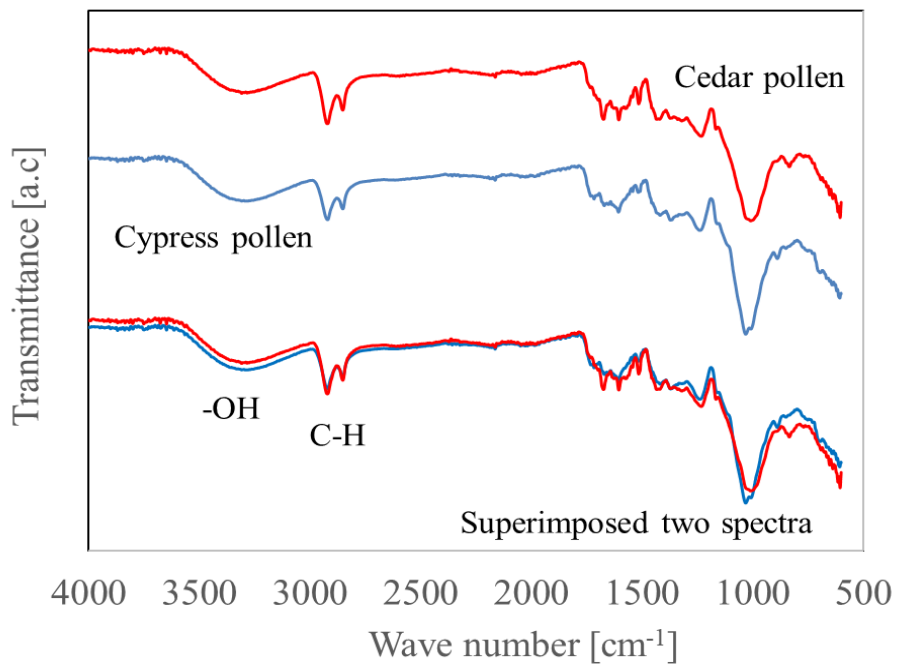Figure 4-2. Particle size distributions of cedar pollen and cypress pollen

Figure 3. Fourier-transform infra-red spectra of cedar pollen and cypress pollen

4.2.2　Measureing pollen HSPs

The HSPs of each pollen sample were determined by measuring the contact angles for different solvents using the capillary penetration method. The contact angle threshold values for a poor solvent and good solvent were then determined, and the HSPs were determined using the Hansen dissolution sphere method. The capillary penetration method is described first. A pollen sample was placed in an iron container and compressed. To obtain a stable measurement, the compression pressure was first determined. Packing volume when pollen is compressed at each pressure are shown in Figure 4-4. When both pollen pressures were over 500 MPa, the packing volume was saturated. Therefore, the packing pressure was set to 500 MPa so that the variation of the packing volume is reduced. The iron container was 70 mm high, had an inner diameter of 10 mm, and had a hole with a diameter of 8 mm on the lower surface to allow solvent to enter. Tests were performed using 26 organic solvents. In each test, the solvent of interest was allowed to enter the container and the mass of solvent that had penetrated the sample was determined at 1 s intervals. The effective radius r of each capillary in the capillary bundle is difficult to measure. Therefore, assuming that the contact angle of the solvent with the best wettability with respect to pollen is 30°, r was calculated backward using Equation 2-1. The method used to determine r is described in detail here. When measuring the HSPs using the capillary penetration method, poor solvents and good solvents can be identified if the relative contact angles of the solvents are known, and this allows the HSPs to be calculated. The relative contact angle can be determined if the reference solvent contact angle is arbitrarily set and r is determined. However, when determining r, setting the contact angle of the solvent with the best wettability to a small value will increase the measurement variation of the contact angle. The contact angle of the reference solvent was therefore changed, and the difference between the two measured contact angles was determined. The point at which the difference was at a minimum was defined as the realistic contact angle. This contact angle was 30°. The contact angles for the different solvents would have remained in the same order

whatever reference solvent contact angle was used, so the reference solvent contact angle used will not have affected the HSPs that were calculated. This method is described in detail in the results and discussion sections of 4.4.1.

The contact angle was calculated using equation 2-1, and the poor solvent and good solvent thresholds were determined, then the HSPs were determined using the Hansen solubility sphere method. The contact angle threshold was not arbitrary, and was set as described next. An appropriate contact angle threshold was determined after assessing the contact angles for various solvents and the distances Ra between the HSPs for various solvents and the pollen HSPs. The contact angle will have been small when the affinity between the pollen and solvent was high. The distance Ra between the HSPs for a solvent and pollen will have been small when the solvent and pollen had a strong affinity for each other. Therefor the contact angle and Ra will have correlated, and the contact angle threshold is more appropriate when the correlation coefficient was higher. To confirm all the correlation coefficient, the HSPs for the pollen surfaces were calculated for all thresholds. The distances Ra between the pollen surface HSPs and the HSPs for various solvents were then calculated. The threshold with the highest correlation coefficient was selected in the correlation coefficient between Ra and contact angle. The contact angle calculation method is also described in detail in the results and discussion sections of 4.4.1.

Finally, the Hansen dissolution sphere method was performed. The HSPs for the solvents used in the capillary penetration method were plotted on a 3D graph. The smallest radius sphere (Hansen sphere) was created with the data for a good solvent within the sphere and the data or a poor solvent outside the sphere. The coordinates for the center of the sphere were defined as the HSPs for the target substance.
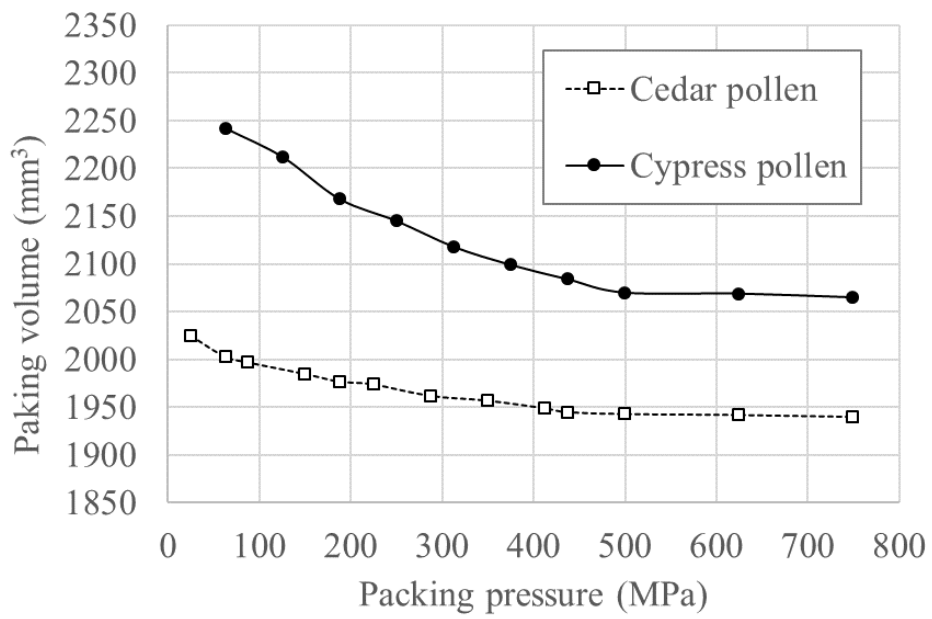
Figure 4-4. Relationships between the packing pressure and packing volume for cedar and cypress pollen particles

4.3　Reasults

4.3.1　Cedar and cypress pollen measurements

　The solvents used to measure the cedar pollen and cypress pollen HSPs are shown in Table 4-1. The densities, viscosities, and surface tensions shown in Table 4-1 were taken from the literature [4-25]. The contact angle measurement for each solvent was performed twice, and the results are shown in Table 4-1. The contact angles in Table 4-1 were calculated by determining r as described next. The difference between the contact angles found when the two cedar pollen measurements were made using 1-nonanol and the difference between the contact angles found when the two cypress pollen measurements were made using 1-nonanol are shown in Figure 4-5. The contact angle variation for both cedar and cypress pollen decreased at about 30°, so the contact angle for 1-nonanol was set to 30°. Next, r was calculated backwards with a contact angle of 30°. The r for cedar pollen was 1.4 μm, and the r for cypress pollen was 1.6 μm. The contact angle for each solvent was calculated using these r values and equation 2-1.

Table 4-1. Solvent data and parameters used to calculate the Hansen solubility parameters for cedar pollen and cypress pollen

	Hansen solubility parameter			Density	Viscosity	Surface tension	Cedar pollen				Cypress pollen			
	δ_d (MPa)$^{1/2}$	δ_p (MPa)$^{1/2}$	δ_h (MPa)$^{1/2}$	kg/m^3	mPa·s	mN/m	Contact angle			Score	Contact angle			Score
							1	2	Ave		1	2	Ave	
1-Nonanol	16.0	4.8	11.0	812.1	14.300	27.71	30.0	30.6	30.3	1	32.0	30.0	31.0	1
1-Octanol	16.0	5.0	11.2	824.0	8.925	27.53	44.8	42.6	43.7	1	57.8	58.9	58.3	1
1-Heptanol	16	5.3	11.7	823.0	5.810	23.03	51.4	50.5	51.0	1	55.5	58.5	57.0	1
1-Hexanol	15.9	5.8	12.5	819.0	5.200	23.60	53.8	52.9	53.4	1	61.2	60.4	60.8	1
1-Decanol	16.0	4.7	10.5	829.7	13.800	28.01	55.7	53.7	54.7	1	58.3	56.6	57.5	1
1-Undecanol	16.1	3.9	9.9	833.4	17.200	26.74	54.1	56.8	55.5	1	57.0	59.6	58.3	1
1-Butanol	16	5.7	15.8	810.0	3.000	23.80	62.3	61.5	61.9	0	60.7	62.3	61.5	0
1-Pentanol	15.9	5.9	13.9	814.4	3.600	25.60	63.5	65.3	64.4	0	67.0	67.8	67.4	0
1-Methoxy-2-propanol	15.6	6.3	11.6	923.4	1.750	27.10	63.3	67.5	65.4	0	67.9	67.3	67.6	0
1-propanol	16	6.8	17.4	803.0	1.938	23.71	67.9	67.1	67.5	0	71.1	71.0	71.1	0
Ethanol	15.8	8.8	19.4	789.3	1.060	22.10	72.7	72.5	72.6	0	75.6	75.2	75.4	0
Tetrahydrofuran	16.8	5.7	8.0	889.2	0.550	26.40	73.7	74.9	74.3	0	73.4	73.5	73.4	0
Acetone	15.5	10.4	7.0	785.0	0.316	23.70	77.4	76.9	77.1	0	76.4	76.4	76.4	0

Table 4-1. (Continued)

| | Hansen solubility parameter | | | Density | Viscosity | Surface tension | Cedar pollen | | | | Cypress pollen | | | |
| | δ_d $(MPa)^{1/2}$ | δ_p $(MPa)^{1/2}$ | δ_h $(MPa)^{1/2}$ | kg/m^3 | $mPa \cdot s$ | mN/m | Contact angle | | | Score | Contact angle | | | Score |
							1	2	Ave		1	2	Ave	
Ethyl acetate	15.8	5.3	7.2	900.6	0.449	23.75	77.8	76.9	77.4	0	74.7	76.4	75.6	0
Dimethyl Formamide	17.4	13.7	11.3	944.0	0.802	35.20	79.4	76.0	77.7	0	81.2	80.7	80.9	0
1,4-Dioxane	17.5	1.8	9.0	1033.8	1.310	36.90	79.4	79.4	79.4	0	80.9	81.3	81.1	0
1-Dodecanol	16.0	4.0	9.3	824.3	7.520	27.65	79.3	80.5	79.9	0	80.4	81.1	80.8	0
Methanol	14.7	12.3	22.3	791.3	0.595	22.55	81.2	82.6	81.9	0	83.9	83.8	83.8	0
N-Methyl Formamide	17.4	18.8	15.9	1000.0	1.650	39.50	80.9	83.1	82.0	0	82.6	82.6	82.6	0
Toluene	18.0	1.4	2.0	866.9	0.587	28.53	82.6	82.6	82.6	0	82.9	83.0	82.9	0
1-Methyl-2-pyrrolidone	18.0	12.3	7.2	1027.9	1.650	41.00	85.1	83.9	84.5	0	86.2	85.7	86.0	0
Benzyl Alchol	18.4	6.3	13.7	1045.0	5.582	39.71	89.8	89.7	89.7	0	89.9	90.0	89.9	0
Aniline	20.1	5.8	11.2	1022.0	4.429	42.79	90.0	90.0	90.0	0	90.0	90.0	90.0	0
γ- Butyrolactone	18.0	16.6	7.4	1125.4	1.700	44.60	90.0	90.0	90.0	0	90.0	90.0	90.0	0
Salicylaldehyde	19.0	10.5	12.0	1146.0	2.500	49.00	90.0	90.0	90.0	0	90.0	90.0	90.0	0
Nitrobenzene	20.0	10.6	3.1	1203.7	2.010	43.35	90.0	90.0	90.0	0	90.0	90.0	90.0	0
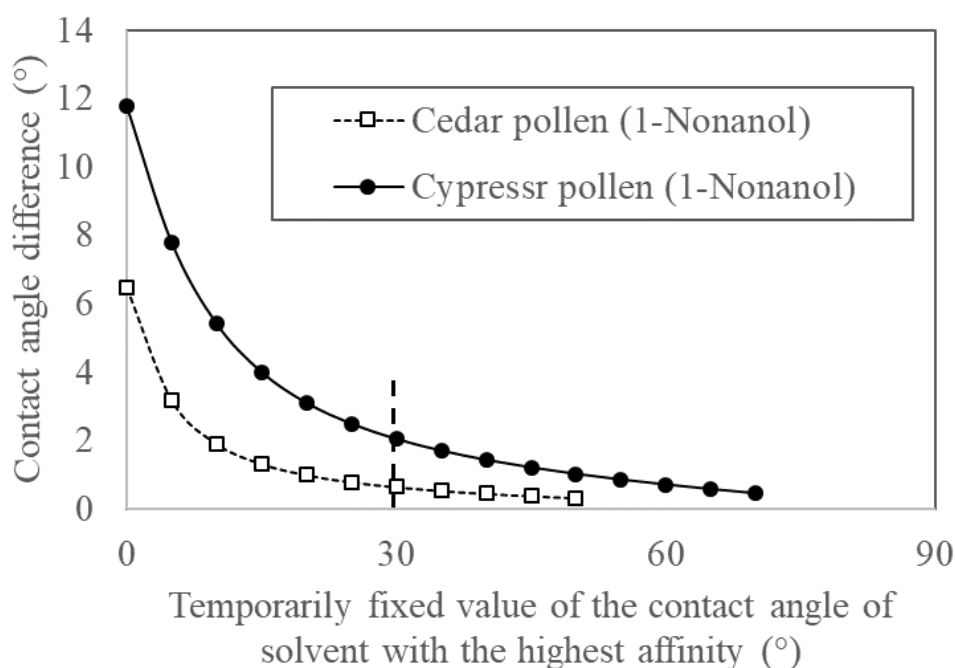
Figure 4-5. Relationships between the "provisional fixed contact angles of solvents with the strongest affinities for pollen" and the "differences between the contact angles determined in the two measurements"

The contact angle threshold was determined from the correlation between the contact angle and the distance Ra between the solvent and pollen HSPs. The threshold solvents for cedar and cypress pollen, the correlation coefficients, and the HSPs with threshold solvent contact angle as threshold are shown in Tables 4-2 and 4-3. It can be seen from Table 4-2 that the highest correlation coefficient for cedar pollen (0.769) was found when 1-hexanol was classed as a good solvent. It can be seen from Table 4-3 that the highest correlation coefficient for cypress pollen (0.748) was found when 1-hexanol was classed as a good solvent. As a representative example, the relationships between the contact angles for different solvents and the distance Ra between the HSPs for the solvents and the pollen HSPs when 1-hexanol was classed as a good solvent are shown in Figure 4-6. The contact

angles for the different solvents and the distance Ra between the HSPs for the solvents and the pollen HSPs positively correlated.

Hansen spheres for the cedar pollen and cypress pollen surfaces were created using the Hansen dissolution sphere method using the results described above for good and poor solvents. The Hansen spheres are shown in Figure 4-7. Cedar pollen and cypress pollen both gave clean spheres. The cedar pollen HSPs were $(\delta_d, \delta_p, \delta_h) = (15.8, 5.4, 11.7)$ and the cypress pollen HSPs were $(\delta_d, \delta_p, \delta_h) = (16.0, 4.7, 11.3)$. The states of the cedar and cypress pollen samples after they had been removed from the container after measurements had been made with typical good solvents and poor solvents are shown in Figure 4-8. 1-Nonanol was found to be a good solvent for both cedar pollen and cypress pollen, and penetrated the pollen samples. The poor solvent γ-butyrolactone did not penetrate the pollen samples, and the pollen remained a free-flowing powder.

Table 4-2. Threshold solvents, Hansen solubility parameters for cedar pollen using the threshold solvents, and correlation coefficients for the relationships between the Ra values and contact angles

| Threshold solvent | Hansen solubility parameter | | | Correlation coefficie | Contact angle |
	δ_d $(MPa)^{1/2}$	δ_p $(MPa)^{1/2}$	δ_h $(MPa)^{1/2}$		$(°)$
1-Nonanol					30.3
1-Octanol	Because of almost the same HSP, Hansen sphere was not drawn.				43.7
1-Heptanol					51.0
1-Hexanol	15.80	5.40	11.70	0.769	53.4
1-Decanol	16.10	5.30	11.50	0.755	54.7
1-Undecanol	15.90	4.80	11.20	0.759	55.5
1-Butanol	16.30	0.60	13.90	0.675	61.9
1-Pentanol	16.30	3.70	13.20	0.726	64.4
1-Methoxy-2-propanol	16.10	4.80	12.90	0.752	65.4
1-propanol	16.10	5.20	13.70	0.733	67.5
Ethanol	15.70	6.30	14.60	0.707	72.6
Tetrahydrofuran(THF)	15.50	8.90	13.20	0.684	74.3
Acetone	15.50	9.00	13.20	0.679	77.1
Ethyl acetate	14.90	9.00	12.70	0.709	77.4

Table 4-3. Threshold solvents, Hansen solubility parameters for cypress pollen using the threshold solvents, and the correlation coefficients for the relationships between the Ra values and contact angles

Threshold solvent	Hansen solubility parameter			Correlation coefficie	Contact angle
	δ_d $(MPa)^{1/2}$	δ_p $(MPa)^{1/2}$	δ_h $(MPa)^{1/2}$		$(°)$
1-Nonanol					31.0
1-Decanol	Because of almost the same HSP, Hansen sphere was not drawn.				57.5
1-Heptanol					57.0
1-Undecanol	17.30	3.20	12.00	0.604	58.3
1-Octanol	16.00	4.40	11.00	0.735	58.3
1-Hexanol	16.00	4.70	11.30	0.748	60.8
1-Butanol	16.60	1.00	14.00	0.658	61.5
1-Pentanol	16.50	3.80	13.20	0.701	67.4
1-Methoxy-2-Propanol	16.00	4.80	12.90	0.742	67.6
1-Propanol	16.10	5.30	13.70	0.716	71.1
Tetrahydrofuran (THF)	16.00	8.50	12.30	0.664	73.4
Ethanol	15.50	9.00	13.20	0.659	75.4
Ethyl Acetate	15.30	8.30	13.20	0.700	75.6
Acetone	14.90	9.10	12.70	0.689	76.4
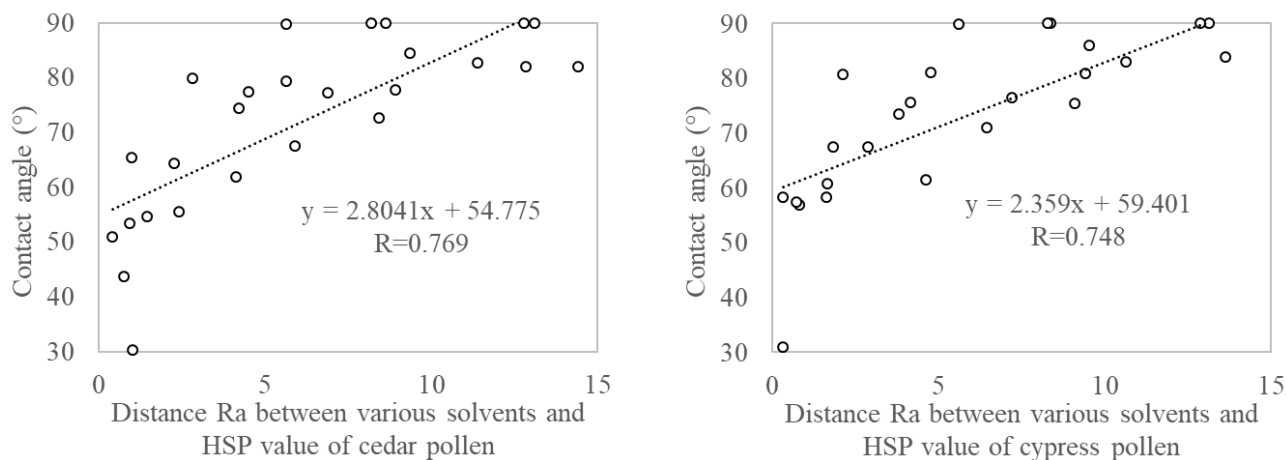
Figure 4-6. Relationships between the contact angles and "the distances Ra between the solvent and pollen Hansen solubility parameters" using 1-hexanol as a good solvent for cedar and cypress pollen
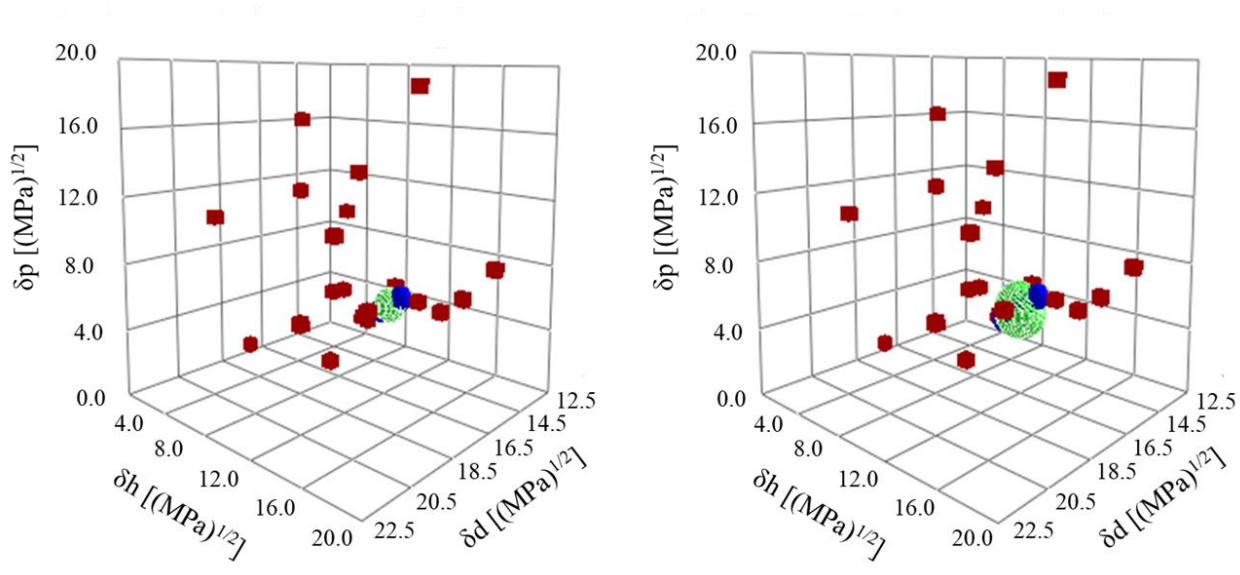

Figure 4-7. Hansen spheres for the cedar and cypress pollen surfaces. Blue spheres are for "good" solvents and red cubes are for "bad" solvents. The center of the green sphere is the Hansen solubility parameter.
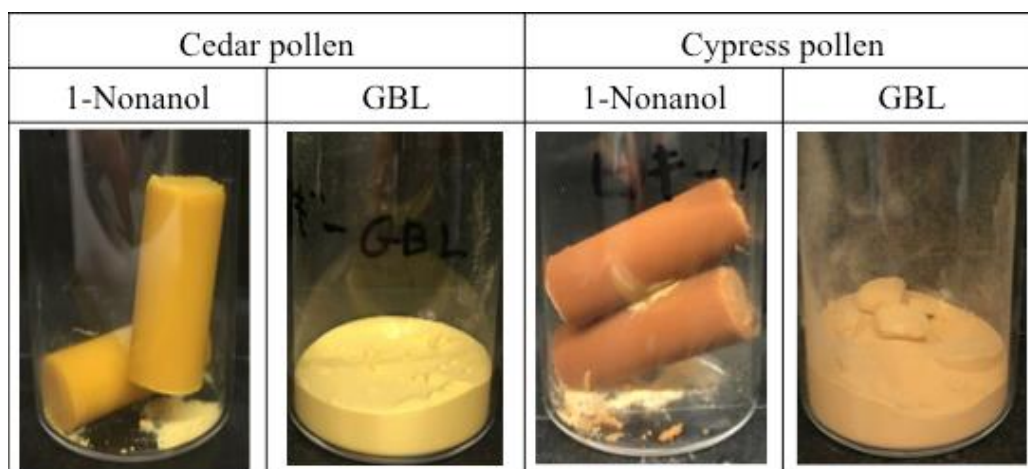
Figure 8. Pollen samples after measurements had been made using the capillary penetration method (GBL = γ-butyrolactone)

4.3.2 Carbon numbers and contact angles for alcohols

The calculated cedar and cypress pollen HSPs were also evaluated in another way. Various alcohols were used for the HSPs measurements, and the relationship between the number of carbon atoms in an alcohol and the contact angle was assessed. The relationships between the number of carbon atoms in an alcohol and the cedar pollen and cypress pollen contact angles are shown in Figure 4-9. Clear relationships were found between the numbers of carbon atoms in the alcohols and the contact angles for both cedar and cypress pollen. The cedar and cypress pollen contact angles were extremely small for 1-nonanol (which has nine carbon atoms). I therefore concluded that the cedar and cypress pollen HSPs were close to $(\delta_d, \delta_p, \delta_h) = (16.0, 4.8, 11.0)$, which are the HSPs for 1-nonanol. The distance Ra between the 1-nonanol and pollen HSPs was close to 1.0 for cedar pollen and 0.4 for cypress pollen, confirming that the HSPs were appropriate.
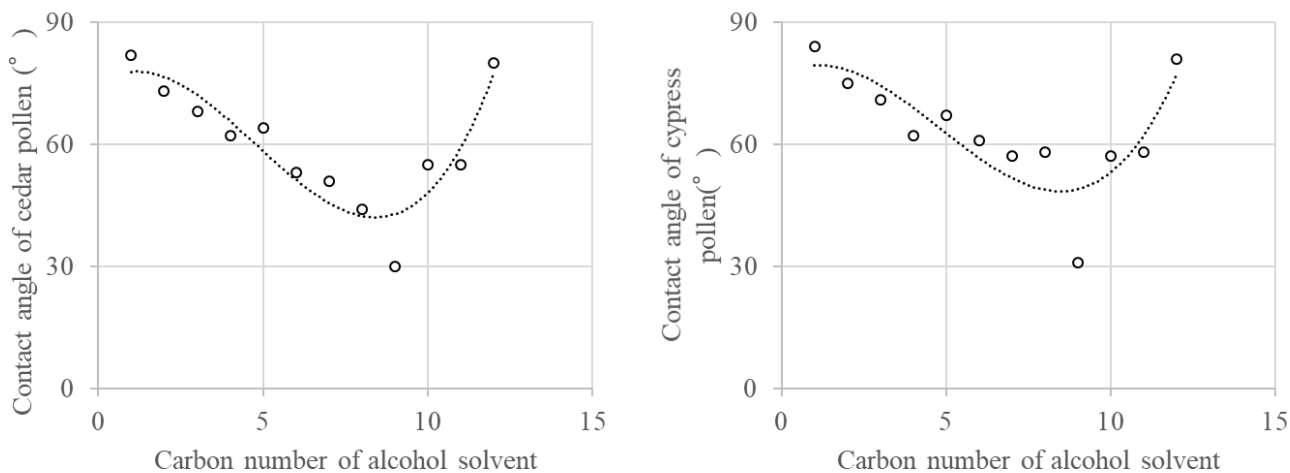
Figure 4-9. Relationships between the numbers of carbon atoms in the alcohols and the pollen contact angles

4.3.3　Liquids compatible with pollen

The cedar and cypress pollen HSPs were measured and confirmed as described above. Here, I will identify liquids with strong affinities for pollen surfaces that could be used to decrease the incidence of hay fever. Solvents with around nine carbon atoms (e.g., 1-nonanol) were found to have strong affinities for pollen. Liquid mixtures with HSPs similar to the measured HSPs for cedar and cypress pollen are shown in Tables 4-4 and 4-5, respectively. The ratios shown in the tables are the volumetric ratios of the components of the solvent mixtures. The mixtures shown in Tables 4-4 and 4-5 had smaller Ra values than 1-nonanol, had strong affinities for pollen surfaces, and were considered to be suitable for use as mists to efficiently collect pollen.

Table 4-4. Solvent mixtures with strong compatibilities with cedar pollen and distance Ra values between the Hansen solubility parameters for cedar pollen and the solvent mixtures

	δd [(MPa)$^{1/2}$]	δp [(MPa)$^{1/2}$]	δh [(MPa)$^{1/2}$]	δt [(MPa)$^{1/2}$]	Ra -
Cedar pollen	15.8	5.4	11.7	20.4	-
t-Butyl Alcohol : THF = 54 : 46	15.9	5.4	11.6	20.4	0.2
Hexylene Glycol : sec-Butyl Acetate = 56 : 44	16	5.4	11.7	20.5	0.4
Dipropylene Glycol Methyl Ether : Cyclohexanol = 76 : 24	16	5.3	11.8	20.6	0.4

Table 4-5. Solvent mixtures with strong compatibilities with cedar pollen and distance Ra values between the Hansen solubility parameters for cypress pollen and the solvent mixtures

	δd [(MPa)$^{1/2}$]	δp [(MPa)$^{1/2}$]	δh [(MPa)$^{1/2}$]	δt [(MPa)$^{1/2}$]	Ra
Cypress pollen	16.1	4.8	11.3	20.2	-
Heptane : Ethylene Glycol = 56 : 44	16	4.8	11.4	20.2	0.2
Ethanol : Cyclohexane = 57 : 43	16.2	5	11.1	20.3	0.3
n-Amyl Acetate : 1-Propanol = 54 : 46	15.9	4.9	11.3	20.1	0.4

4.4 Discussion

4.4.1 Method for determining the effective radius r

It is difficult to measure the effective radius r of an individual capillary tube in a capillary bundle. Therefore, r is often calculated by temporarily setting the contact angle of the solvent giving the highest degree of wettability to 0°. However, it is unlikely that the contact angle of the solvent giving the highest degree of wettability within the test range will be 0°. If additional experiments are performed and there is a solvent with better wettability, the contact angle will be negative. In addition, as explained in section 4.3.1, the contact angles variation increases on the low contact angle side. The measured contact angle was therefore considered to be somewhat different from the true contact angle. More realistic r values were obtained using the method described next. First, the change in measured contact angle when the set contact angle for the solvent giving the highest degree of wettability was changed was plotted on a graph. The angle at which the error was decreased markedly was used as the contact angle reference value. The method described here cannot be used to accurately determine the r value but will give a value close to the true value.

4.4.2 Method for determining the contact angle threshold

Because the HSPs change depending on how the threshold is determined, it may be pointed out that the determination method is arbitrary. Therefore, in this paper, the following method was adopted to eliminate arbitrariness. First, all the HSPs on the pollen surface when the threshold was comprehensively changed were calculated. Next, the distance Ra between the HSPs for the pollen surfaces and the HSPs for all of the solvents used in the measurements were calculated. The Ra values and contact angles should positively correlate because Ra and contact angle will be small when there if a strong affinity between the solvent and pollen surfaces. This calculation was performed for each threshold value, and

the correlation coefficient for each was calculated. The threshold with the highest correlation coefficient was used.

The threshold value was automatically determined through the calculations that were performed. The contact angle of the solvent used in the experiment was not only a good or poor solvent, but the contact angle value of each solvent played a role in determining the threshold. The method therefore effectively used the measurement data and gave accurate HSPs.

4.4.3   HSPs for cedar and cypress pollen surfaces

The HSPs for the cedar and cypress pollen surfaces were calculated to eliminate arbitrariness and give values close to the true values, as discussed in section 4.4.2. The relationships between the carbon numbers of the alcohols and the contact angles confirmed that the HSPs were accurate.

The HSPs for the pollen surfaces will help when selecting mist ingredients and filter materials for air purifiers to collect pollen. Selecting a liquid or mixture with HSPs similar to the pollen surface HSPs (e.g., the solvent mentioned in section 4.3.3) will give a good pollen collection efficiency. From a scientific point of view, the mixed liquids were chosen to have the lowest possible R_a value. However, in actual products, it is necessary to consider the effects on the human body, and it is necessary to select substances that are not harmful to health.

4.5   Conclusions

The aim of the study was to identify a solvent mixture that could efficiently collect pollen (which is harmful to human health). The surface physical properties of pollen particles were investigated by measuring the HSPs of cedar and cypress pollen. The pollen HSPs were measured using a capillary permeation method that allowed measurements to be made irrespective of the shapes and sizes of the particles. The measured cedar pollen HSPs were $(\delta_d, \delta_p, \delta_h) = (15.8, 5.4, 11.7)$, and the measured cypress pollen HSPs were $(\delta_d, \delta_p, \delta_h) = (16.0, 4.7, 11.3)$. These HSPs were confirmed by the relationship between the numbers of carbon atoms in the alcohols that were tested and the contact angles. Of the solvents used, 1-nonanol had the strongest affinities for both cedar pollen and cypress pollen. A 56:44 v/v mixture of hexylene glycol and sec-butyl acetate was found to have the strongest affinity for cedar pollen, and a 56:44 v/v mixture of heptane and ethylene glycol was found to have the strongest affinity for cypress pollen. It would therefore be expected that mists of these solvent mixtures in air purifiers and other systems would efficiently remove cedar and cypress pollen from air.

4.6 References

[4-1] J. Buters, M. Prank, M. Sofiev, G. Pusch, R. Albertini, I. Annesi-Maesano, C. Antunes, H. Behrendt, U. Berger, R. Brandao, S. Celenk, C. Galan, Ł. Grewling, B. Jackowiak, R. Kennedy, A. Rantio-Lehtimäki, G. Reese, I. Sauliene, M. Smith, M. Thibaudon, B. Weber, L. Cecchi, Variation of the group 5 grass pollen allergen content of airborne pollen in relation to geographic location and time in season the HIALINE working group, J. Allergy Clin. Immunol. 136 (2015) 87–95.e6.

[4-2] M. Prank, D.S. Chapman, J.M. Bullock, J. Belmonte, U. Berger, A. Dahl, S. Jäger, I. Kovtunenko, D. Magyar, S. Niemelä, A. Rantio-Lehtimäki, V. Rodinkova, I. Sauliene, E. Severova, B. Sikoparija, M. Sofiev, An operational model for forecasting ragweed pollen release and dispersion in Europe, Agric. For. Meteorol. 182–183 (2013) 43–53.

[4-3] F. Zhao, A. Elkelish, J. Durner, C. Lindermayr, J.B. Winkler, F. Ruioff, H. Behrendt, C. Traidl-Hoffmann, A. Holzinger, W. Kofler, P. Braun, C. Von Toerne, S.M. Hauck, D. Ernst, Common ragweed (Ambrosia artemisiifolia L.): Allergenicity and molecular characterization of pollen after plant exposure to elevated NO2, Plant Cell Environ. 39 (2016) 147–164.

[4-4] M. Turkalj, I. Banic, A review of clinical efficacy, safety, new developments and adherence to allergen-specific immunotherapy in patients with allergic rhinitis caused by allergy to ragweed pollen (Ambrosia artemisiifolia), Patient Prefer. Adherence. 11 (2017) 247–257.

[4-5] K. Honda, H. Saito, N. Fukui, E. Ito, The Relationship between Pollen Count Levels and Prevalence of Japanese Cedar Pollinosis in Northeast Japan, Allergol. Int. 62 (2013) 375–380.

[4-6] N. Yamamoto, J. Nishikawa, M. Sakamoto, T. Shimizu, H. Matsuki, Indoor and outdoor concentrations of Japanese cedar pollens and total suspended particulates: A case study at a kindergarten in Japan, Build. Environ. 45 (2010) 792–797.

[4-7] L. Pahus, M. Gouitaa, T. Sofalvi, K. Alagha, D. Gras, P. Chanez, D. Charpin, Cypress pollen allergy is responsible for two distinct phenotypes of allergic rhinitis different from other pollinosis, Eur. Ann. Allergy Clin. Immunol. 50 (2018) 28–35.

[4-8] J.T.M. Buters, C. Antunes, A. Galveias, K.C. Bergmann, M. Thibaudon, C. Galán, C. Schmidt-Weber, Pollen and spore monitoring in the world, Clin. Transl. Allergy. 8 (2018) 1–5.

[4-9] Y.S. Cheng, J.C. Lu, T.R. Chen, Efficiency of a Portable Indoor Air Cleaner in Removing Pollens and Fungal Spores, Aerosol Sci. Technol. 29 (1998) 92–101.

[4-10] F. Orlandi, T. Bonofiglio, C. Sgromo, L. Ruga, B. Romano, M. Fornaciari, An applied aerobiological study to test the efficacy of pollen filters in limiting indoor pollen contamination, Grana. 50 (2011) 73–80.

[4-11] T.J. O'Meara, J.K. Sercombe, G. Morgan, H.K. Reddel, W. Xuan, E.R. Tovey, The reduction of rhinitis symptoms by nasal filters during natural exposure to ragweed and grass pollen, Allergy Eur. J. Allergy Clin. Immunol. 60 (2005) 529–532.

[4-12] Y. Takikawa, Y. Matsuda, T. Nonomura, K. Kakutani, S.I. Kusakari, H. Toyoda, An electrostatic-barrier-forming window that captures airborne pollen grains to prevent pollinosis, Int. J. Environ. Res. Public Health. 14 (2017) 3–7.

[4-13] S. Kanzaki, K. Hashiguchi, K.-I. Wakabayashi, K. Suematsu, K. Okubo, Histamine antagonist Bepotastine suppresses nasal symptoms caused by Japanese cedar and cypress pollen exposure., J. Drug Assess. 5 (2016) 15–23. doi:10.1080/21556660.2016.1237365.

[4-14] S.J. McEldowney, R.K. Bush, Pollen immunotherapy: selection,prevention, and future directions, Curr Allergy Asthma Rep. 6 (2006) 420–426.

[4-15] J.H. Hildebrand, R.L. Scott, The Solubility of Nonelectrolytes, third ed. (Dover Publications Inc., New York, 1950).

[4-16] C.M. Hansen, Hansen Solubility Parameters: A User's Handbook (CRC Press, Boca Raton, 1999).

[4-17] C.M. Hansen, A.L. Smith, Using Hansen solubility parameters to correlate solubility of C 60 fullerene in organic solvents and in polymers, Carbon N. Y. 42 (2004) 1591–1597.

[4-18] H.T. Ham, Y.S. Choi, I.J. Chung, An explanation of dispersion states of single-walled carbon nanotubes in solvents and aqueous surfactant solutions using solubility parameters, J. Colloid Interface Sci. 286 (2005) 216–223.

[4-19] S. Acevedo, A. Castro, E. Vásquez, F. Marcano, M.A. Ranaudo, Investigation of physical chemistry properties of asphaltenes using solubility parameters of asphaltenes and their fractions A1 and A2, Energy and Fuels. 24 (2010) 5921–5933.

[4-20] T. Sato, S. Araki, M. Morimoto, R. Tanaka, H. Yamamoto, Comparison of hansen solubility parameter of asphaltenes extracted from bitumen produced in different geographical regions, Energy and Fuels. 28 (2014) 891–897. doi:10.1021/ef402065j.

[4-21] T. Sato, Y. Hamada, M. Sumikawa, S. Araki, H. Yamamoto, Solubility of oxygen in organic solvents and calculation of the Hansen solubility parameters of oxygen, Ind. Eng. Chem. Res. 53 (2014) 19331–19337.

[4-22] J.U. Wieneke, B. Kommob, O. Gaer, I. Prykhodko, M. Ulbricht, Systematic investigation of dispersions of unmodified inorganic nanoparticles in organic solvents with focus on the hansen solubility parameters, Ind. Eng. Chem. Res. 51 (2012) 327–334. [4-23] S.H. Wang, J.H. Liu, C.T. Pai, C.W. Chen, P.T. Chung, A.S.T. Chiang, S.J. Chang, Hansen solubility parameter analysis on the dispersion of zirconia nanocrystals, J. Colloid Interface Sci. 407 (2013) 140–147.

[4-24] S. Tsutsumi, K. Kondo, Y. Kato, N. Fujiwara, H. Yamamoto, Determination of Hansen solubility parameters of particles using a capillary penetration method, Chem. Phys. 521 (2019) 115–122.

[4-25] Organic Synthetic Association, Solvents Pocket Book (Ohmsha. Ltd, Tokyo, 1967).

Chapter 5 Conclusion and future prospects

5.1 Chapter 1 Summary and future prospects

An outline of the principles of the HSP and its calculation and measurement are described. Research related to the HSP is introduced.

In future, it is expected that research will be conducted to improve accuracy by understanding more detail of the parameter, such as the subdivision of the London dispersion δ_d and hydrogen-bonding δ_h forces. Various proposals have been made regarding methods of evaluating affinity; such methods are expected to further increase with the development of analyzers.[5-1,5-2,5-3,5-4,5-5] Application to research on fine particle dispersion, which is described in this paper, is active.[5-6,5-7,5-8,5-9,5-10] Research in biotechnology and medical applications is also increasing. HSP use in all fields is expected to be reported in the future.[5-11,5-12,5-13,5-14,5-15]

5.2 Chapter 2 Summary and future prospects

Measurement of HSP values of relatively large fine particles with high specific gravity is difficult using existing DLS or sedimentation methods. I therefore devised a method of HSP measurement using capillary penetration.[5-16, 5-17] The proposed method was verified and compared with results obtained using DLS.[5-18] Using 1 μm spherical silica particles, which can be measured by DLS, it was confirmed that the new method could measure particles of this size. In addition, it was confirmed that non-spherical silica particles of 63 μm diameter or less, which were difficult to measure by DLS, could be measured. HSPs of relatively large particles were able to be measured by applying the traditional permeation-rate method. In addition, its combination with HSP was effective for the capillary-penetration method. It is pointed out that the capillary-penetration method cannot measure the absolute value of contact angle and can only perform relative comparisons; however, when the capillary-penetration method and HSP are combined, the HSP value is determined

using the relative value of the contact angle measured by the capillary-penetration method, which can compensate for the disadvantages of the permeation-rate method.

5.3 Chapter 3 Summary and future prospects

In Chapter 3, I attempted to improve the performance of bonded magnets containing non-spherical and high-specific-gravity magnetic powders using the HSP measurement technique for fine particles that was established in Chapter 2. Based on past experience and knowledge, various composite materials, including bonded magnets, have been designed.[5-19,5-20,5-21,5-22,5-23,5-24,5-25,5-26,5-27,5-28] HSPs were applied to quantitatively evaluate the design of this composite material. A bonded magnet mainly comprises a magnetic powder and a resin: improving compatibility of these components can improve the fluidity of injection molding and still achieve high magnetic properties. I first measured the HSP of the magnetic powder and the resin, and then tried to bring the HSP on the surface of the powder closer to that of the resin by treating the surface of the powder. To clarify the relationship between the selected surface-treatment agents and HSP, the HSP of the surface-treatment agent was obtained in advance by calculation using the group-contribution method. The HSP of the treated magnetic powder was also measured. There was a correlation between the calculated distance R_a of the HSPs of the surface-treatment agent and resin and the injection fluidity of the magnetic powder. Furthermore, there was a high correlation between the HSP value of the treated powder and the fluidity. With the most-compatible UPTMS surface-treatment agent, fluidity that could be molded was obtained, even at the high density of 5700 kg/m^3. This result suggested that the material design of a bonded magnet can be quantified using HSPs. This approach can be applied to other composite materials and used to quantify complicated composite material designs. In the future, this method will be expanded to other composite materials, such as structural, heat-conductive, friction, and electrically conductive materials.

5.4 Chapter 4 Summary and future prospects

In Chapter 4, application to pollen particles was attempted using the penetration-rate method established in Chapter 2. Hay fever, such as that attributed to cedar and ragweed, has become a worldwide problem.[5-29,5-30,5-31,5-32,5-33,5-34,5-35] To date, countermeasures, such as the use of air purifiers,[5-36] pollen filters,[5-37] and electrostatic repulsion,[5-38] have been studied. In this chapter, the HSPs of pollen were measured with a view to its efficient collection. I identified the HSPs of pollen particles and proposed a mixed solvent with a high affinity for pollen. I also examined a method for determining the threshold for separating good and poor solvents, which is always a problem in the measurement of HSPs of particle surfaces, and proposed a method to effectively use the measured contact angle data to derive more accurate HSPs. A mixed solvent is proposed for this application from a chemical point of view, so it is necessary to study liquids and filter materials in consideration of their effects on the human body and the environment. I hope that HSPs will contribute to the development of pollen allergy countermeasures in the future.

5.5   References

[5-1] H.J. Lim, K. Lee, Y.S. Cho, Y.S. Kim, T. Kim, C.R. Park, Experimental consideration of the Hansen solubility parameters of as-produced multi-walled carbon nanotubes by inverse gas chromatography, Phys. Chem. Chem. Phys. 16 (2014) 17466–17472.

[5-2] G.C. Vebber, P. Pranke, C.N. Pereira, Calculating Hansen solubility parameters of polymers with genetic algorithms, J. Appl. Polym. Sci. 131 (2014).

[5-3] M. Weng, Determination of the Hansen solubility parameters with a novel optimization method, J. Appl. Polym. Sci. 133 (2016).

[5-4] M.J. Louwerse, A. Maldonado, S. Rousseau, C. Moreau-Masselon, B. Roux, G. Rothenberg, Revisiting Hansen Solubility Parameters by Including Thermodynamics, ChemPhysChem. 18 (2017) 2999–3006.

[5-5] C. Andecochea Saiz, S. Darvishmanesh, A. Buekenhoudt, B. Van der Bruggen, Shortcut applications of the Hansen Solubility Parameter for Organic Solvent Nanofiltration, J. Memb. Sci. 546 (2018) 120–127.

[5-6] J. Ma, R.M. Larsen, Use of Hansen solubility parameters to predict dispersion and strain transfer of functionalized single-walled carbon nanotubes in poly(vinylidene fluoride) composites, J. Thermoplast. Compos. Mater. 27 (2014) 801–815.

[5-7] S. Gårdebjer, M. Andersson, J. Engström, P. Restorp, M. Persson, A. Larsson, Using Hansen solubility parameters to predict the dispersion of nano-particles in polymeric films, Polym. Chem. 7 (2016) 1756–1764.

[5-8] M. Huth, C.W. Chen, V. Wagner, Measurement of Hansen solubility parameters for organophilic fluoromica and evaluation of potential solvents for exfoliation, Appl. Clay Sci. 155 (2018) 120–125.

[5-9] M. Huth, C.W. Chen, J. Köhling, V. Wagner, Influence of Hansen solubility parameters on exfoliation of organophilic fluoromica, Appl. Clay Sci. 161 (2018) 412–418.

[5-10] S. Süß, T. Sobisch, W. Peukert, D. Lerche, D. Segets, Determination of Hansen parameters for particles: A standardized routine based on analytical centrifugation, Adv. Powder Technol. 29 (2018) 1550–1561.

[5-11] B.J. Carberry, J. Farrell, J.E. Kennedy, Evaluation and characterisation of urinary catheter coating utilising Hansen solubility parameters and FEA analysis, Surf. Coatings Technol. 276 (2015) 456–463.

[5-12] L. Paseta, G. Potier, S. Abbott, J. Coronas, Using Hansen solubility parameters to study the encapsulation of caffeine in MOFs, Org. Biomol. Chem. 13 (2015) 1724–1731.

[5-13] B. Hossin, K. Rizi, S. Murdan, Application of Hansen Solubility Parameters to predict drug-nail interactions, which can assist the design of nail medicines, Eur. J. Pharm. Biopharm. 102 (2016) 32–40.

[5-14] M.M.R. Devalapalli, H.S. Cheruvu, T. Yertha, V.B. Veeravalli, S. Sampathi, S. Shivakumar, Hansen solubility parameters for assay method optimization of simvastatin, ramipril, atenolol, hydrochlorothiazide and aspirin in human plasma using liquid chromatography with tandem mass spectrometry, J. Sep. Sci. 40 (2017) 3662–3674.

[5-15] D. Obradović, F. Andrić, M. Zlatović, D. Agbaba, Modeling of Hansen's solubility parameters of aripiprazole, ziprasidone, and their impurities: A nonparametric comparison of models for prediction of drug absorption sites, J. Chemom. 32 (2018) 1–12.

[5-16] J. E.Jaine, M. R.Mucalo, Measurements of the wettability of catalyst support materials using the Washburn capillary rise technique. Powder Technol. 276 (2015) 123–128.

[5-17] S. Tsutsumi, K. Kondo, Y. Kato, N. Fujiwara, H. Yamamoto, Determination of Hansen solubility parameters of particles using a capillary penetration method, Chem. Phys. 521 (2019) 115–122.

[5-18] S.Süß, T.Sobisch, W.Peukert, D.Lerche, D.Segets, Original Research Paper Determination of Hansen parameters for particles: A standardized routine based on analytical centrifugation. Advanced Powder Technol. 29 (2018) 1550-1561.

[5-19] X.W. Li, R.G. Song, Y. Jiang, C. Wang, D. Jiang, Surface modification of TiO 2 nanoparticles and its effect on the properties of fluoropolymer/TiO 2 nanocomposite coatings, Appl. Surf. Sci. 276 (2013) 761–768.

[5-20] S. Kango, S. Kalia, A. Celli, J. Njuguna, Y. Habibi, R. Kumar, Surface modification of inorganic nanoparticles for development of organic-inorganic nanocomposites - A review, Prog. Polym. Sci. 38 (2013) 1232–1261.

[5-21] S.H. Wang, Y. Sen Sun, A.S.T. Chiang, H.F. Hung, M.C. Chen, K. Wood, Carboxylic acid-directed clustering and dispersion of ZrO2 nanoparticles in organic solvents: A study by small-angle x-ray/neutron scattering and NMR, J. Phys. Chem. C. 115 (2011) 11941–11950.

[5-22] Z.M. Dang, Y.J. Xia, J.W. Zha, J.K. Yuan, J. Bai, Preparation and dielectric properties of surface modified TiO 2/silicone rubber nanocomposites, Mater. Lett. 65 (2011) 3430–3432.

[5-23] S. Mallakpour, A. Barati, Efficient preparation of hybrid nanocomposite coatings based on poly(vinyl alcohol) and silane coupling agent modified TiO2 nanoparticles, Prog. Org. Coatings. 71 (2011) 391–398.

[5-24] W. Zhou, Effect of coupling agents on the thermal conductivity of aluminum particle/epoxy resin composites, J. Mater. Sci. 46 (2011) 3883–3889.

[5-25] W. Chuang, J. Geng-sheng, P. Lei, Z. Bao-lin, L. Ke-zhi, W. Jun-long, Influences of surface modification of nano-silica by silane coupling agents on the thermal and frictional properties of cyanate ester resin, Results Phys. 9 (2018) 886–896.

[5-26] I. Jang, K.H. Shin, I. Yang, H. Kim, J. Kim, W.H. Kim, S.W. Jeon, J.P. Kim, Enhancement of thermal conductivity of BN/epoxy composite through surface modification with silane coupling agents, Colloids Surfaces A Physicochem. Eng. Asp. 518 (2017) 64–72.

[5-27] Q. Chen, J. Asuncion, J. Landi, B.M. Ma, The effect of the coupling agent on the packing density and corrosion behavior of NdFeB and SmCo bonded magnets, J. Appl. Phys. 85 (2002) 5684–5686.

[5-28] J.U. Otaigbe, J. Xiao, H. Kim, S. Constantinides, Influence of filler surface treatments on processability and properties of polymer-bonded Nd-Fe-B magnets, J. Mater. Sci. Lett. 18 (1999) 329–332.

[5-29] J. Buters, M. Prank, M. Sofiev, G. Pusch, R. Albertini, I. Annesi-Maesano, C. Antunes, H. Behrendt, U. Berger, R. Brandao, S. Celenk, C. Galan, Ł. Grewling, B. Jackowiak, R. Kennedy, A. Rantio-Lehtimäki, G. Reese, I. Sauliene, M. Smith, M. Thibaudon, B. Weber, L. Cecchi, Variation of the group 5 grass pollen allergen content of airborne pollen in relation to geographic location and time in season the HIALINE working group, J. Allergy Clin. Immunol. 136 (2015) 87–95.e6.

[5-30] M. Prank, D.S. Chapman, J.M. Bullock, J. Belmonte, U. Berger, A. Dahl, S. Jäger, I. Kovtunenko, D. Magyar, S. Niemelä, A. Rantio-Lehtimäki, V. Rodinkova, I. Sauliene, E. Severova, B. Sikoparija, M. Sofiev, An operational model for forecasting ragweed pollen release and dispersion in Europe, Agric. For. Meteorol. 182–183 (2013) 43–53.

[5-31] F. Zhao, A. Elkelish, J. Durner, C. Lindermayr, J.B. Winkler, F. Ruioff, H. Behrendt, C. Traidl-Hoffmann, A. Holzinger, W. Kofler, P. Braun, C. Von Toerne, S.M. Hauck, D. Ernst, U. Frank, Common ragweed (Ambrosia artemisiifolia L.): Allergenicity and molecular characterization of pollen after plant exposure to elevated NO2, Plant Cell Environ. 39 (2016) 147–164.

[5-32] M. Turkalj, I. Banic, S.A. Anzic, A review of clinical efficacy, safety, new developments and adherence to allergen-specific immunotherapy in patients with allergic rhinitis caused by

allergy to ragweed pollen (Ambrosia artemisiifolia), Patient Prefer. Adherence. 11 (2017) 247–257.

[5-33] K. Honda, H. Saito, N. Fukui, E. Ito, K. Ishikawa, The Relationship between Pollen Count Levels and Prevalence of Japanese Cedar Pollinosis in Northeast Japan, Allergol. Int. 62 (2013) 375–380.

[5-34] N. Yamamoto, J. Nishikawa, M. Sakamoto, T. Shimizu, H. Matsuki, Indoor and outdoor concentrations of Japanese cedar pollens and total suspended particulates: A case study at a kindergarten in Japan, Build. Environ. 45 (2010) 792–797.

[5-35] L. Pahus, M. Gouitaa, T. Sofalvi, K. Alagha, D. Gras, P. Chanez, D. Charpin, Cypress pollen allergy is responsible for two distinct phenotypes of allergic rhinitis different from other pollinosis, Eur. Ann. Allergy Clin. Immunol. 50 (2018) 28–35.

[5-36] Y.S. Cheng, J.C. Lu, T.R. Chen, Efficiency of a Portable Indoor Air Cleaner in Removing Pollens and Fungal Spores, Aerosol Sci. Technol. 29 (1998) 92–101.

[5-37] F. Orlandi, T. Bonofiglio, C. Sgromo, L. Ruga, B. Romano, M. Fornaciari, An applied aerobiological study to test the efficacy of pollen filters in limiting indoor pollen contamination, Grana. 50 (2011) 73–80.

[5-38] Y. Takikawa, Y. Matsuda, T. Nonomura, K. Kakutani, S.I. Kusakari, H. Toyoda, An electrostatic-barrier-forming window that captures airborne pollen grains to prevent pollinosis, Int. J. Environ. Res. Public Health. 14 (2017) 3–7.

Acknowledgments